ELSEVIER

Spectrochimica Acta Part B 57 (2002) 1361–1452

SPECTROCHIMICA ACTA PART B

www.elsevier.com/locate/sab

Review

Reaction cells and collision cells for ICP-MS: a tutorial review

Scott D. Tanner*, Vladimir I. Baranov, Dmitry R. Bandura

Perkin Elmer SCIEX, 71 Four Valley Drive, Concord, Ont., Canada L4K 4V8

Received 12 December 2001; accepted 20 June 2002

Abstract

This paper reviews the literature published to September 2001 relating to the history, design, operation and application of linear radio-frequency (r.f.)-driven multipole collision cells and reaction cells in combination with inductively coupled plasma mass spectrometry. The available material is supplemented with original experimental data that demonstrates the principles presented. The relation of these devices to collision cells for organic mass spectrometry and to the three-dimensional ion trap is discussed in its historical context. A general tutorial on the fundamentals of ion collision and reaction, including thermochemistry, energy transfer and reaction kinetics, is given. Consideration is given to some of the fundamental aspects of operation and design of linear r.f. devices. This historical and fundamental framework then allows the tutorial to focus on the promotion and control of ion–molecule chemistry in linear r.f.-multipole cells for elemental analysis. Vacuum requirements are considered in some detail, and deal in particular with the issue of contamination of the reaction gas. Special attention is paid to the thermal characteristics of the ions in the cell, as this has important implications for the application of the available databases of thermochemical and thermal kinetic data to the development of analytical methods. Calculation and experimental validation of the efficiency of the ion–molecule chemistry leads to the recognition that secondary, sequential chemistry can play a limiting role in the realization of the potential of the cell method. The two principal means of controlling the analytical impact of the secondary chemistry, through post-cell kinetic energy discrimination and through in-cell mass-bandpassing are discussed and contrasted through spectral data acquired for different reaction gas types and pressures. The available literature on the application of collision cells and reaction cells for the analysis of samples of high purity, environmental, geological and biological materials is critically reviewed.

Keywords: Collision cell; Reaction cell; ICP-MS; Collision induced fragmentation; Ion–molecule chemistry

*Corresponding author. Tel.: +1-905-660-9006x262; fax: +1-905-660-2623.
E-mail address: scott.tanner@sciex.com (S.D. Tanner).

0584-8547/02/$ - see front matter © 2002 Elsevier Science B.V. All rights reserved.
PII: S0584-8547(02)00069-1

Contents

1. Introduction

It is our opinion that ion–molecule chemistry, enacted in a radio-frequency (r.f.)-driven multipole that is pressurized with a reactive gas, will dominate high performance elemental analysis by inductively coupled plasma mass spectrometry (ICP-MS) in the near- and mid-future. Ion–molecule reactions have been studied for several decades, having their principal application in interstellar and ionospheric chemistry [1,2]. The basic tenets governing the kinetics and reactivity are well understood [3–11]. The r.f.-only multipole has found significant application for the study of near-thermal or energy-selected ion–molecule reactions, particularly when operated at low r.f. amplitude and high frequency [12–14]. In addition, the r.f.-only 'collision cell' has been important in organic tandem mass spectrometry for 20 years, where it is used to promote collision induced dissociation (CID) and to confine and transport the resultant fragment ions to a downstream mass analyzer [15–19]. Two important papers appeared in 1989 that discussed the potential of CID and reactivity for the inorganic application [20,21]. It was shown [20] that CID is an ineffective process for several polyatomic ions obtained from the ICP, but that ion–molecule chemistry using O_2 [20], Xe, CH_4 or C_2H_6 [21] was very specific and efficient. Perhaps because of perceived deficiencies, difficulties or expense, or because attention was focused on other perceived instrument deficiencies, the subject remained dormant for several years. The catalyst for the recent resurgence in interest was the 1994 publication of Barinaga and Koppenaal [22] in which it was observed that argide ions were nearly absent in the spectra obtained by ICP-IT-MS (ion trap), and this was importantly ascribed, at least in part, to charge transfer reactions of these ions with adventitious water molecules. Subsequent work by the same group [23–26] showed highly effective application of ion–molecule chemistry with other gases (H_2, O_2 and CH_4) for general and specific challenges.

The first commercial enactment of a pressurized multipole, specific for the ICP-MS application in the form of a hexapole collision cell, was reported by Turner et al. [27], and is now available from Micromass as the Platform™ (a similar technology is used with a different intent in the Micromass IsoProbe™). Originally, it was claimed in this work that the effective process was CID using He as the collision gas. Later, H_2 was used as a reaction gas in mixture with He. For reasons now apparent, reactions with H_2 and impurities in the collision gas were principally responsible for the observed benefit. Subsequent commercial entries were made by Perkin Elmer-SCIEX (ELAN® DRC™), Thermo Elemental (PQ ExCell®), and Agilent (7500c).

It is the intent of this work to review the technology of pressurized r.f.-driven multipole cells and to review the fundamentals of ion–molecule chemistry as it might be applied to the

ICP-MS application. The adoption of these technologies is just now taking place, such that insufficient information related to operation or the development of methods has been published. Accordingly, we will complement our review of the existing literature with examples from our own laboratory. The resultant manuscript thus becomes a tutorial review, where we provide our own interpretation and understanding of the processes discussed.

2. Experimental

In support of some of the theoretical considerations presented in this work, we include some previously unpublished demonstrative data obtained in our laboratory. These data were obtained using several generations of the prototypes of the ELAN DRC and including the commercial instrument itself. The hardware and the operating modes of these instruments have been described [28,29]. The DRC (Dynamic Reaction Cell™) is a high precision quadrupole that is enclosed and may be pressurized. It is operated at a low, user-selected r.f. amplitude, typically 200 V_{rf} measured peak-to-peak. The frequency of the r.f. signal is adjusted dynamically in accordance with the user-selected value of the operating parameter RPq (related to the Mathieu parameter q, defined below). A DC potential may be applied between pole pairs, having an amplitude defined by the user-selected operating parameter RPa (related to the Mathieu parameter a, also defined below). The flow of gas into the cell is controlled by a mass flow controller (Model 1479, MKS, Andover, MA). Two principal modes of operation of these systems are supported: the standard mode (which emulates conventional ICP-MS), in which the reaction cell is operated at low pressure ($\approx 10^{-5}$ torr) obtained by shutting off the reaction gas flow and venting the cell to the high vacuum (mass analyzer) chamber, and the DRC mode, obtained by closing the vent and pressurizing the cell with a reactive (or non-reactive) gas. All of the reported data were obtained under normal 'robust' plasma conditions. Typical operating conditions and voltages are given in Ref. [30].

The data given in Sections 8.3, 8.4 and 9.2 were obtained using a prototype of the ELAN DRC^{Plus}, which differs from the earlier instrument with the addition of electrodes inserted between the active rods of the reaction cell quadrupole, as described in Section 7.5, to provide an axial accelerating field of approximately 0.2 V/cm.

3. Nomenclature (definitions)

Various terms used in the discussion of reaction energetics and r.f. multipole theory have proper definitions, but they are often misused or micro-defined. Therefore, we define our usage of these terms with specific reference to the pressurized multipole cell used for ICP-MS:

A *bimolecular process* is a reaction (or collision) involving two particles, as is described by the reaction

$$A + B \rightarrow C + D \tag{3.1}$$

A *termolecular reaction* involves three particles, where the intermediate transition state of a bimolecular process is stabilized by collision with a third particle which removes an amount of energy. These reactions are also called *clustering reactions* or *association reactions*, and may be described by the reaction

$$A + B + M \rightarrow AB + M \tag{3.2}$$

which is actually comprised of the two steps:

$$A + B \rightarrow AB^* \tag{3.3}$$

$$AB^* + M \rightarrow AB + M \tag{3.4}$$

It is convenient to distinguish a bimolecular process from a termolecular process on the basis of the pressure dependence of the rate of reaction. The reaction rate of a bimolecular process is linearly dependent on the reaction gas density, whereas that for a termolecular process is dependent on the product of the pressure and the reaction gas density. In the instance where a buffer gas is not used (i.e. the cell is pressurized only by the reaction gas), a bimolecular process is first order, and a termolecular is second order, with respect to the cell pressure.

Thermochemistry refers to the energy balance in a reaction process. The 'reaction enthalpy', $\Delta H_{r,T}$,

is the difference between the sums of the gas phase heats of formation, $\Delta H_{f,T}$, of the reactants and products at the temperature T. When the enthalpy is negative, the reaction is said to be *exothermic*, and when positive it is *endothermic*. An exothermic reaction releases energy to the environment and, thus, is *thermodynamically allowed*. An endothermic reaction absorbs energy from the environment and is thermodynamically disallowed. An exothermic process may proceed, and is often fast. An endothermic process usually does not proceed, or is very slow (taking place only for those reactants with energies in the high energy tail of the distribution). In fact, the true discriminator of a thermodynamically allowed gas phase reaction is the 'free energy of reaction', $\Delta G_{r,T}$, which includes an entropy term ($\Delta G_{r,T}=\Delta H_{r,T}-T\Delta S_{r,T}$), but in most instances the entropy difference between reactants and products of a bimolecular process in the gas phase is negligible.

A *thermal condition* is one under which an ensemble of particles has a Maxwell–Boltzmann energy distribution which has the same temperature in all degrees of freedom. A thermal ensemble can be adiabatic (insulated from the container) or can be in equilibrium with the container walls. Therefore, a 'thermal ion beam' is an oxymoron, due to its obvious anisotropy.

A *non-thermal condition* is one under which an ensemble of particles has a non-Maxwell–Boltzmann energy distribution in one or more degrees of freedom. It can be adiabatic (insulated from the container) or be out of equilibrium with the container walls. An example of a non-thermal ensemble is an ion beam.

A *thermal process*, with respect to the subject of this paper, is a reaction that proceeds under thermal conditions. That is, the process is exothermic and an external source of energy is absent or is irrelevant.

A *non-thermal process*, with respect to the subject of this paper, is a reaction that proceeds when the reactants are not in equilibrium or are not adiabatically insulated from the container walls that are themselves not in equilibrium with the reactants. Such a reaction can be endothermic under thermal conditions and requires an external energy source to proceed under non-thermal conditions.

To *thermalize* a system is to convert a non-thermal ensemble into a thermal ensemble, usually by means of spontaneous energy redistribution (equilibration). Thermalization in the case of an ion beam injected into a pressurized multipole can be achieved (to some extent) by means of multiple collisions with a buffer gas under thermal conditions.

A *lab normal condition* is one under which a thermal ensemble of ions is in equilibrium with a buffer gas under thermal conditions. In most practically important instances, the thermal ensemble of ions should be adiabatically insulated from the r.f. drive of a pressurized multipole.

An *adiabatic* condition, with special reference to an r.f. multipole device, is one in which the ions do not, on average, gain energy from the applied r.f. field. This condition is achieved when the fundamental frequency of ion motion is essentially uncoupled from the applied r.f. frequency, and conveniently describes a case of insulation of the ion flow from the r.f. field. It is generally considered that an adiabatic condition is achieved for r.f.-only multipole devices only when the stability parameter q (see below) is less than approximately 0.3 [12].

The parameters a and q describe the regions of stable or unstable trajectories in an r.f. multipole field. In general:

$$a=2n(n-1)\frac{eV_{dc}}{m\omega^2 r_0^2} \tag{3.5}$$

$$q=n(n-1)\frac{eV_{rf}}{m\omega^2 r_0^2} \tag{3.6}$$

where n is the order of the multipole (number of pairs of poles), e is the elementary charge, V_{dc} is the DC voltage applied between pole pairs and V_{rf} is the peak-to-peak r.f. voltage (note that this definition follows that of Dawson [31]), m is the ion mass, ω is the r.f. angular frequency (the applied r.f. frequency multiplied by 2π), and r_0 is the radius of the inscribed circle that is tangential to the inner surfaces of the rods of the multipole array.

Stability, as referred to multipole operation, describes the region in (a, q) parametric space which allows transmission of ions through an infinitely large theoretical multipole field (field only, no multipole array present). Ions inside of the stability region belong to a stable trajectory.

Acceptance, referred to a multipole array, describes the (position, velocity) space (r, $\mathrm{d}r/\mathrm{d}t$ in cylindrical coordinates) for which an ion belonging to a stable trajectory has a maximum radial displacement less than r_0. The acceptance of the multipole is directly related to the transmission efficiency.

Collisional energy damping and *collisional focusing* are concomitant phenomena (a chicken and egg conundrum) referring to the loss of axial ion energy and the reduction of the width of the ion energy distribution towards thermalization with a collision gas. This process manifests itself in migration of ions towards the axis of a multipole.

In this paper, we use the term pressure in two senses. The term pressure is appropriate in discussion of collision frequency, and applies to consideration of vacuum system requirements and, amongst other things, to collisional stabilization of reaction intermediate complexes (termolecular reactions). However, we often refer to pressure as indicative of the number of collisions that an ion suffers in transit through a device, where we have assumed a fixed length for the device (12.5 cm for the cell length, unless otherwise specified). A more correct term for the latter usage is *gas thickness*, which is given by the product of the gas density and the length of the device. An increase in pressure results in an increase in the number of collisions that an ion suffers for a given device, but where devices differ in length, gas thickness gives a better comparison of the total number of collisions.

4. History

4.1. Tandem mass spectrometry

The two dimensional r.f.-driven collision cell was first introduced to mass spectrometry by Yost and Enke [15] in the triple quadrupole configuration. A r.f.-only enclosed quadrupole (the collision cell) was placed between two mass analyzing quadrupoles. Ions of interest, called the 'parent ions', from the composite of ions from the ion source are mass-selected in the first quadrupole (Q1). These ions are injected at a selectable energy into the collision cell (Q2) which has been pressurized with a target (collision) gas. Upon impact at the collision energy with the collision gas, the ions are fragmented. The resultant daughter ions are confined in the r.f. field and transmitted to the second mass analyzer (Q3) where the daughter ions are mass analyzed. The process is shown schematically in Fig. 1. The fragmentation process has been called CID or collision activated dissociation. In its initial enactment, the collision cell was operated at relatively low pressures that allowed only a few collisions. In this instance, a significant fraction of the incident ion energy was retained and each collision occurred at significant energy. The process of fragmentation may be a single collision event or a multiple collision event in which the vibrational degrees of freedom of the polyatomic ion are pumped in sequential collisions to the state of fragmentation. Another enactment of the device used a cross-molecular beam in an open construction collision cell [18,19]. It is clear that the fragmentation pathways are a function of the incident energy of the ions, the mass ratio of the ion-to-target gas, and the number of degrees of freedom of the ion and the target gas. In essence, the daughter ion spectrum may be viewed as a jigsaw puzzle from which the structure of the parent ion may be determined. This mode of operation may be termed a daughter ion scan. With two mass analyzers, other modes of operation are also feasible, including neutral loss scan (where the two mass analyzers are scanned in concert with a fixed mass offset), and parent ion scan (where the Q3 mass analyzer is held to transmit a fixed daughter ion m/z and the Q1 analyzer is scanned to determine which parent ions give rise to the daughter ion fragment).

The triple quadrupole is more properly described as a tandem mass spectrometer, in recognition that subsequent iterations of the device included higher order multipoles (specifically hexapole and octapole) as the collision cell [32]. The advantage claimed for the higher order multipole in this

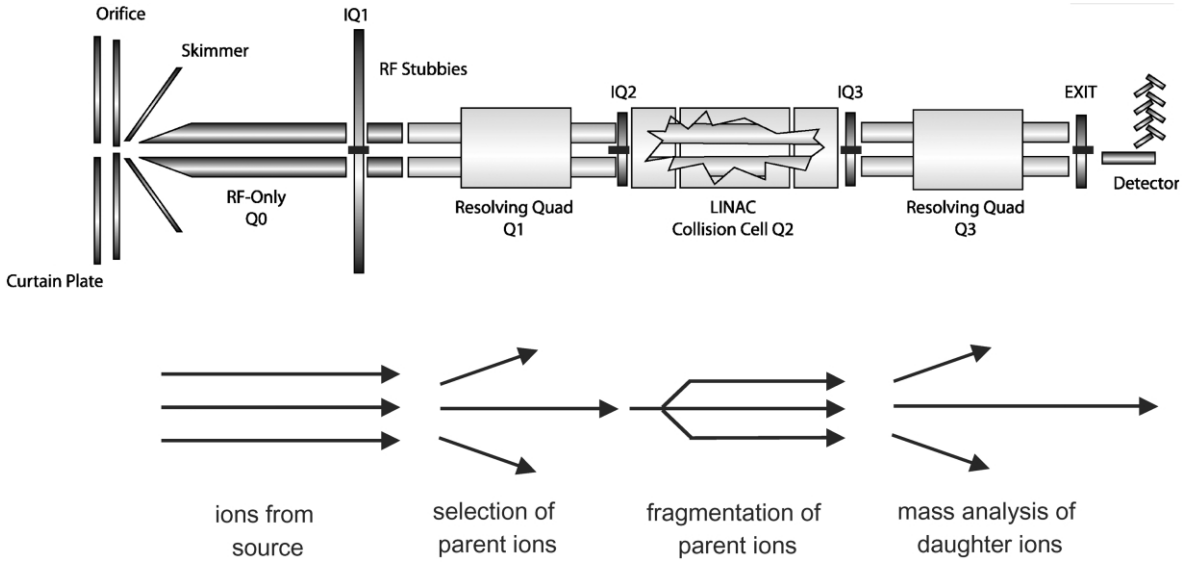

Fig. 1. Schematic of a tandem quadrupole MS/MS system for organic mass spectrometry. Ions are produced in a corona or electrospray source and transmitted through a vacuum interface and r.f.-only multipole ion guide. Ions of interest (parent ions) are selected by a first mass-analyzing quadrupole and are transmitted to a collision cell where they are fragmented in collisions with an inert gas at energies that exceed the bond strength(s) of the parent ion. The daughter ions are confined and transmitted to the second mass-analyzing quadrupole. The daughter ions provide structural information regarding the parent ion. Several types of linked scan modes are possible. (Figure provided by MDS SCIEX.)

application is more efficient confinement and transport of the daughter ions, due to the deeper and steeper pseudo-potential well and wider stability region of these devices as compared to a quadrupole [12,33–36]. In practice, the r.f.-only hexapole and octapole show a practical increase in the mass range of confinement of the order of 10% towards high mass and 30% at low mass [32]. The higher order multipoles are reported to provide lower transmission efficiency than the quadrupole at high ion energy, but comparable transmission at low energies (presumably the conditions appropriate for the ICP-MS application) [32].

Tandem MS has also been enacted in situ in an ion trap mass spectrometer, wherein the trap is operated to confine and then isolate the parent ion, an auxiliary r.f. field is applied to excite the ion and induce CID, and the daughter ions are trapped and mass analyzed [37]. Multiple sequential fragmentation events may be obtained (MS^n) through sequential isolation and excitation [37]. In the 2D quadrupole, such MS^n operation requires $(2n-1)$ multipole devices in series [38,39]. Recent work with a 2D ion trap has shown the ability to accomplish MS^n in a single 2D collision cell [40].

Of course, it was recognized early on that, alternative to CID, the tandem MS collision cell could be used to promote ion–molecule reactions. Hence, the neutral loss scan could also be used as a neutral gain scan, where the ion reacts by addition or substitution to produce a product ion of higher m/z. In some instances [41,42], this capability is used to facilitate resolution of isobars by discrimination on the basis of thermochemical properties (e.g. on the basis of proton affinity relative to ammonia as a reaction gas, where only the higher proton affinate isobar survives the cell), in a manner similar to conventional chemical ionization ion sources. It is also well known that the quadrupole may be operated in a notch filter mode, in which an auxiliary excitation frequency at the fundamental frequency of motion (which is mass dependent) is applied in order to selectively

eject a particular m/z. Watson et al. [43] used this capability to delineate the sequence of reactions that might take place in a cell operated under multiple collision conditions. In this instance, the authors selected a parent ion (Fe^+ from iron carbonyl) in Q1 and introduced this ion into the cell operated with 1 mtorr of allyl chloride. A number of organic and organometallic ions were observed in the daughter ion spectrum, and several of these were perceived to be due to sequential reactions of previous daughter ions. Notch filtering at $m/z=41$ caused the suppression of a number of ions which were thus identified as products of subsequent reactions of the $C_3H_5^+$ ion, which itself is a daughter ion of the Fe^+ reaction with allyl chloride; other ions were not affected by the notch filtering at $m/z=41$, indicating that these ions were not progeny of $C_3H_5^+$.

Tandem MS has found exceptional application in organic mass spectrometry, most commonly with operation of the collision cell for CID. It has been widely used for environmental analyses, perhaps most notably for the determination of dioxins in soils and incineration ashes [44]. With the advent of various incarnations of electrospray ionization [45], it has had a profound impact on pharmaceutical drug discovery [46] and related fields such as proteomics [47,48]. A good introduction to tandem MS, though by now a little dated, is the book by Busch et al. [49].

The first application of tandem MS with the ICP ion source was reported by Douglas [20]. The initial intent was to perform CID on polyatomic ions (e.g. Ar_2^+, ClO^+, $ArCl^+$ and CeO^+) in order to obviate their interference on isobaric atomic ions. Clearly, the collision energy must be sufficiently large to promote such fragmentation (i.e. the deposited energy must exceed the bond strength). At 50 eV (in the laboratory frame), it was observed that the loss cross-section (proportional to the loss rate) of atomic ions is comparable to that for the polyatomic ions. This was ascribed to the occurrence of charge transfer reactions of the atomic ions with the argon gas target. That is, the collision energy required to successfully fragment many metal polyatomic ions exceeds the difference in the ionization potentials (IPs) of the isobaric atom and the reaction gas. As a result, conditions which enable CID of the polyatomic ions also generally promote charge transfer of the elemental ion of interest, resulting in a corresponding loss in sensitivity. This is in addition to the simple scattering loss of both the polyatomic ion and the atomic ion. Hence, it was recognized that CID was unlikely to provide large gains in the metal ion to molecular ion ratios. On the other hand, it was found that some atomic ions rapidly oxidize in reaction with O_2, but that the oxide ion frequently does not further oxidize to the dioxide. Operation of the triple quadrupole in the neutral gain mode (for $\Delta m=16$ amu) with O_2 as the reaction gas transmits only those ions that add 16 amu (O) in the collision cell. Accordingly, Ce^+ is transmitted (as CeO^+), but CeO^+ is not transmitted (as CeO_2^+) since CeO^+ does not further oxidize, as is shown in Fig. 2. The cautious conclusion that 'for some special cases…ion–molecule chemistry may provide a way around persistent interferences' has greater significance in hindsight. Shortly after this was discussed, Rowan and Houk described the direct coupling of the ICP with a reaction cell and mass analyzer [21], omitting the Q1 mass analyzer. This is the point of divergence of the ICP-MS application from the conventional collision cell. We will return to it after introducing some further relevant art.

An additional important characteristic that has profound influence on the use and operation of pressurized multipole cells for ICP-MS is collisional focusing of both the energy and spatial distributions. It is not clear which is the cause and which the effect; these might be viewed as concomitant phenomena. In the ICP-MS application, the ions are generally introduced into the cell with a relatively high axial translational energy (strongly influenced by the ion optical configuration) and a low radial energy (resulting from the transverse cooling of the ions in the expansion through the interface). Collisions with gas molecules in the cell cause retardation of the axial motion and, as will be seen later, consequent excitation of the radial energy. Subsequent collisions exponentially decrease the magnitude and distribution of these energies, ultimately yielding a nearly thermal energy distribution in all dimensions (under certain conditions). Coincident with this reduction of the

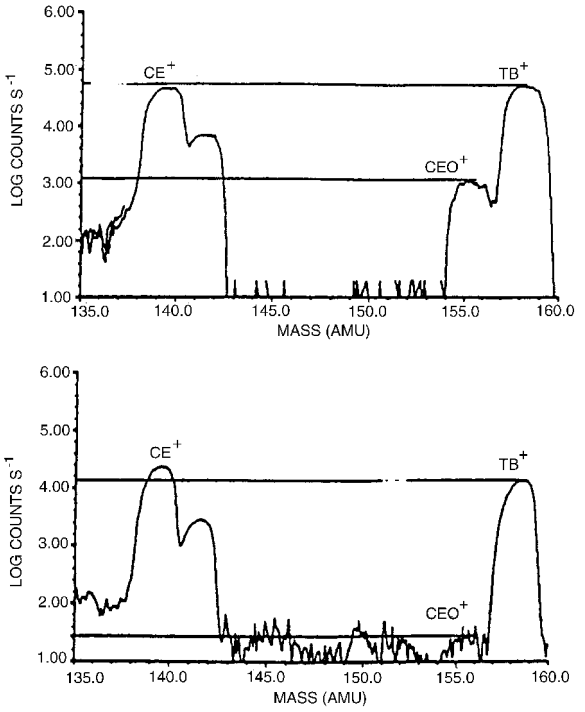

Fig. 2. Spectra obtained using an ICP source on a tandem quadrupole MS/MS system, for a sample containing cerium and terbium. (a) The first mass analyzer is operated in r.f.-only mode and no collision gas is used. Approximately 2% CeO^+/Ce^+ is observed, corresponding to the composition typical for the plasma itself. (b) Both mass analyzers are operated to provide nominal unit mass resolution, and they are synchronously scanned with the second analyzer operating at 16 amu higher than the first, and the mass transmitted by the first analyzer is shown. Collision gas (air) was introduced to the cell to promote oxidation. Only ions that add 16 mass units in the collision cell are detected. Ce^+ and Tb^+ are both oxidized and are thus observed. CeO^+ is not efficiently further oxidized and is correspondingly significantly suppressed in the detected spectrum. (From Ref. [20] with permission.)

ion energy, the ions migrate to the axis of the multipole. Since the cell's extraction aperture is on-axis, this migration causes an increase in the efficiency of transmission of the ions out of the cell. The consequence of the spatial focusing effect is an increase in sensitivity, providing that the collisional focusing outweighs scattering or reactive losses. Energy focusing leads to an improvement in the mass resolution of the downstream mass analyzer. The efficiency of these collisional effects is dependent on the number of degrees of freedom of the ion and neutral, the total number of collisions, the number of collisions per r.f. cycle, the relative masses of the ion and neutral and the operating point (a, q) of the multipole. These phenomena are described in the general case by Douglas et al. [50,51] and by Krutchinsky et al. [52], and in the specific case of the quadrupole reaction cell for ICP-MS by Baranov and Tanner [28]. The simultaneous improvement in transmission efficiency and mass resolution of daughter ions of renin substrate has been shown by Thomson et al. [53], and of Pb^+ ions (by ICP-MS) by Turner et al. [27]. A novel application of the collision cell, taking advantage principally of its energy focusing characteristics, is incorporated in the Isoprobe from Micromass, which replaces the electric sector of a double focusing mass spectrometer with a hexapole collision cell pressurized with He [54]. This yields a single focusing magnetic sector ICP-MS instrument that has sufficient resolution for isotope measurement and is now available as either a single collector or multi-collector system.

4.2. Pressurized multipole ion guides for reaction studies

Multipole ion guides have long been used to study ion–molecule reaction chemistry. As an example, Ervin and Armentrout [13] reported on the translational energy dependence of the cross-section for the Ar^+ reaction with hydrogen (H_2, D_2 and HD) using a pressurized octapole ion beam guide. The subject is thoroughly reviewed, as far as the classic application is concerned, by Gerlich [12]. The principal conclusions (page 62 of Ref. [12]) are that, for the study of near-thermal ion–molecule chemistry, 'the frequency should be as high as possible, the buffer gas should be light relative to the ion mass, and the r.f. trap should have a wide field-free region with steep confining walls. If collisions play a role, quadrupole ion traps should be avoided.' In effect, the argument is that the influence of the r.f. field should be minimized. Accordingly, the r.f. device should be operated under conditions of adiabaticity (commonly considered to be for $q<0.3$), and the

collision frequency should be less than the applied frequency. A higher order multipole is desirable since these have a wider region of low r.f. field near the axis, with steeper fields closer to the rods, and because they have a wider stability region (they confine and transmit product ions over a wider mass range). Indeed, these characteristics are desirable when it is intended to study reaction kinetics and product ion distributions under conditions of defined energy (including near-thermal). However, we will argue below that other more practical considerations take precedence in the ICP-MS application where it is desired to remove interferences (which may include the products of reactions within the cell) rather than trap them.

4.3. The ion trap as a reaction cell

The two dimensions multipole confines ions in only 2Ds, so that ions can leak out of the cell along the axis; therefore, there is restricted control over the time that ions spend in the cell (the trapping time). In addition, when operated as a reaction cell, the pressure is usually higher (1–20 mtorr), so that the mean free path is shorter and the ions gain less energy between collisions from the r.f. field. Accordingly, multi-step dissociation of polyatomic ions is relatively inefficient. For small ions with few internal degrees of freedom, scattering loss is more probable than dissociation.

The 3D quadrupole ion trap may be regarded as a 2D quadrupole that is rotated through its transverse axis bisecting a pair of rods (according to the original theory, the trap is asymmetric with $r_0^2=2z_0^2$, where $2z_0$ is the distance between the endcaps, though in practice the trap is often 'stretched' [55]). It is characterized by well-defined stability boundaries similar to those of the quadrupole mass filter. It is commonly pressurized with an inert gas, which serves to retard the energy of externally injected ions (thus allowing their entrapment) and causes the ions to migrate to the center of the trap, which provides improved mass resolution and sensitivity. While they are in widespread use as mass analyzers (and as tandem mass analyzers), they have also been used as near-thermal and non-thermal ion reactors for nearly three decades. The subject is thoroughly reviewed in the excellent book by March and Hughes [56] and the more recent set of books edited by March and Todd [37].

The 3D ion trap is usually operated at relatively low pressure, of the order of 1 mtorr. The efficiency of an ion–molecule reaction in the trap, therefore, is dominated by the trapping time: a longer trapping time leads to more complete reaction. Provided that the r.f. amplitude is low and the frequency is high (low q), the ions gain only a small amount of energy between collisions from the r.f. field, and the collision energy approximates thermal energies. In this event, the chemistry is more-or-less characterized as a thermal process. At higher q, or when auxiliary excitation at the fundamental frequency of motion of the ion is applied, the ions can be translationally excited. In addition, the internal energy of the ion can be excited step-by-step in multiple collisions. Accordingly, the ion trap can also be used as a super-thermal reactor such that even very endothermic processes (such as dissociation of TaO^+ [57] and $BaOH^+$ [58]) can be promoted. Hence, multi-step CID of polyatomic ions is possible with the 3D ion trap.

Much of the recent interest in collision and reaction cells derives from the work of the group of Koppenaal [22–26]. In recognition that the ion trap has a limited dynamic range of ion confinement (of the order of 10^3–10^4 ions before space charge effects are prominent), the original concept for the ICP-IT [22] included a quadrupole ion guide interface that could be used to notch filter (i.e. remove) the Ar^+ ions. Surprisingly, even without the notch filtering capability, few Ar^+ or argide polyatomic ions were observed in the spectrum obtained with the ion trap. It was realized [22,23] that, at least in part, this was the result of reactions of these ions (whose corresponding neutrals have high IPs) with adventitious water in the ion trap. This then led to the intentional addition of H_2 to the ion trap in order to promote reactions with Ar^+ leading to its consequent efficient removal from the spectra [24]. The method was shown to be extremely efficient, with 6 orders of magnitude reduction of the expected Ar^+ ion signal and little simultaneous loss of other elemental ions of analytical interest. More recently, Furuta et al.

[59], presenting initial results obtained with the first commercial ICP-trap-MS (the Hitachi P-5000) and using He as the trapping gas, have shown relatively efficient conversion of CaO^+ to $CaOH^+$, presumably due to reaction with impurity gases in the ion trap. Eiden et al. [26] have summarized the attractive performance characteristics of the ICP ion trap for the ICP-MS application.

The 2D multipole can act as an analog of the 3D ion trap when ions are pulsed into the cell and the end cap potentials are adjusted to confine the ions. Trapping times as long as 5 s with efficiency approaching 100% have been reported [40]. Ions may be extracted from the trap either axially through the exit aperture when the potential is dropped, or radially through a slot in one of the poles. It should be evident that many of the scan modes available to the 3D trap are also potentially applicable to the 2D configuration, including the application of auxiliary r.f. excitation for ion isolation or fragmentation. It seems reasonable that the 2D trap can be operated at low pressure, has higher trapping efficiency than the 3D trap, and can confine more ions because the space charge limit is higher (approx. proportional to the length of the 2D trap). Accordingly, the 2D trap offers intriguing benefits that should be explored. The increased space charge limit may be particularly significant for the ICP-MS application where the input ion flux is high.

4.4. Pressurized multipole cells for ICP-MS

To this point we have but briefly noted the important 1989 contribution from Rowan and Houk [21]. This work was singular in that it showed tremendous potential for ion–molecule chemistry enacted in a pressurized multipole cell for the ICP-MS application, but the work was then essentially ignored until the introduction of a commercial equivalent 8 years later. The Rowan and Houk instrument contained two quadrupoles, the first of which was operated in the r.f.-only mode synchronously with the mass filter quadrupole through capacitive coupling. A schematic is given in Fig. 3. The first (r.f.-only) quadrupole could be pressurized with an external gas (xenon, methane and ethane were reported). Therefore, the instrument might be viewed as a triple quadrupole without the first mass filter. Accordingly, all ions that passed the ion optical region were introduced into the first quadrupole cell, which could be pressurized. The authors made the further notable distinction against a triple quadrupole collision cell in that 'collisions are used to remove unwanted ions already present…polyatomic ions must be lost efficiently, relative to analyte ions' [21]. The mean DC potential of the quadrupole arrays (the quadrupole rod offsets) were independently adjustable. Highly specific and efficient suppression of certain isobaric interferences were reported while retaining a substantial portion of the analyte signal. In particular, improvements in the signal-to-background ratio were obtained for Fe^+ (removal of ArO^+ by Xe) and Se^+ (removal of Ar_2^+ by CH_4). Perhaps of the greatest importance, Rowan and Houk recognized that the resultant mass spectrum contained ions that were formed within the collision cell; obviously these were either primary or secondary products of reactions of the ions obtained from the ICP with the reaction gas. Further, it was shown that these product ions, which themselves can act as isobaric interferences for other analyte ions, could be discriminated against by application of a potential hill downstream of the collision cell (which, in this case, was applied simply by making the DC rod offset of the collision cell slightly more negative than that of the mass filter). Accordingly, ions that were produced in the cell and, as a result, had lower kinetic energies than the incompletely thermalized analyte ions derived from the source, were prevented from entering the mass filter. It should be emphasized that this approach, which we term 'kinetic energy discrimination', is effective only when there is a discernable difference in the ion energy distributions of the analyte ions and of the ions produced in the cell; that is, it is not effective when the ion population is nearly (or fully) thermalized in the cell.

Kinetic energy discrimination of analyte and interference ions has a substantial impact on the efficiency of the ion–molecule chemistry that might be used to resolve plasma–ion interferences, and, arguably, is a distinguishing characteristic of

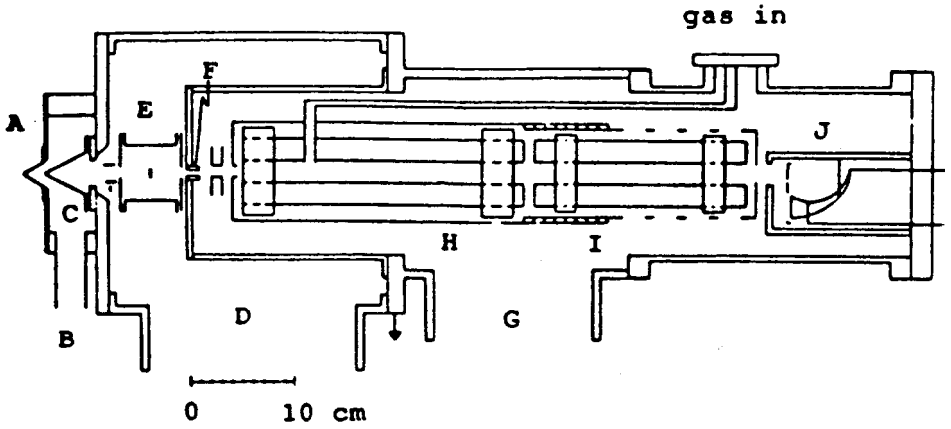

Fig. 3. Schematic of the cell-based ICP-MS instrument of Rowan and Houk [21], the first reported configuration that introduced the plasma ion beam into a pressurized multipole for chemical modification before mass analysis. (From Ref. [21] with permission.)

cell operation. In a broad sense, current commercial instrumentation may, in part, be distinguished on this basis. In our opinion, this is one of the major distinctions between collision cells and reaction cells. However, with the commercial introduction of this technology in quadrupole ICP-MS instruments (the four currently available instruments are shown schematically in Fig. 4), designation of the terms 'collision cell' and 'reaction cell' has created some confusion.

The collision cell has a long history of association with CID, perhaps principally in the MS/MS configuration. The large majority of practitioners are hence familiar with a mode of operation that is most concerned with only the first few collisions; these are at relatively high energies so that the center-of-mass energy exceeds at least the weakest chemical bond in the (polyatomic) ion with the intent to cause *fragmentation* of the parent ion with *trapping* of the resultant daughter ions. Certainly, it is common now to operate the collision cell at elevated pressures so as to enhance transmission of the ions through collisional focusing, but this effect is subsequent and supplementary to the initial fragmentation process. Perhaps the principal distinguishing feature is that the collision cell, in its historical application, is used to promote processes that are endothermic under lab normal conditions: usually fragmentation that is endothermic by at least the weakest bond strength. It has not been common to introduce ions into a collision cell at energies that do not promote fragmentation (other than for purposes of ion collisional focusing and transmission), and it has certainly not been common to use a collision cell for atomic ions.

When the 'collision cell' is used to promote ion–molecule chemistry, as we now realize is the principal mechanism in the ICP-MS application (Section 5), it has been called a 'molecule ion reactor' [60], 'ion guide' [13], 'beam guide' [12] or 'reaction chamber' [43]. It is obvious that ion–molecule collision precedes energy transfer, fragmentation or chemical reaction. Indeed, fragmentation might be considered an endothermic reaction. Nevertheless, the distinctions in the operating conditions are evident. In our opinion, to call a 'reaction cell' a 'collision cell' could be considered infringing on the common usage of the latter term. The confusion in the ICP-MS application likely stems from early misunderstanding or commercial interest.

It is clear that Rowan and Houk [21] understood that the operative mechanism in their early work that combined a pressurized cell with an ICP-MS instrument was ion–molecule chemistry, and also that the ions were not thermalized. However, the first commercial application [27] reverted to inferring that the improvements were obtained as a result of collisional fragmentation. As long as the

attention was focused on polyatomic (argide) ions and the mechanism was understood to be collisional fragmentation, the term collision cell seemed to apply. Eiden et al. [25] modified the octapole ion guide of their ion trap instrument to allow pressurization with reactive gases, and called the device a collision cell. They showed at least 4 orders of magnitude suppression of Ar^+ using H_2 as a reaction gas, and demonstrated specific ion–molecule chemistries for the distinction of other isobars, notably the elimination of $^{129}Xe^+$ interference on $^{129}I^+$ and $^{90}Y^+$, $^{90}Zr^+$ on $^{90}Sr^+$ with the addition of O_2 as a reaction gas, and the removal of Kr^+ interference on Sr^+ with CH_4 [25]. Baranov and Tanner [28] then described a quadrupole cell operated at relatively high pressure with reactive gases (O_2, NH_3, N_2) and discussed the process and importance of thermalization of the ions. They promoted the potential for near-thermal ion–molecule chemistry to provide specific and efficient 'chemical resolution' [61], and used the term 'reaction cell' to distinguish their approach. The confusion then began, with various manufacturers and researchers using the terms interchangeably or even together, as in 'collision and reaction cell' [62–64]. The distinguishing characteristic that appears to have been overlooked is that the 'reaction cell' was intuitively understood to involve thermal chemistry, or at the least near-thermal conditions, so that the reactions are governed by the thermochemical properties of the ions and the reaction gas. Accordingly, we subsequently proposed a distinction based on the thermal characteristics of the cell [65]. We justify this distinction on the premise that a near-thermal energy distribution means that the reaction kinetics are governed by the thermal properties of the ions and neutrals, and that the reaction rates correspond to those that are measured for thermal systems (e.g. selected ion flow tube (SIFT) instruments [11,66]). Hence, the distinction is intimately related to the operating pressure and type of gas used in the cell, though the measurable characteristic is the ion energy distributions (or, equivalently, the efficiency of kinetic energy discrimination to improve the analytical result).

The Micromass Platform and the Thermo Elemental PQ ExCell both use an r.f.-only hexapole as the r.f. device of the cell, and in both instances the plasma gas expansion through the sampler–skimmer interface is directed into the on-axis entrance of the cell. To discriminate against plasma photons and metastables, the Platform collision cell is tilted off-axis while the ExCell employs a deflecting chicane lens downstream of the cell. The Agilent 7500c uses an r.f.-only octapole that is tilted off-axis as the cell r.f. device. An off-axis aperture lens downstream of the skimmer and before the collision/reaction cell serves to simultaneously disrupt the directed flow of the plasma gas into the cell and blocks the transmission of plasma photons and metastables. Kinetic energy discrimination is enabled on all three instruments by biasing the pole bias (rod offset) of the collision cell negative relative to the mass analyzer rod offset. These instruments are typically operated with either He or H_2 or a combination of these as the collision/reaction gas, though the use of Xe has been shown by Mason [67].

The several generations of the Perkin Elmer SCIEX ELAN DRC use a quadrupole cell that may be operated either r.f.-only or r.f./DC, the frequency and amplitudes of which are selected on the basis of the chemistry that is enacted. It is typically operated with relatively heavy reaction gases (NH_3, CH_4, O_2, CH_3F, N_2O or others) and usually at pressures that provide near-thermal conditions. Discrimination against ions produced within the cell is preferably accomplished by establishing the appropriate mass bandpass (via the Mathieu parameters a and q, proportional to the ELAN parameters RPa and RPq) of the quadrupolar field (discussed in Section 8.4.2). Kinetic energy discrimination can also be employed when a low mass collision gas is used at relatively low pressure (i.e. under non-thermal conditions, see Section 8.4.1). Plasma photons and metastables are blocked by an on-axis shadow stop, which also serves to disrupt the directed motion of the beam.

All four instruments adjust the pressure inside the cell by controlling the rate of flow of gas into the cell. At low flow, the cell gas is primarily plasma gas entrained from the ion optics chamber. In general, this is an undesirable state, since the sampled plasma gas contains as much as 17% oxygen and hydrogen [68]. Increasing the cell

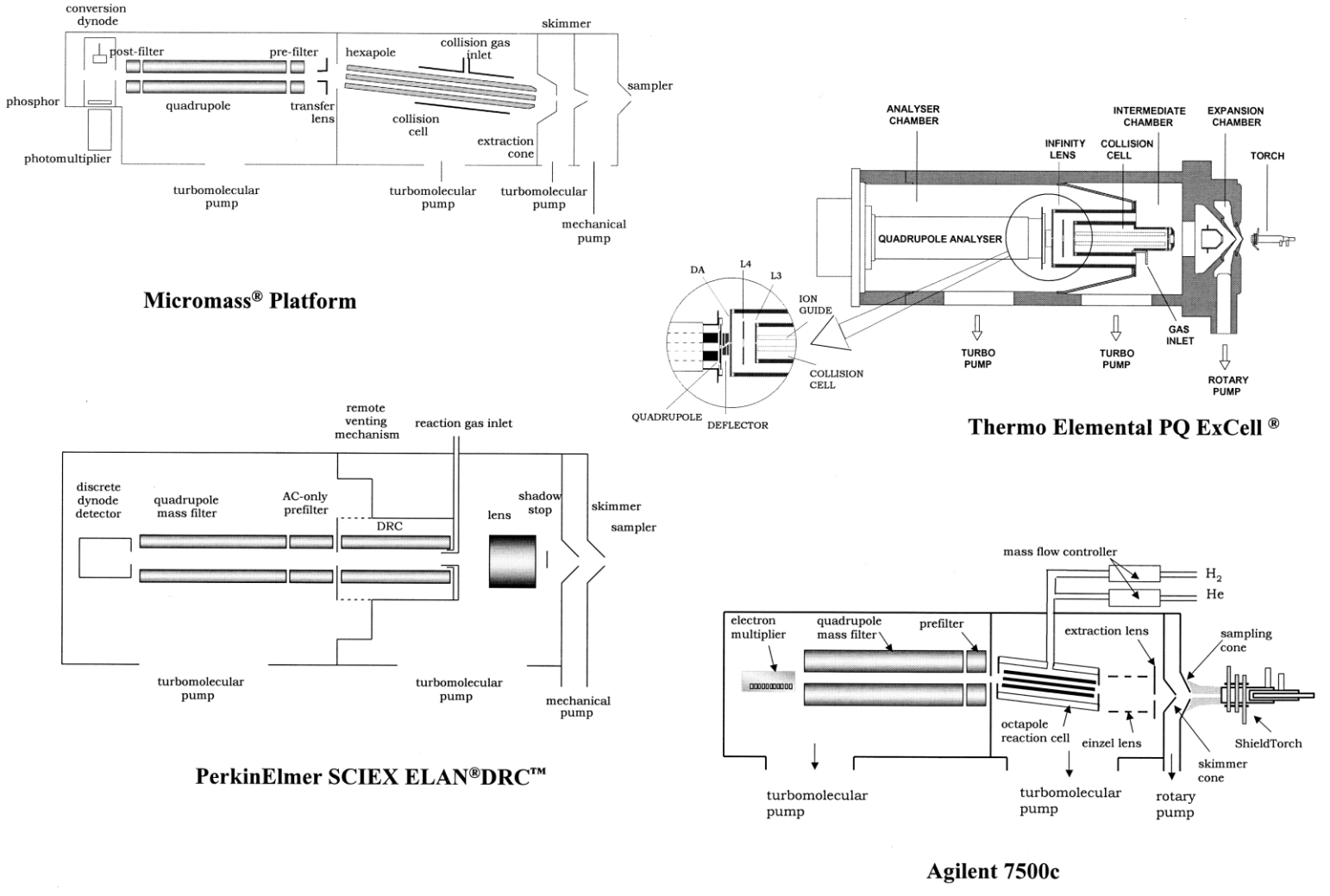

Fig. 4. Schematics of the four cell-based quadrupole analyzer instruments that are presently commercially available: the Micromass® Platform (figure courtesy Andrew Eaton), the Perkin Elmer SCIEX ELAN® DRC™ (figure from the authors), the Thermo Elemental PQ ExCell® (figure courtesy Jonathan Batey) and the Agilent 7500c (figure courtesy Setsuo Muramoto).

pressure should eventually achieve a state where reaction gas flows out from the entrance aperture, thus excluding the plasma gas: the efficiency of this exclusion, and its dependence on instrument design, is discussed in Section 8.1. Some of these instruments may emulate conventional ICP-MS by stopping the flow of reaction gas and operating either at the ambient pressure of the chamber (typically less than 1 mtorr) or by active venting to the lower pressure mass analyzer chamber, thus to achieve nearly or fully collisionless conditions so that the cell simply acts as an r.f.-driven multipole ion guide.

5. Collisional processes

All interactions of ions with molecules are collisional processes, and a liberal interpretation might include energy transfer and collisional fragmentation as reaction processes. We distinguish the latter two as collisional events, preferring to consider reactive processes as those that include transfer of one or more particles between the reacting partners. For example, fission results in the transformation of the reactant species, but has conventionally been considered a physical phenomenon. In large measure, the distinction might be made on the basis of the energetics of the collision. The authors tend to consider particle transfer events that take place at, or near, thermal conditions to be chemical reactions, though this presents a challenge to describe energy-selected endothermic processes, such as those studied by the ion guide technique [12,13], as the reactions that they clearly are. Because we distinguish between fragmentation and reaction, we present these in separate Sections of this review. The discussion presented here of collisional processes, including energy transfer and collisional fragmentation, is taken closely from Ref. [65]. The reader is referred to the review by Douglas [51] for a more general and thorough discussion.

5.1. Energy transfer

In an elastic (no internal excitation) non-reactive collision of an ion of mass m_1 and kinetic energy E_1 with a stagnant ($E_2=0$) neutral of mass m_2, the energies after collision are given by:

$$E'_1 = E_1\left[\frac{m_1^2+m_2^2}{(m_1+m_2)^2}\right] \tag{5.1}$$

$$E'_2 = E_1 - E'_1 \tag{5.2}$$

As $m_2 \to 0$, $E'_1 \to E_1$, and no energy transfer takes place, with the reactant ion leaving the interaction with the same energy with which it entered. If $m_2 = m_1$, the collision partners exit with equal energy, so that the incident ion loses half of its initial energy. Multiple collisions of the ion result in sequential loss of kinetic energy and results in energy damping (a reduction in the width and magnitude of the kinetic energy distribution). Thus, the ion loses energy according to the reduced mass of the collision partners: a larger neutral/ion mass ratio increases the rate of energy damping of the ion. Complete damping to the thermal condition, if possible, means that the ion simply executes an essentially 'random walk' through the cell. A large ion energy at the entrance to the cell (source potential plus expansion energy minus cell offset potential) requires more collisions for energy damping. For a given cell pressure, a higher initial energy also results in a reduction of efficiency because the ion progresses farther into the cell before the energy is damped, and hence the number of collisions is reduced. Further, higher energy lowers the probability of reaction during collision, compromises the specificity of the thermal chemistry, and increases the potential for sputtering cell materials.

5.2. Collisional fragmentation

Transfer of energy to internal degrees of freedom during the collision defines an inelastic collision. The energy that is transferred can be distributed amongst the various internal degrees of freedom: for a polyatomic ion, these include rotational, vibrational and electronic. Subsequent collisions can transfer (relax) this energy to translation (kinetic energy, heat). If an energy that exceeds the bond strength accumulates in a single vibrational degree of freedom, the chemical bond may rupture and the polyatomic ion fragments. This

process is commonly known as CID. Fragmentation may be successful in a single collision, in which case a relatively high collision energy is required (to account for the distribution of the energy in the various degrees of freedom). It can also occur through multiple collisions, where the internal energy is accumulated by sequential energy pumping to the dissociation limit. The latter is most effective in a 3D ion trap (or 2D trap with confinement using repulsive endcap potentials) because the ion can be confined in three dimensions for a long period of time. In these devices, auxiliary excitation may be used to further increase the collision energy, thus improving the efficiency of CID. For a given r.f. amplitude and frequency, CID is promoted more efficiently under conditions of fewer than 1 collision per r.f. cycle (i.e. at low pressure) because the ion gains higher kinetic energy from the r.f.-field between collisions. In a 2D multipole without endcap trapping (i.e. a collision cell), multi-collision CID is relatively inefficient because the ions are unconstrained in the axial direction. Though CID is of paramount importance for organic tandem MS applications, the efficiency required of the process is modest: seldom are more than 90% of the polyatomic ions fragmented since it is only necessary to produce sufficient fragment ions in order to identify the parent polyatomic.

Eqs. (5.1) and (5.2) describe the energetics of collisions in the LAB frame (the energies that are apparent to an outside observer). The transfer of energy to internal modes of excitation is best understood in the center-of-mass frame of reference. Assuming a stationary neutral molecule, the energy with which the center-of-mass moves, or the energy *of* the center-of-mass, E_{CM}, is proportional to the LAB energy of the ion, E_1, according to:

$$E_{CM} = E_1\left[\frac{m_1}{(m_1+m_2)}\right] \tag{5.3}$$

For the same collision pair, the energy *in* the center-of-mass, which is the maximum amount of energy that may be converted into internal excitation, $E_{int,max}$, is given by:

$$E_{int,max} = E_1 - E_{CM} = E_1\left[\frac{m_2}{(m_1+m_2)}\right] \tag{5.4}$$

For single collision fragmentation, it is thus desirable to use a neutral having as large a mass as possible. Unfortunately, this condition also maximizes scattering losses. Bandura et al. [65] have considered the energetics of fragmentation of Ar_2^+ (a particularly favorable case, since the bond strength is only 1.2 eV [69]), assumed to enter the cell with a LAB energy of 8 eV (3 eV from the plasma potential offset, 4 eV from the supersonic expansion, and assuming that the ion penetrates sufficiently into a cell having an offset potential of -1 V that the cell potential defines the potential near the ion). Recursive use of Eqs. (5.1), (5.3) and (5.4) allows estimation of the *maximum* possible energy transfer as a function of the number of collisions under two extreme conditions:

1. prior collisions are elastic (no internal excitation is obtained in prior collisions); and
2. maximum internal excitation in the vibrational bond is achieved and accumulated on each collision.

It is shown that single-collision fragmentation of Ar_2^+ is possible (but not necessarily obtained) using neutral Ar as the collision gas, for which each of the first two collisions permits energy transfer in excess of the bond strength (the third and further collisions provide insufficient energy transfer). Interestingly, this projects a maximum efficiency of 86% for single-collision fragmentation of Ar_2^+ with Ar. He and H_2 are incapable of facilitating single-collision fragmentation under the conditions given. Of course, given the above, pumped sequential fragmentation (case 2) with Ar is possible, since even the first collision is sufficient if maximum excitation is obtained. With He as the collision gas, a minimum of 4 collisions, each providing maximum transfer of energy to the vibrational bond, are required for pumped fragmentation. Pumped fragmentation with H_2 as the collision gas requires more than 4 collisions, and it should be noted that internal excitation of H_2 competes with the fragmentation of the ion.

A more effective alternative process for removal of the argon dimer ion is chemical reaction. There

are no exothermic reaction channels for Ar_2^+ with either Ar or He. However, reaction with H_2 is relatively rapid (yielding ArH^+), having a thermal rate constant of 4.9×10^{-10} cm^3/s [10], and charge transfer is exothermic for reaction with atomic O and H neutrals (and their molecular combinations) that may be entrained from the plasma gas. Accordingly, it is far more likely that the removal of the argon dimer ion is achieved through chemical reaction than through collisional fragmentation. An analytically useful reaction gas is CH_4, for which Ar_2^+ reacts by charge transfer with a rate constant of 5.7×10^{-10} cm^3/s, and with which Se^+ has no bimolecular reaction [70].

6. Ion–molecule reactions

6.1. Reaction thermochemistry

Enthalpy is a state property, meaning (in part) that it is defined for the set of thermodynamic properties of a system (which include temperature, pressure, composition, etc.). It is the heat effect defined as the sum of the internal energy of the system plus the expansion work performed on the surroundings for a constant pressure process. As noted by Sussman [71], 'its *raison d'être* is convenience'. The enthalpy of formation (commonly called the heat of formation) of species X, $\Delta H_{f,T}(X)$, is the amount of heat required to produce X from its standard state components at temperature *T*. The 'standard state' of an element is the normal state of aggregation at atmospheric pressure at the specified temperature. Accordingly, at room temperature the standard state of H is H_2, that of O is O_2, and that of Ar is Ar. The heats of formation of standard states at 298 K are defined as zero. Tabulations of the heats of formation of ions and neutrals, such as Ref. [9], are valuable because they allow determination of the enthalpy of a proposed reaction, which will be shown to be determinant of the thermodynamic viability of that reaction for analytical application (subject only to kinetic validation; see Section 6.2).

6.1.1. Enthalpy of reaction

The change of enthalpy in a reaction:

$$A^+ + B \rightarrow C^+ + D \tag{6.1}$$

is (the sum of the heats of formation of the products) minus (the sum of the heats of formation of the reactants):

$$\Delta H_r = \Delta H_f(C^+) + \Delta H_f(D) - \Delta H_f(A^+) - \Delta H_f(B) \tag{6.2}$$

If the enthalpy of reaction is negative, the reaction is exothermic and might proceed. If the enthalpy of the reaction is positive, the reaction is endothermic and will not take place unless additional energy is contributed to the process (by excess axial kinetic energy before relaxation in a collision/reaction cell or by the r.f.).

In reality, the reaction energy is given by the free energy of reaction:

$$\Delta G_r = \Delta H_r - T\Delta S_r \tag{6.3}$$

where *T* is the temperature (in K) and ΔS is the entropy change of the reaction (defined the same as for enthalpy). Few people bother calculating the free energy, in part because it is more difficult, the entropy data is not as commonly available, and the fact that the entropy change of a simple small-particle-transfer reaction (charge transfer, H-atom transfer or proton transfer) is usually close enough to zero. The entropy term is important in some condensation reactions and is particularly important in association reactions.

In some instances, the enthalpy of formation (heat of formation) of one or more of the species is not known or reported, or there may be reason to doubt the reported value (i.e. different resources were used for the same reaction). In some cases, the heat of formation may be calculated from other information. For example, we may wish to determine the reaction energetics of oxidation and hydroxylation of Sr:

$$Sr^+ + O_2 \rightarrow SrO^+ + O \tag{6.4}$$

$$SrO^+ + H_2O \rightarrow SrOH^+ + OH \tag{6.5}$$

We know the following enthalpies of formation (X, $\Delta H_f(X)$), where the enthalpy is given in kcal/mol) [9]: Sr^+ (170.6), O_2 (0, by definition), SrO^+ (149), O (59.6), H_2O (−58), OH (9.3),

from which we can derive the enthalpy of Eq. (6.4) as

$$\Delta H_r(\text{Eq. 6.4}) = 149 + 59.6 - 170.6 - 0 = 38 \text{ kcal/mol} \quad (6.6)$$

The reported [9] heat of formation of $SrOH^+$ is 74 kcal/mol, which seems questionable. We know the heat of formation of SrOH (−49.1 kcal/mol), and we know the IP of SrOH (5.1 eV). So we can calculate the heat of formation of $SrOH^+$ as

$$SrOH \rightarrow SrOH^+ + e^- \quad (6.7)$$

The heat of formation of the electron is 0, so the heat of formation of $SrOH^+$ is

$$\Delta H_f(SrOH^+) = \Delta H_r - \Delta H_f(e^-) + \Delta H_f(SrOH) = (5.1 \times 23.06) - 0 + (-49.1) = 68.5 \text{ kcal/mol} \quad (6.8)$$

So the heat of Eq. (6.5) is

$$\Delta H_r(\text{Eq. 6.5}) = 68.5 + 9.3 - 149 - (-58) = -13.2 \text{ kcal/mol} \quad (6.9)$$

Of course, this is the same as simply summing reactions, where Eq. (6.5) is the same as the sum of Eqs. (6.10) and (6.11):

$$SrO^+ + H_2O + e^- \rightarrow SrOH + OH$$
$$\Delta H_r = (-49.1) + 9.3 - 149 - (-58) - 0 = -130.8 \quad (6.10)$$

$$SrOH \rightarrow SrOH^+ + e^- \quad \Delta H_r = IP = 5.1 \text{ eV} = 5.1 \times 23.06 = 117.6 \text{ kcal/mol} \quad (6.11)$$

where

$$\Delta H_r(\text{Eq. 6.5}) = \Delta H_r(\text{Eq. 6.10}) + \Delta H_r(\text{Eq. 6.11}) = -130.8 + 117.6 = -13.2 \text{ kcal/mol} \quad (6.12)$$

This is a simple and obvious example, but it will allow you to combine reactions where necessary: the heat of reaction of a sum of reactions is the sum of the heats of the individual reactions.

In some instances, the only available thermochemical data is an 'appearance potential', which is an experimental parameter that can in some instances be converted to an enthalpy of formation. In a simple case, the sample is placed in a low-pressure vessel and is subjected to electrons, in an attempt to induce ionization. The electron energy is increased until the product ion appears. This is then the appearance potential of that ion. If the ion is simply the ionized neutral sample, the appearance potential is an approximation to the IP of the neutral sample. If the product ion is a dissociation product of the ionization, then the appearance potential is the sum of the IP of the sample and the heat of dissociation reaction. For example:

$$A + e^- \rightarrow A^+ + 2e^- \qquad AP(A^+) \sim IP(A) \quad (6.13)$$

$$A + e^- \rightarrow B^+ + C + 2e^-$$
$$AP(B^+) \sim IE(A) + \Delta H_f(B^+) + \Delta H_f(C) - \Delta H_f(A^+) \quad (6.14)$$

where we obtained the $AP(B^+)$ through combining the reactions:

$$A + e^- \rightarrow A^+ + 2e^- AP(A^+)\∼IP(A) \quad (6.15)$$

$$A^+ \rightarrow B^+ + C$$
$$\Delta H_r = \Delta H_f(B^+) + \Delta H_f(C) - \Delta H_f(A^+) \quad (6.16)$$

Clearly, the appearance potential must be defined with reference to a particular parent neutral (i.e. the appearance potential of CH_2^+ from CH_4).

A convenient means to gain a qualitative perspective of reaction energetics is to scatter-plot a thermodynamic property against the mass (or identity) of analyte and interference ions and overlay on this horizontal lines that correspond to the value of this property for potential reaction gases. Each horizontal line then bisects the scatter-plot into endothermic/exothermic reactions with respect to that reaction gas. (Of course, just because a particular type of reaction is endothermic does not preclude a different reaction channel for the pair from being exothermic.) An example is given in Fig. 5a, which plots the IP of the elements and possible ICP-MS plasma interferences (argon, argides, oxides and hydroxides of elements) against the masses of the most abundant corresponding ions. The elements are indicated by filled circles and the 'interferences' by open circles. Several horizontal lines are given, corresponding to the IPs of potential reaction gases. The (posi-

tive) ions of species that are above a line are exothermic for charge transfer with that gas, and those that are below the line are endothermic for charge transfer with that gas. For example, Ar^+ and N_2^+ are exothermic for charge transfer with H_2, but all other ions shown are endothermic. On the other hand, NO is endothermic for charge transfer with most analyte ions and is exothermic for charge transfer with a majority of interference ions. A similar 'reaction energetics' figure is given in Fig. 5b for O-atom affinities. In this instance, the horizontal lines correspond to the O-atom affinities of the gas having one less O-atom than indicated (i.e. the neutrals indicated would be the product of an oxidation reaction). Hence, ions that have a higher affinity than an indicated reaction gas (i.e. that appear above the line) are exothermic to extract an O-atom from the indicated gas, and ions that are below (providing that these ions contain an oxygen atom) are exothermic for donation of an O-atom to a neutral that would form that gas (i.e. for reaction with the gas having one less O-atom than indicated).

6.1.2. Specificity of thermal ion–molecule reaction

The enthalpy of reaction is, of course, a thermal property. It is properly defined only when the ions and neutrals are thermalized. An exothermic reaction releases energy to the environment and is termed 'thermodynamically allowed'. Reactions leading to polyatomic products (either the product ion or product neutral) generally release the enthalpy of reaction principally into internal degrees of freedom (vibration and rotation of chemical bonds). The energy eventually ends up as thermal (kinetic) energy as a result of energy transfer in subsequent collisions. An endothermic reaction absorbs energy from the environment and, thus, is thermodynamically 'not allowed'. The enthalpy of reaction is not correlated with kinetics (the rate of reaction) except in one very important aspect: under thermal conditions, an exothermic reaction may take place but an endothermic reaction may not. If an exothermic small particle transfer reaction occurs, it usually occurs with high probability (i.e. close to the collision rate) and is relatively fast. In principle, this is because such processes do not generally exhibit an activation energy barrier. In turn, this is due to the relatively strong ion-induced dipole electrostatic interaction. Hence, thermochemistry provides a high degree of specificity for ion–molecule reactions. If a reaction gas is chosen such that it has an exothermic channel with either the analyte ion or the isobaric interference ion, and thermal conditions prevail, the allowed reaction is likely to take place and the disallowed reaction is not. This difference provides 'chemical resolution'. An example is the chemical resolution of Ca^+ from Ar^+ using NH_3 as the reaction gas. The IP of Ar (15.76 eV) is greater than that of NH_3 (10.16 eV), which in turn is greater than that of Ca (6.11 eV). Thus, the IP of NH_3 is sandwiched between Ar and Ca, and charge transfer is allowed for Ar^+ but disallowed for Ca^+. It is observed experimentally [10] that the Ar^+ reaction is fast and the Ca^+ reaction is exceptionally slow (if it proceeds at all). Passing the ion beam through a cell containing NH_3 as the reaction gas therefore promotes reactive loss of Ar^+ while Ca^+ is essentially unaffected, thus achieving chemical resolution. It is important to recognize that the provision of (near) thermal conditions is essential: if the collision energy (in the center of mass) is sufficiently large to overcome the endothermicity of the disallowed (under lab normal conditions) reaction, the specificity is potentially forfeit.

6.2. Kinetics

The enthalpy of reaction determines the thermodynamic viability of a proposed reaction. The actual value of the reaction for analytical purposes is dependent on the kinetics, by which we mean the rate of the reaction. The density of a reactant or product ion, which is proportional to the ion signal observed, is exponentially dependent on the rate constant, the density of the reactant neutral, and the reaction time. In addition, the product ion distribution (the identity of the product ions and their branching ratio, for multiple products or reaction channels) is of critical importance. In this section we discuss theoretical aspects of the reaction dynamics, compare experimental reaction rates with theoretical collision rates, review the major types of ion–molecule reactions, and consider how

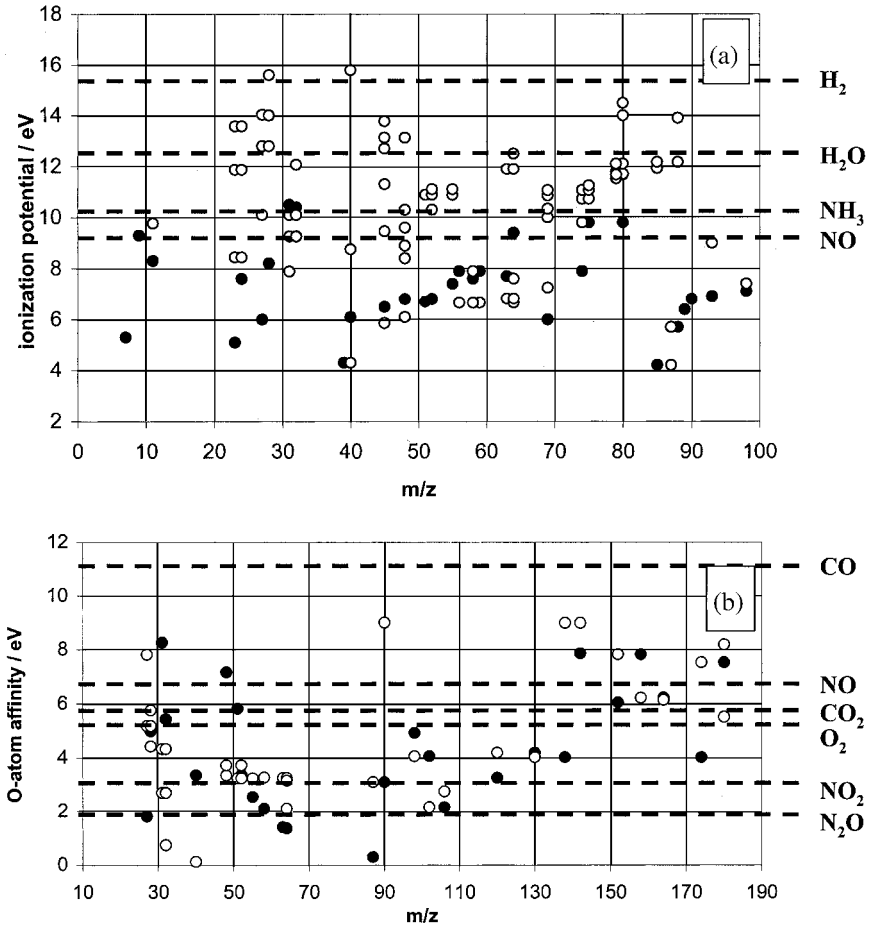

Fig. 5. Some thermochemical properties of some atomic ions and potential atomic and polyatomic interference ions. Solid points represent the atomic ions usually of interest for inorganic analysis, and the open points represent argon, argide, oxide, hydroxide and other potential interference ions. (a) Ionization potentials. The horizontal lines indicate the IPs of potential reaction gases. Ions above a horizontal line are thermodynamically favorable (though not necessarily kinetically favorable) for charge transfer with the indicated neutral. (b) Oxygen-atom affinities. The horizontal lines indicate the O-atom affinities of gases having one less oxygen than the indicated neutral. Ions above a line are thermodynamically favorable to extract an oxygen atom from the indicated neutral; oxides of the ions below the line a favorable to donate an oxygen atom to a neutral having one less O-atom than the indicated neutral.

these characteristics affect the observation of ion signals in the 2D r.f.-driven multipole.

6.2.1. The Langevin collision theory

According to the Langevin approach (which has certain limitations, as will be discussed), the ion is considered as a point charge and all its interactions are predetermined by the polarizability, α, of the molecule. In this instance, the ion–molecule potential as a function of the internuclear distance, r, may be taken as:

$$\Phi(r) = -\left(\frac{1}{4\pi\varepsilon_0}\right)^2 \frac{e^2\alpha}{2r^4} \tag{6.17}$$

where ε_0 is the permittivity of free space. The potential is presented in SI units. Accordingly, the molecular polarizability is in $\mathrm{J\,(m/V)^2}$ and the elementary charge (e) in Coulombs. In the CGS

system of units, α and e would be in cm^3 and e.s.u., respectively. An ion–molecule reaction can occur only when the distance between the centers of the ion and molecule are less than a critical value. Integrating in two dimensions, this determines a cross-section, σ, which can be shown to depend on the relative velocity v as:

$$\sigma(v) = \frac{e}{2\varepsilon_0 v}\left(\frac{\alpha}{\mu}\right)^{1/2} \tag{6.18}$$

where $\mu = (m_1 m_2)/(m_1 + m_2)$ is the reduced mass for the collision of partners having masses m_1 and m_2. Consequently, the cross-section is inversely proportional to the relative velocity. This property of the cross-section of an ion–molecule reaction in the Langevin theory is very important because the rate constant $v\sigma(v) = k_L$ for Eq. (6.1) may be deduced from:

$$-\frac{d[A^+]}{dt} = [A^+][B]v\sigma(v) \tag{6.19}$$

as

$$k_L = \frac{e}{2\varepsilon_0}\left(\frac{\alpha}{\mu}\right)^{1/2} \tag{6.20}$$

and is, thus, independent of energy.

It is generally accepted that the ion-induced-dipole model, Eq. (6.17), satisfactorily describes the interaction at impact energies less than an electron volt. For higher energies the Langevin theory is not applicable. Moreover, the force between a real molecule and ion is strongly repulsive at short distances and weakly attractive at large distances. Also, the polarizabilities of molecules are not scalars but tensors, and not all collisions are reactive. Given these limitations, k_L can be regarded as the maximum limiting rate of an ion–molecule reaction (for non-polar molecules) and is widely used for comparison with the observed reaction rate, k. The ratio k/k_L is generally considered as a reaction efficiency of an ion–molecule collision and describes the fraction of collisions that lead to reaction.

Assuming that neutral reactant B is present in abundance and its concentration is independent of the reaction time, Δt, and ion concentration, Eq. (6.19) may be integrated. The result is:

$$[A^+] = [A^+]_0 e^{(-k\Delta t[B])} \tag{6.21}$$

where $[A^+]_0$ is the initial concentration of ions. Units for the rate constant, k, are equal to $\{1/\Delta t[B]\}$, usually given in cm^3/s or more accurately $cm^3/(\text{molecule s})$. The reaction time or concentration of the reaction gas may be kept constant during the ion–molecule reaction, in which case the logarithm of the ion concentration should decay linearly as a function of Δt or [B]. In the special case of the linear reaction cell, which obviously has a constant length, it is much more convenient to vary the reaction gas flow. A plot of the ion signal as a function of the reaction gas flow yields a reaction profile. Its characteristic feature should be a semilogarithmic linear decay of the parent ion (A^+ in the case of Eq. (6.1)). As can be seen from Eq. (6.21), the slope of the decay of the ion signal is proportional to the reaction rate constant. A steep decay indicates a fast reaction. If several ions react with the same reactant under the same conditions and form different reaction profiles, the steepest one indicates the fastest ion–molecule reaction assuming that other losses are similar.

6.2.2. Measurement of reaction rate constants

Rate constants of ion–molecule reactions have been measured using a variety of techniques, including high pressure ion sources [72], ion traps [37], ion cyclotron resonance [73], flowing afterglows (FAs) [74] and SIFTs [11,66]. In many instances, the reported values are remarkably consistent, while in others there is substantial variation. The instances of disparate results have incited vigorous debate. In most instances, argument has focused on the validity of the assumption of thermal conditions (hence, perhaps, the present authors' preoccupation with this characteristic). The rates of certain reactions (e.g. spin-forbidden reactions and others that show an unusual activation energy) can be very sensitive to the energy distribution of the ions and to residual internal excitation of the ions. It is our opinion that rate constants measured with the SIFT technique provide the most reliable thermal data. In this method, ions are produced (by electron impact, thermal

ionization, or other means) and mass-filtered to select the ions of interest. This step, which is additional to the FA method, ensures that subsequent concomitant reactions of other source ions, or reactions with source gases, do not interfere with the data analysis. The mass-selected ions are then extracted into a flight tube where they are entrained in a flow of He ($\approx$0.35 torr) and allowed to undergo many ($>10^5$) collisions to ensure thermalization at the temperature of the He (which should be equilibrated with the flight tube). A reaction gas is added downstream, and the ions are allowed to react as they flow towards the exit of the tube (having a constant reaction time, Δt), whereupon they are extracted for mass analysis and detection. Knowledge of the flow characteristics of the flight tube (mixing, wall effects, velocity distribution, etc.) and of the dependence of the ion signals on the flow rate (density) of the reaction gas allows determination of the thermal rate constant with high accuracy and precision. As well, the products of the reaction can, in most instances, be determined as these are also transported through the tube and are mass-analyzed. The product ions themselves can also react, and the data can be deconvoluted to yield rate constants for each step of the sequential chemistry. An important development for the focus of this work is the adaptation of an ICP ion source to a SIFT apparatus in the laboratory of Diethard Bohme at York University, Canada [75–77]. With this modification, rate constants of virtually any ion that the analytical atomic spectroscopist may encounter with a variety of neutral reaction gases can be determined, and this capability will significantly enhance method development for the ICP-MS application.

It should be noted that some research groups (notably those of Armentrout [14] and Schwarz [78]) have specialized in the measurement of rate constants of energy-selected ions. The reactions of ions having a known and well-defined energy, sometimes 'thermalized' in a pressurized octapole and accelerated into a collision cell, are studied as a function of the incident ion energy. In most instances, the reactions are studied under relatively rarefied conditions so that, typically, the average ion undergoes only a single collision (or less), and this ensures that the energy distribution is not significantly altered during the promotion of the reaction. In every instance, the ions are 'non-thermal', having an excess axial kinetic energy. The dependence of the reaction rate and products on the axial energy is interpreted in terms of the reaction endothermicity (if appropriate) or activation energy.

Anicich has expended considerable effort in tabulating thermal bimolecular rate constants [10]. Two of the adjectives in the preceding sentence are exceedingly important. The referenced tabulation is for thermal reactions and, hence, does not include the very many energy-selected rate constants that have been reported. Secondly, the tabulation includes, for the most part, only bimolecular processes and, with few exceptions, excludes association (clustering) reactions. Hence, reliance on this database for the ICP-MS application must be tempered with the recognition that three-body reactions may proceed even when the tabulation indicates 'no reaction'. Anicich has included a variety of measurement techniques in his compilation without comment on the validity of the assumption of thermalization, and has included in many instances rate constants at temperatures other than room temperature. In instances where there are multiple reports of rate constants, Anicich has 'evaluated' the data on the basis of his considerable experience to recommend a value.

It will become common to report 'relative rates' measured with cell-based ICP-MS instruments [79,80]. These rates are expressed as the number of orders of magnitude of reaction per unit of reaction gas flow (i.e. the logarithmic slope of the measured reaction profile). In many instances, there is good correlation between the absolute rate constants and the 'relative rates' [79,80]. However, several important considerations should be noted:

1. By and large, the cell-based ICP-MS instruments are not operated under strictly thermal conditions, so the relative rates cannot be considered 'thermal'.
2. The relative rates of reaction cannot be converted to absolute rate constants since the reaction time and the pressure are not known accurately (though an effective rate constant

might be determined through normalization to a known rate constant).
3. Incursion of plasma or background gas into the cell can significantly affect the apparent relative rate of reaction, especially for relatively non-reactive gases.
4. The apparent relative reaction rates may be affected by differing rates of scattering loss or collisional focusing.
5. Care must be taken in the units in which the reaction gas flow is measured. As will be discussed in Section 8.1, the units of flow that are reported depend upon the calibration of the mass flow controller (if used). It is common to use a mass flow controller calibrated for Argon with gases other than Argon, and the resultant flow units should be indicated as Ar-equivalent flow units (though in a prior publication [65] we have referred to these as 'arbitrary units'). These may be converted to absolute flow units if the calibration correction coefficient is known.

6.2.3. Ion–molecule reaction profiles in a r.f.-driven reaction cell

6.2.3.1. Types of ion–molecule reactions. The generic ion–molecule reaction given in Eq. (6.1) includes several categories or types of processes that transform the reacting species. It is generally understood that, in the ICP-MS application, the most important, useful and abundant type of reactions are charge transfer of the type:

$$A^+ + B \rightarrow B^+ + A \quad (\text{e.g. } Ar^+ + NH_3 \rightarrow NH_3^+ + Ar) \tag{6.22}$$

because the first applications were to the resolution of interferences caused by the argide ions (Ar^+ and ArX^+, where X may be Ar, O, Cl, C, Na and so on). The corresponding neutral argides have high IPs and their charge transfer reactions often proceed with high efficiency near the collision rate.

The experimental observation that thermal charge transfer reactions occur near the collision rate allows an opportunity to dispel a common misunderstanding related to the rates of resonant charge transfer reactions. For atomic species at high kinetic energy, where the collision cross-section approximates the hard sphere limit, interaction times are short and it is known that charge transfer processes (in this regime they are sometimes called stripping reactions) that are resonant typically proceed at a higher rate. In effect, this may be re-stated as: atomic non-resonant charge transfer processes at high energy are relatively inefficient. At thermal energies the interaction time is longer, in part due to the development of the ion–dipole attraction, and electron transfer is more efficient. In the thermal instance, where charge transfer, whether resonant or not, proceeds on each collision, it is not possible to distinguish the rates on the basis of resonance.

With the development of the reaction cell technique, it has become apparent that the scope of application is considerably broader than simple charge transfer, and it is to be expected that a variety of classes of ion–molecule reactions will be applied to resolve other interferences. Since small particle transfer reactions are often fast, a second important class of reactions involves hydrogen-containing substances. The several types of these include:

Proton transfer:

$$AH^+ + B \rightarrow BH^+ + A \quad (\text{e.g. } ArH^+ + H_2 \rightarrow H_3^+ + Ar) \tag{6.23}$$

Hydrogen atom transfer:

$$A^+ + BH \rightarrow AH^+ + B \quad (\text{e.g. } Ar^+ + H_2 \rightarrow ArH^+ + H) \tag{6.24}$$

Hydride ion (H^-) transfer:

$$A^+ + BH \rightarrow B^+ + AH \tag{6.25}$$

So-called 'condensation reactions' involve transfer of atoms other than hydrogen, and sometimes result in rearrangement to a thermodynamically stable form. Oxidation reactions are promising due to their apparent selectivity and speed:

$$A^+ + BO \rightarrow AO^+ + B \quad (\text{e.g. } Ce^+ + N_2O \rightarrow CeO^+ + N_2) \tag{6.26}$$

This latter type of ion–molecule reaction is very sensitive to the thermodynamic stabilities of the product oxide ions and of the residual (neutral) leaving molecule. For example, N_2O is attractive as an oxidizing agent because the corresponding reactions include N_2 as a product molecule. CO_2

is also a promising reactant due to the thermodynamic stability of CO as a leaving group. O_2 has a different application because a very strong A^+–O bond is required for this reaction to proceed. However, as a result, some reactions with oxygen have very high specificity.

Clustering is a common reaction between many electron donor molecules and ions, which can be rationalized in terms of the ligand–ion mutual electron donation. Association or clustering reactions of the type:

$$A^+ + B \rightarrow AB^+ \quad (\text{e.g. } Ni^+ + NH_3 \rightarrow Ni^+ \cdot NH_3) \tag{6.27}$$

generally play a negative role in reaction cell ion chemistry when applied to the ICP-MS. Ammonia is a good clustering ligand, meaning that it forms adducts readily and hence can be an analytical complication unless steps are taken to control the appearance of cluster ions (Section 8.4.2). This type of reaction is often observed with water molecules, which are present in many reaction gases in trace quantities. Water also facilitates oxidation, hydroxylation, H-atom transfer and proton transfer reactions.

More complicated multistep ion–molecule reactions may be observed in the reaction cell environment but are usually considered as a nuisance. This does not mean that they cannot be used to advantage; an example is the sequential oxidation of Sr^+ by N_2O followed by H-atom transfer from CH_4 [65,80].

6.2.3.2. Plasma ion reactive decay. As was discussed in Section 6.2.2, the r.f.-driven reaction cell operated under multiple collision conditions is an unsuitable environment for accurate determination of thermal ion–molecule reaction rate constants. Within the validity of certain assumptions regarding flow characteristics, the number density of the reaction gas in the cell is directly proportional to its flow rate. If the ions were fully thermalized throughout the cell, the reaction time would be determined by the macroscopic flow speed of the reaction gas and this depends on the manner in which the gas is added and the relative flow rates through the entrance and exit apertures of the cell. However, reaction cells have not been operated under strictly thermal equilibrium conditions. Usually, the ions are injected into the cell with some energy, and in addition they experience the r.f. field which alters the ion trajectory (Section 8.2.1). From basic principles, a semilogarithmic linear decay of the reacting ion should be obtained if the loss process is first order with respect to the gas density. A bimolecular reaction is such a process, but it should be realized that other (non-reactive, physical) processes can also emulate the dependence with different associated rates. For reactive loss, first order decay can be observed at the relatively low operating pressure of this technique if the number of thermalizing collisions is small in comparison with the total number of collisions or if the ion–molecule reaction happens on every collision.

For example, a semilogarithmic linear decay of the parent plasma ion signal is typical for reaction cells operated under conditions close to thermal [28]. As can be seen in Fig. 6, the reaction of the La^+, Tb^+, Ho^+ and Tm^+ ions with CO_2 in our laboratory with an ELAN DRC demonstrate linear decay in the semilogarithmic plot. These analyte ions react with CO_2 by formation of the corresponding oxides:

$$M^+ + CO_2 \rightarrow MO^+ + CO \tag{6.28}$$

where M^+ is La^+, Tb^+, Ho^+ or Tm^+. Evidently, the response of the parent plasma ion is related to the probability of reaction during the collision. Broadly, all events of close interaction between an ion and a neutral can be divided into two generic groups: reactive and non-reactive collisions. Non-reactive collisions do not change the chemical nature of the colliding atoms and molecules. The usual outcome of such an event is energy exchange between different degrees of freedom of the colliding partners. Chemical reaction leads to an exchange of mass, charge or energy, which is followed by transformation of the reactants into new chemical entities. From Eq. (6.20) it is clear that the mean collisional frequency φ_L of ions is:

$$\varphi_L = [B]k_L = [B]\frac{e}{2\varepsilon_0}\left(\frac{\alpha}{\mu}\right)^{1/2} \tag{6.29}$$

and that the probability for the ion to travel n

times longer than $1/\varphi_L$ without collision is equal to $P_n = e^{-n}$. Assuming that every collision leads to reaction, this simple dependence allows us to estimate the number of collisions (or the reaction gas pressure) that are required in order to attenuate the ion signal by a given factor. For example, 10 reactive collisions are able to reduce the ion signal by approximately 4 orders of magnitude ($1/P_{10} = 2.2\times10^4$), but 30 reactive collisions will achieve 13 orders of magnitude ($1/P_{30} = 1.1\times10^{13}$)! Of course, if the rate of the ion–molecule reaction is half the collision rate (reaction efficiency of 50%), the 13 orders of magnitude will require twice as many collisions: half reactive and half non-reactive.

We know that if the reaction time was independent of the reaction gas flow (i.e. if the reaction cell was buffered with a non-reactive gas) and the ions were thermalized throughout the reaction cell and the number density of the reaction gas was accurately known, the slope of the logarithmic decay of the ion signal intensity versus the reaction gas flow would yield the reaction rate constant. All these conditions and many others are not essential for an analytical instrument (though they are for an instrument intended for kinetic measurements), and one should not attempt to obtain accurate kinetic data from a reaction cell designed for the ICP-MS analytical application. Therefore, why bother with a discussion of the rate constants? There is important information that can be extracted from the reaction dynamics, and this information can be vital for method development. For example, from comparison of the observed reaction profiles in Fig. 6, one may conclude that the rate constants for ion–molecule reactions of lanthanide ions with CO_2 decay in the order $k(La^+) > k(Tb^+) > k(Ho^+) > k(Tm^+)$. Therefore, we gain information on the efficiency of these reactions, and this guides us on the corresponding reaction cell conditions necessary for transformation of the ions for analytical purposes. Even some qualitative information can be obtained from this comparative study despite the reservations about limitations of rate determinations using a r.f.-driven reaction cell. Assuming that the fastest reaction (for La^+) has a relative rate constant equal to 1, it is simple to estimate the other rate constants obtained under

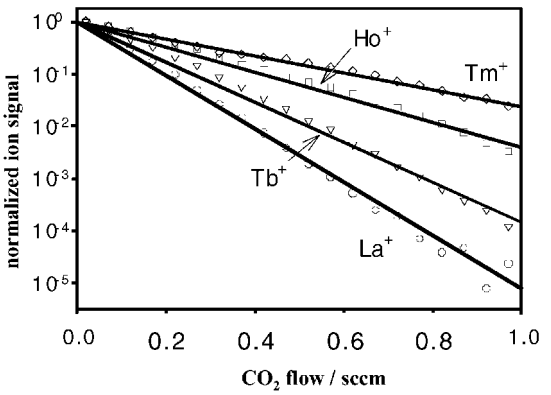

Fig. 6. Ion signals for lanthanide ions as a function of CO_2 reaction gas flow (in true sccm). The steepest slope indicates the fastest reacting ion with the indicated gas.

the same conditions (Table 1). It is useful to know that, in order to get comparable attenuation of Tm^+ in reaction with CO_2, the reaction cell pressure should be at least three times higher than in the case of La^+ reaction. In a relative sense, only 1 reactive collision occurs for every 3 collisions between Tm^+ and CO_2. Fortunately, the collision rate constants, k_L, for these analytes are very similar and no additional correction is required for this estimation. This is not exactly true for a similar assessment of the reactions of Ar^+, Ar_2^+ and ArO^+ with ammonia, even though the effect is small or even negligible.

One of the most efficient and important practical reactions in the ICP-MS application is the charge exchange between Ar^+ and NH_3:

$$Ar^+ + NH_3 \rightarrow NH_3^+ + Ar \qquad (6.30)$$

which has been observed under strictly thermoequilibrium conditions using a SIFT apparatus to proceed with a reaction rate equal to 1.7×10^{-9} cm^3/s [10]. The reaction is considered to be fast in comparison with the collision rate (Table 2). Consequently, its efficiency, given by the ratio of the experimental reaction rate to the calculated Langevin collision rate, is more than 100%. Clearly, the reaction rate cannot exceed the collision rate, and this instance demonstrates a significant error that is introduced by the simplifications of the Langevin theory. The average dipole orienta-

Table 1
Comparative rate constants for reaction of the La^+, Tb^+, Ho^+ and Tm^+ ions with CO_2 under the DRC operating conditions

$M^+ + CO_2$, M	k (relative)	Relative number of required collisions (estimation)[a]	$k_L \times 10^9$ (cm^3/s)	Relative number of collisions (corrected)
La^+	1	1	0.69	1
Tb^+	0.75	1.3	0.68	1.3
Ho^+	0.47	2.13	0.68	2.13
Tm^+	0.31	3.19	0.68	3.19

[a] Number of required collisions for equal attenuation of an analyte ion (see text).

Table 2
Comparative rate constants for reaction of the Ar^+/Ca^+, Ar_2^+ and ArO^+/Fe^+ ions with NH_3 under the DRC operating conditions

$X^+ + NH_3$, X	k (relative)	Relative number of required collisions (estimation)[a]	$k_L \times 10^9$ (cm^3/s)	Relative number of collisions (corrected)
Ar^+	0.97	1.03	1.01	1.04
Ar_2^+	0.45	2.2	0.94	2.1
ArO^+	1	1	0.97	0.97
Ca^+	0.08	12.5	1.01	12.6
K^+	0.04	25		
Fe^+	0.15	6.7	0.97	6.5

[a] Number of required collisions for equal attenuation of an analyte ion (see text).

tion (ADO) theory [6] is an improved collision theory model that includes the charge-induced orientation of the molecular dipole moment that increases the collision rate for polar molecules. Calculation according to the ADO theory (required parameters for ammonia: mass 17 amu, polarizability $= 2.26 \times 10^{-24}$ cm^3, dipole moment $= 1.3 \times 10^{18}$ e.s.u.) yields a collision rate equal to $2.1 \times 10^{-9} cm^3/s$, which puts the efficiency of the reaction under consideration slightly below 100%.

The number of reactive collisions required to decrease the Ar^+ ion intensity from $\sim 10^9$ to 10 cps is close to 20, which under our experimental conditions corresponds to an NH_3 flow of approximately 0.53 sccm (~ 1.0 Ar-equivalent sccm), as seen in Fig. 7a. Chemical conversion of ArO^+ in a similar reaction is marginally faster. In addition, the initial ion current of ArO^+ is significantly smaller and, as a result, less flow of ammonia is required. Reaction between the argon dimer ion and ammonia is slower, and the initial Ar_2^+ signal is intermediate between that of Ar^+ and ArO^+; consequently, reduction of the Ar_2^+ signal to the instrument baseline using this gas is not obtained even at the highest flows consistent with instrument operation (Section 8.1).

6.2.3.3. Reactive decay of an interfering plasma ion. In Fig. 7a a wide range of NH_3 flows in the DRC was used, and a curvature in the high flow region can be observed. Let us consider this curvature more closely.

Usually, the ion–molecule reaction profile has two slopes if the reactant ion m/z is comprised of two (or more) populations that react differently. Using a mass-spectrometer to measure the ion concentration (number density) one cannot distinguish between different populations easily. For instance, a mixture of an ion in the ground and excited electronic states might form two slopes in the reaction profile. Two isobaric ions ($^{40}Ar^+$ and $^{40}Ca^+$, e.g.) will possibly react with different speeds. In both cases, the observed reaction profile would present an unresolved combination of two reaction profiles. For instance, ArO^+ interferes with iron. Both ions are generated in the plasma, are unresolved in the quadrupole mass spectrum, but have different reactivity toward many reaction

gases. If iron is present in trace quantities (as in DIW), ArO^+ dominates the combined ion signal (and the reaction profile) until it is sufficiently reactively removed that it is no longer the major component of the $m/z=56$ signal. It is our experience that, even inside a clean room facility, contaminants in the DIW are at the level of several ppt and it is very difficult to exclude them completely. In Fig. 7b it is evident that Fe^+ reacts much more slowly with ammonia than does ArO^+. A similar observation holds for Ar^+ and Ca^+, which also have very different properties and reactivities (Table 2). The difference in reactivity between isobaric ions is an essential feature of method development for interference reduction. Because of the difference in the reaction rate constants, the same extent of signal suppression in reaction with ammonia requires ten times more collisions for Ca^+ than for Ar^+. A larger difference in the reaction rate constants provides higher specificity of the ion–molecule reaction and, as a result, better detection power of an instrument based on the reaction cell technology.

As an additional confirmation that the observed curvatures in the reaction profiles are due to residual contamination in DIW, one can compare the relative reaction rate constants of the contamination as evidenced by the slope of the second, high flow part of the reaction profile with the reaction rate (slope) obtained from a solution containing the contaminant (or analyte). As can be seen in Fig. 7b, the observed slopes (reaction rates) for the Ca^+ or Fe^+ dominated signals (at high flow) are nearly identical to those of the corresponding background decay rates in Fig. 7a. This gives some confirmation that the limiting signals in the DIW sample are due to contamination by Ca and Fe. Certainly, such an analysis is conclusive only in the case of a negative result.

6.2.3.4. Product ions of the primary ion–molecule reaction. What happens to the product ion of an ion–molecule reaction? Charge should be conserved in a chemical reactor if there is no external means of quenching it. All reaction cells have some physical boundaries and in a multipole environment some charged particles can disappear from the cell by striking the rods or entrance/exit lenses.

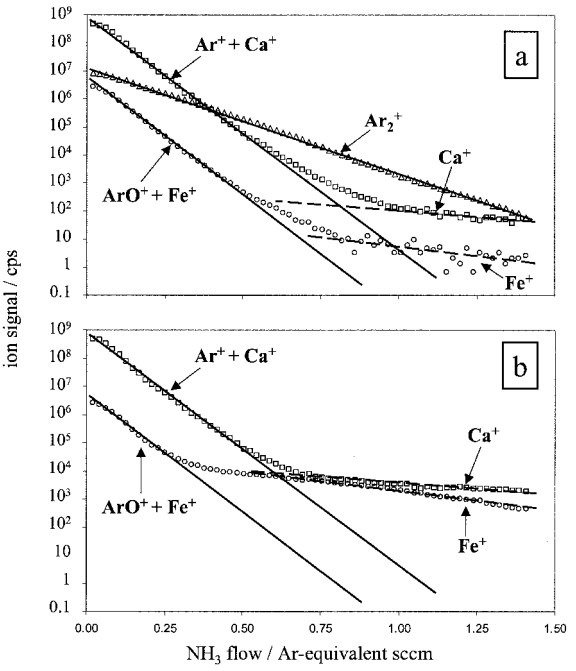

Fig. 7. Reaction profiles for $m/z=40$, 56 and 80 ions with ammonia reaction gas (a) for high purity water and (b) for a solution containing 100 ppt Ca and Fe. Ar^+ and ArO^+ react relatively quickly, and Ar_2^+ reacts more slowly, with ammonia. The curvature of the $m/z=40$ and 56 signals at high ammonia flow indicates the presence of other ions at the same mass that react much more slowly with ammonia than do Ar^+ and ArO^+; these other ions become predominant once the majority of the Ar^+ and ArO^+ ions are reacted away. The initial decays for both (a) and (b) are similar, indicating the predominance of fast-reacting Ar^+ and ArO^+. The second linear portions of the profiles in (b) indicate the relative reaction rates of Ca^+ and Fe^+; the similarity of these slopes with those at high flow in (a) provides evidence that the residual signal in the latter is due to contaminant Ca and Fe in the high purity water. The gas flow is given in Ar-equivalent sccm (Table 4).

Conservation of charge can be forfeit due to collisional scattering or to ion rejection according to the stability characteristics of the multipole field. Under certain operating conditions (Section 8.4.2), the r.f./DC field of a quadrupole is able to confine ions and successfully deliver them to the exit aperture, but under other conditions is also able to reject them according to their mass-to-charge ratio. In addition, product ions might emerge at the same mass as an analyte ion, which creates a new interference. For example, the NH_3^+ ion that is a

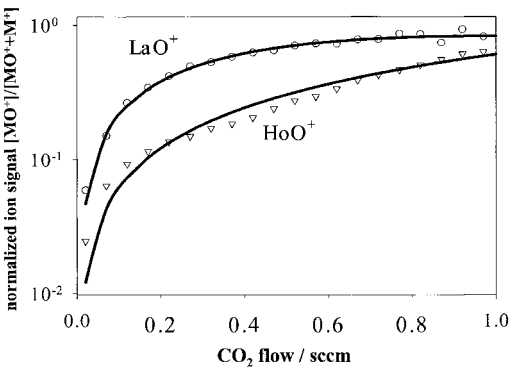

Fig. 8. Signals for the product ions of reactions of La and Ho with CO_2 (see also Fig. 6). The more rapid increase of the LaO^+ signal reflects the faster reaction of La^+. Further, the approach to unity of the normalization to the total ($M^+ + MO^+$) signal indicates that oxidation is the primary reaction channel for these ions.

product of Eq. (6.30) might react further if certain stability conditions are met:

$$NH_3^+ + NH_3 \rightarrow NH_4^+ + NH_2 \qquad (6.31)$$

Eqs. (6.22) and (6.23) are examples of charge and proton transfer reactions, respectively, that are common under most experimental conditions. In our instance, the product ions NH_3^+ and NH_4^+ of charge and proton transfer reactions, respectively, could not be reliably observed. In part, this is because $m/z=17$ and 18 ion signals were already large (isobaric OH^+, OH_2^+), resulting from dominant plasma ions. Other abundant ions (e.g. N_2^+, ArH^+) for which the corresponding neutral has a higher IP or lower proton affinity than ammonia can also contribute to their formation, and resolution of the source reactions is not feasible without prior mass selection of the reactant ions.

In addition, particularly in the case of a quadrupole when operated with a restricted bandpass, the large mass-to-charge difference between the reactant and product ions means that both are not necessarily simultaneously stable. It will be shown (Section 8.4.2) that the DRC is operated in a bandpass mode defined by the parameters q and a for the mass that is currently being analyzed by the mass analyzer. Concomitant ions of other mass-to-charge in the reaction cell are confined according to the stability parameters q and a corresponding to their masses:

$$q_1 m_1 = q_2 m_2, \quad \text{or} \quad q_2 = q_1(m_1/m_2) \qquad (6.32)$$

as implied by Eqs. (3.5) and (3.6). Under conditions for which the Ar^+ reactant ion is at $q>0.39$ ($a=0$), the NH_3^+ product ion is at high $q>0.9$ and is consequently unstable. Conversely, when the (lower mass) product ion is stable, the operating point for the (higher mass) reactant ion is at very low q, under which conditions the efficiency of confinement in the quadrupole field is reduced due to scattering (Section 7.2). Accordingly, the existence of a charge transfer reaction channel can only be inferred by observing a reactive loss of the reactant ion without observing a concomitant product ion whose intensity change accounts for the loss of the reactant ion.

Determination of the products of atom transfer (hydrogen and oxygen) reactions is more straightforward because of the small mass shift of the products. For example, the products of the La^+ and Ho^+ oxidation reactions with CO_2 can be clearly observed, as shown in Fig. 8. Comparison with the decay profiles of Fig. 6 shows that the rate of increase of the product oxide ions is proportional to the rate of decay of the parent metal ions. For a reaction that proceeds through only one reaction channel, the magnitude of the rates of reactant decay and product appearance should be equal. However, there are several competing processes that interfere with the observation of the reaction kinetics. Perhaps the most important of these effects are scattering and collisional focusing, both of which are functions of the mass ratio of the ion and neutral, the operating point of the multipole, and the number of degrees of freedom of the ion and neutral.

6.2.3.5. Scattering versus reactivity for parent and product ions. Plasma ion decay in the presence of a reaction/collision gas is not always evidence of ion–molecule reaction. Similarly, product ion decay is not always indicative of a subsequent reaction channel. There was no doubt concerning the character of ion decays in the case of Eq. (6.28) because the corresponding product oxide ions could be easily observed and the rates of reaction were substantial. However, simple scatter-

ing in the cell is able to mimic reactivity and it can be challenging to distinguish between this and slow (inefficient) reaction. For instance, in the presence of ammonia, K^+ and Ca^+ exhibit 'reactivity' which is only 4 and 8% of the reactivity of ArO^+, respectively (Table 2). One can speculate that the observed decays of these ion signals occurs mostly due to scattering in the cell. As was mentioned before, Fe^+ under the same conditions decays just a little faster. However, the chemical nature of this decay is obvious because the cluster ions $Fe^+ \cdot (NH_3)_x$ can be observed when the cell is operated at low q. Scattering is a complex phenomenon of its own. It includes at least three components: simple scattering due to collision with a gas molecule, which moves an ion outside of the acceptance ellipse of the r.f.-driven cell (Section 7.1.5); scattering of product ions due to translational excitation as a result of high exothermicity of the ion–molecule reaction; and 'scattering-like' effects produced by different simultaneous stability of the parent and product ions in the r.f.-field. In addition, space charge related scattering can be observed when the pressurized reaction cell is operated under conditions that promote trapping or storage.

There are several methods of distinguishing between different scattering phenomena. In general, the uncertainty is removed by comparison to a non-reactive ion decay that is measured under the same conditions. For example, confirmation that the decay of a reactant ion signal is not due to instability of its trajectory in the r.f.-field could be obtained by simultaneously monitoring a different analyte ion of similar mass-to-charge but for which reaction with the gas is significantly slower or endothermic. As was shown before, fast ion–molecule reactions (Section 6.2.3.2) are characterized by a linear semilogarithmic reaction profile. If reaction happens on every collision ($k \geqslant k_L$), there is no opportunity for scattering to occur. For reactions that are less efficient, $k < k_L$ or $k \ll k_L$, distinction between reaction and scattering can be difficult, except by comparison to a non-reactive but otherwise homologous ion. Let us consider the interactions of several analyte ions with ammonia under the same conditions. In Fig. 9 the elemental ions under consideration are divided into two

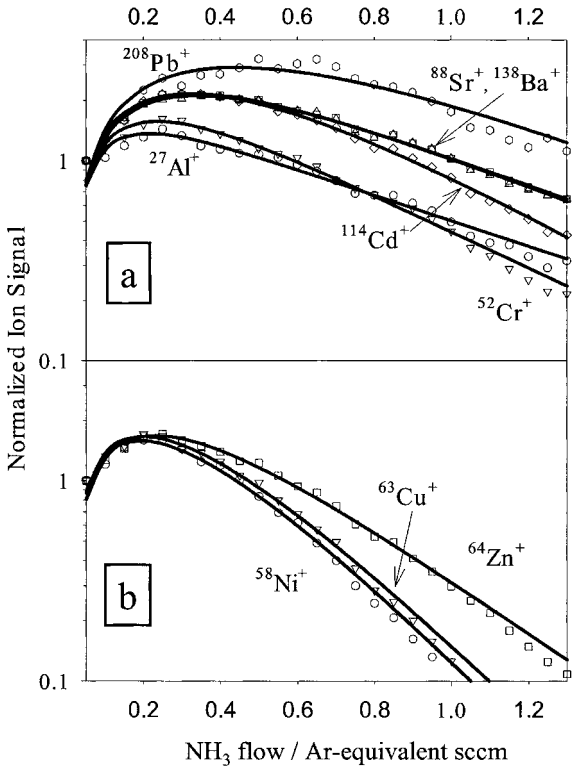

Fig. 9. Reaction profiles of (a) relatively non-reactive atomic ions and (b) relatively reactive atomic ions with ammonia. The ion signals initially increase due to collisional focusing towards the axis of the cell, improving the transmission into the mass analyzer. The slopes of the linear portions of the ion signal profiles are inversely proportional to the reaction rate constant. The gas flow is given in Ar-equivalent sccm (Table 4).

groups: obviously reactive ions (bottom reaction profile) and non-reactive or slowly reacting ions (top profile). Such categorical division is, of course, arbitrary. However, two features in common for the profiles of reactive and non-reactive ions may be evident. First, the rate of collision-induced scattering (as evidenced by the slope of the profiles for non-reactive ions at high flow) should be a function of the reduced mass of the collision partners. However, the initial increase in the observed ion signals as well as slow reactivity of some of the ions can obscure a clear dependence on this. Second, in both cases there is an initial increase in the observed ion signal. This increase is not related to the production of new interferences

and it also cannot be attributed to a new source (not associated with the plasma) of the analyte ions. Rather, it is a result of collisional focusing, discussion of which we defer to Section 8.2.1.

7. Linear r.f. devices

Consider an array of an even number, $2n$, of parallel rods of length l placed evenly about an axis of symmetry, z, such that an inscribed circle of radius r_0 contacts the inner surface of each rod. Further, suppose that opposing pairs of rods are electrically connected and supplied with an AC voltage having radio frequency $f=\omega/2\pi$ and amplitude V_{rf}, with a phase shift of π/n radians between neighboring rods. In addition, all of the rods are supplied with an identical DC voltage, V_{RO}, that defines a rod offset (also called pole bias) potential. An ion that is within this array then has an axial kinetic energy, $E_z=\mathrm{KE}_{\mathrm{source}}+\mathrm{PE}_{\mathrm{source}}-V_{\mathrm{RO}}$, where $\mathrm{KE}_{\mathrm{source}}$ and $\mathrm{PE}_{\mathrm{source}}$ are the kinetic energy that the ion has when it exits the source and the potential at the source, respectively. The ion has a corresponding axial velocity $v_z=\sqrt{2E_z/m}$, where m is the mass of the ion. The (positively charged) ion within the array experiences an oscillating field and is at one moment attracted to the nearest pole at negative voltage, and at the next ($1/f$ seconds later) to the neighboring rod. If the frequency is sufficiently low, or the ion mass, m, is sufficiently small, the ion will collide with the attracting rod before the AC voltage on that rod reverses polarity. If the frequency is sufficiently high, or the ion sufficiently heavy, its inertia will prevent it from reaching the attractive rod before the polarity changes, and the ion will undergo lf/v_z stable oscillations throughout its transit of the array. Operation in this 'r.f.-only' mode (V_{RO} is not considered) provides a high-pass mass filter; only ions having masses above a 'low mass cut-off' are transmitted.

If, in addition, a DC voltage, V_{DC}, is applied between pole pairs, the ion will feel a continuous attraction towards the more negative (DC) pole pair. If the AC frequency is sufficiently low, or the ion mass sufficiently heavy, so that the ion's response to the AC field is laggardly, the ion will drift towards the DC-negative pole, eventually striking that pole. If the ion mass, AC frequency and DC voltage are just right, the ion may have a stable (though tortuous) trajectory through the array. Thus, the addition of a DC bias between pole pairs provides a high mass cut-off in addition to the low mass cut-off of the r.f. It will be seen that, to first order approximation, the low mass cut-off is essentially determined by the amplitude of the r.f., V_{rf}, and the applied AC frequency, ω, while the high mass cut-off is essentially determined by the amplitude of the DC, V_{DC}, and the applied AC frequency, ω.

7.1. General characteristics of r.f. multipoles

7.1.1. Equations of motion

This description of ion motion in an r.f.-driven multipole is overly simplistic. In fact, the ion executes a tortuous trajectory in the r.f. field. In the theoretical instance, the r.f. and DC fields are applied to an infinitely long multipole of order n so as to produce a field of the form:

$$\Phi=\Phi_0(x^2+y^2)^{n/2}\frac{1}{r_0^n}\cos\left(n a\tan\frac{y}{x}\right) \tag{7.1}$$

where $\Phi_0=V_{\mathrm{dc}}-V_{\mathrm{rf}}\cos(\omega t)$.

The ion motion in Cartesian coordinates is determined by the classical equations of motion:

$$\frac{\partial^2 x}{\partial t^2}=\frac{e}{m}E_x;\qquad \frac{\partial^2 y}{\partial t^2}=\frac{e}{m}E_y \tag{7.2}$$

The Cartesian components of the electric field are obtained as the gradient of potential Φ:

$$E_x=-\frac{\partial}{\partial x}\Phi;\qquad E_y=-\frac{\partial}{\partial y}\Phi \tag{7.3}$$

where:

$$\frac{\partial}{\partial x}\Phi=\Phi_0 n\left[\frac{(x^2+y^2)^{1/2}}{r_0}\right]^n \frac{x\cos\left(n a\tan\left(\frac{y}{x}\right)\right)+y\sin\left(n a\tan\left(\frac{y}{x}\right)\right)}{(x^2+y^2)} \tag{7.4}$$

$$\frac{\partial}{\partial y}\Phi = \Phi_0 n\left[\frac{(x^2+y^2)^{1/2}}{r_0}\right]^n \frac{-y\cos\left(n a\tan\left(\frac{y}{x}\right)\right)+x\sin\left(n a\tan\left(\frac{y}{x}\right)\right)}{(x^2+y^2)} \quad (7.5)$$

from which the equations of motion of an ion in a multipole field of order n can be derived according to Eq. (7.2). In the special instance that $n=2$ (a quadrupole), it will be seen that Eqs. (7.4) and (7.5) are independent, and this has important ramifications to which we will return.

7.1.2. Adiabaticity

When it is of interest to study ion–molecule interactions under thermal or defined-energy conditions using an r.f.-driven ion guide, it is desirable to operate such that the r.f.-field does not contribute significantly to the interaction energy. Under the influence of the applied r.f., the ion is periodically accelerated and the amount of r.f. energy transferred into the collision energy is greater for higher r.f. amplitude for a given operating point (a, q). Hence, it is propitious to operate at a relatively low r.f. voltage consistent with the concurrent desire to confine ions within the field. In a simple view, adiabatic conditions apply when the total energy and momentum of the ion ensemble are conserved on average. Hence, the term does not seem to properly apply when the ion undergoes collisions (with the consequent exchange of energy that eventually ends up as radiated heat), though the concept of adiabaticity still applies between collisions. It should be evident that operation at pressures that provide more than 1 collision per r.f. cycle also minimizes the contribution of the r.f. energy to the collision energy [28]. With some liberal interpretation, the concept of adiabaticity can be used to identify conditions where the ion collision energetics are at least minimally affected by the applied r.f. It is generally accepted that ion motion in a multipole operated in the r.f.-only mode at low q satisfies the requirements for conservation of energy and momentum on average, and that operation at high q or with non-zero a deviates from this condition. A general rule of thumb, developed by Gerlich [12], is that adiabatic conditions hold for $q<0.3$, though operation outside of this regime does not necessarily imply substantial deviation from constant-energy conditions (depending as it does on the amplitude of the r.f., the geometry of the multipole, the number of collisions per r.f. cycle and the ratio of ion and neutral masses, the latter applying before thermalization). Gerlich has rigorously considered the conditions that provide 'safe operation' from the point of view of adiabaticity; the interested reader is referred to that work [12].

7.1.3. Hyperbolic versus round rods

To satisfy the detailed theory, the field within the multipole should be hyperbolic. Accordingly, the rods used for the quadrupole mass filter application are often produced with a hyperbolic profile. Round profile rods can emulate a hyperbolic field if the ratio of the radii of the rods to that of the inscribed circle, r/r_0, is appropriately chosen on the basis of theory, experiment or modeling (Monte Carlo is preferred to SIMION [81]). For the quadrupole, an incorrect value for this ratio, $r/r_0=1.16$, was misquoted by Paul et al. [82] and subsequently used by other authors; the more commonly accepted value is 1.148 [31,83], which is chosen because it minimizes the dodecapole distortion. Gibson and Taylor [81] empirically determined that the optimum ratio is in the range $1.12<r/r_0<1.13$ through ion trajectory calculations. Douglas and Konenkov [84] have shown theoretically that at $r/r_0=1.13$ the dodecapole term is essentially offset by higher order contributions, and confirmed the prediction experimentally. The quadrupole is often enclosed in a conductive housing that affects the internal field and can minimize the higher order distortions introduced by the round rod approximation [85]; the calculations of Gibson and Taylor [81] indicate that this effect is extremely small. Some quadrupole manufacturers today have experimentally optimized the r/r_0 ratio in their product configuration, leading to a substantially different value of the ratio, which remains proprietary. A recent study reports on SIMION calculations of the appropriate ratio for hexapole ($n=3$) and octapole ($n=4$)

arrays, recommending $r/r_0 = 0.5375$ and 0.355, respectively [86].

Experimental comparison of quadrupole mass filters having hyperbolic and circular geometries is difficult, in part because of variations in reproducibility of installation and in part because of the dependence of performance on the ion kinetic energy distribution, the ion beam profile at the entrance of the array and fringing fields. Probably the most thorough study was reported by Brubaker [87,88], showing that for a given sensitivity the hyperbolic rods can provide up to twice the resolution of circular rods, diminishing to comparable performance at low (nominal unit mass) resolution. The general conclusion is that under the normal operating conditions (unit mass resolution) there is little difference between round rods and hyperbolic rods.

7.1.4. Auxiliary excitation at the secular frequency of motion

In addition to ion motion at the frequency $\omega = 2\pi f$ of the applied r.f., the ion oscillates at its fundamental (secular) frequency of motion, ω_n,:

$$\omega_0 = \beta\frac{\omega}{2}; \quad \omega_1 = \left(1 - \frac{\beta}{2}\right)\omega;$$
$$\omega_2 = \left(1 + \frac{\beta}{2}\right)\omega; \text{ etc.} \tag{7.6}$$

where $0 \leqslant \beta \leqslant 1$ and is a complicated function of the operating conditions (a, q). This fundamental motion usually, and under adiabatic conditions, appears as a dominant low frequency oscillation having high frequency secondary motion driven by the applied r.f. Application of auxiliary r.f. at a frequency which is in resonance with the secular motion of the ion causes the amplitude of motion to increase, and can therefore be used to excite the specific ion mass to eject these ions or to increase their collision energy in a pressurized multipole.

7.1.5. Acceptance

An ion that satisfies the stability requirements of the multipole (recall that stability assumes an infinitely large and perfect device) is not necessarily transmitted through the multipole. The ion must simultaneously meet the acceptance criteria of the multipole, which results from the finite dimensions of the device. These criteria relate to the radial displacement and radial energy (velocity) of the ion and the phase of the r.f. The acceptance is described as an ellipse in (r, $\mathrm{d}r/\mathrm{d}t$) phase space. In general, the acceptance ellipse constricts at lower r.f. frequency or higher V_{rf} or V_{DC} (higher (a, q)). For a pressurized multipole, the acceptance criteria must be satisfied after each collision in order for the ion to remain confined.

7.1.6. Fringing fields

The ion must also satisfy the stability and acceptance criteria as it enters the multipole. One of the realistic assumptions often adopted is that the magnitude of the r.f./DC decays outside of the array as $1/z^2$. Hence, (a, q) is a function of the ion position when it is external to the cell. When conditions are applied to provide stability for the ion within the array, the fringing field is nearly always destabilizing. However, rejection of an ion usually requires a few r.f. cycles, and the effect of the fringing field can be minimized if the residence time is short (energy is high). Accordingly, it is common to accelerate ions into and out of the multipole. Brubaker [89] has described a means of modifying the fringing fields for the r.f./DC application, described below.

7.2. Quadrupoles

Eqs. (7.4) and (7.5) described the motion of an ion in a multipole of order n. For the quadrupole ($n = 2$), these equations simplify to:

$$\frac{\mathrm{d}}{\mathrm{d}x}\Phi = \frac{2\Phi_0}{r_0^2}x \tag{7.7}$$

$$\frac{\mathrm{d}}{\mathrm{d}y}\Phi = \frac{-2\Phi_0}{r_0^2}y \tag{7.8}$$

and it is clear that motion in the X and Y directions is uncoupled. The trajectory of an ion in a perfect quadrupolar field of infinite length is given by:

$$\frac{\mathrm{d}^2u}{\mathrm{d}\xi^2} + \{a \pm 2q\cos 2(\xi - \xi_0)\}u = 0 \tag{7.9}$$

$$\frac{\mathrm{d}^2z}{\mathrm{d}\xi^2} = 0 \tag{7.10}$$

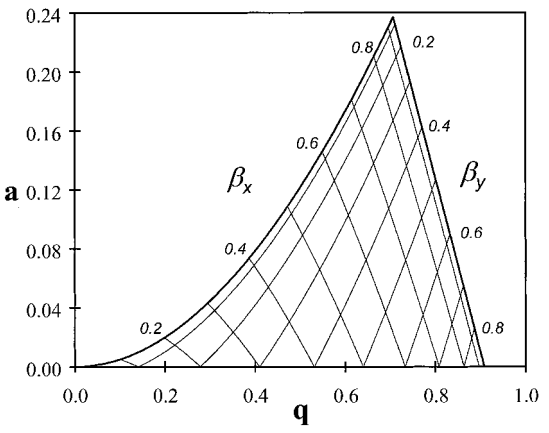

Fig. 10. Stability diagram for an infinitely long and perfect quadrupole in the dimensionless space of (a, q), where a and q are the Mathieu parameters given by Eqs. (3.5) and (3.6) in the text. Ions that are within the enclosed region are considered to be stable, while ions that are outside of this region are considered to be unstable. Also shown are the iso-beta lines that can be used in calculating the frequencies of ion oscillation in the quadrupole.

where $u=(X, Y)$, $\xi=\frac{1}{2}(\omega t)$, ξ_0 is the initial phase of the r.f. field, and a and q are the non-dimensional Mathieu parameters defined in Eqs. (3.5) and (3.6), with $n=2$, and z is defined to be the lengthwise axis of the quadrupole. Because of the independence of motion in X and Y, the stability characteristics of a quadrupole are independent of the initial position of the ion within the array. Accordingly, a single stability diagram is appropriate for the quadrupole, as shown in Fig. 10 in (a, q) space. The diagram describes a binary state: the ion is either stable or unstable, and the transition between these is sharply defined at the $\beta_x=1$ and $\beta_y=0$ boundaries. Recall that a and q are inversely proportional to the ion mass. For a given set of conditions of r.f. and DC amplitude and r.f. frequency, an ion is either stable or not depending on its mass. Specification of (a, q) for a given ion mass then defines a 'scan line' for all other masses that passes through the origin. The range of ion masses that are simultaneously stable (the 'bandpass') is easily established by determining the masses corresponding to interception of the stability boundaries. Clearly, the bandpass narrows as the slope of the scan line increases. Mass filters operate at the apex of the stability diagram. To see this more clearly, the mass can be removed from the parameters a and q (from the axes of Fig. 10), yielding a series of stability curves for each mass as a function of voltage and frequency, as shown in Fig. 11. The scan line that passes through the apex of one stability curve also passes through the apex of the other stability curves for other masses. This describes either of two means of scanning the mass filter: the amplitudes of the r.f. and DC voltage may be adjusted in concert (at a ratio V_{rf}/V_{DC} that defines the resolution) at fixed frequency, or alternatively the voltages may be kept constant and the frequency scanned. Almost all mass filters today operate in the first mode (amplitude-scanned), partially because the mass scale is then linearly dependent on the amplitudes and partially because of the high accuracy and stability of crystal clocks to define the frequency. Typically, the mass filter is operated at r.f. amplitudes up to approximately 7 kV and frequencies of the order of 3 MHz (for the elemental application, for which the maximum scan mass is $\approx$270 amu).

Quadrupole applications can be considered for two general classes: mass filters and ion guides. As noted above, the mass filter application requires operation near the apex of the stability diagram,

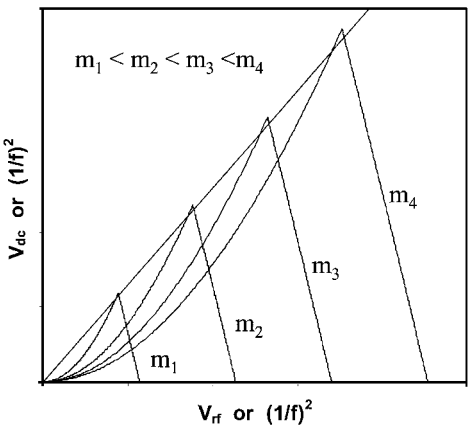

Fig. 11. Quadrupole stability diagrams as a function of ion mass, plotted in $V_{dc,rf}/f^2$ space. Higher masses are stable at higher amplitude of the r.f. and DC and at lower operating frequency. The mass filter is usually operated by scanning the amplitudes of the voltages such that the tips of the stability boundaries are intersected.

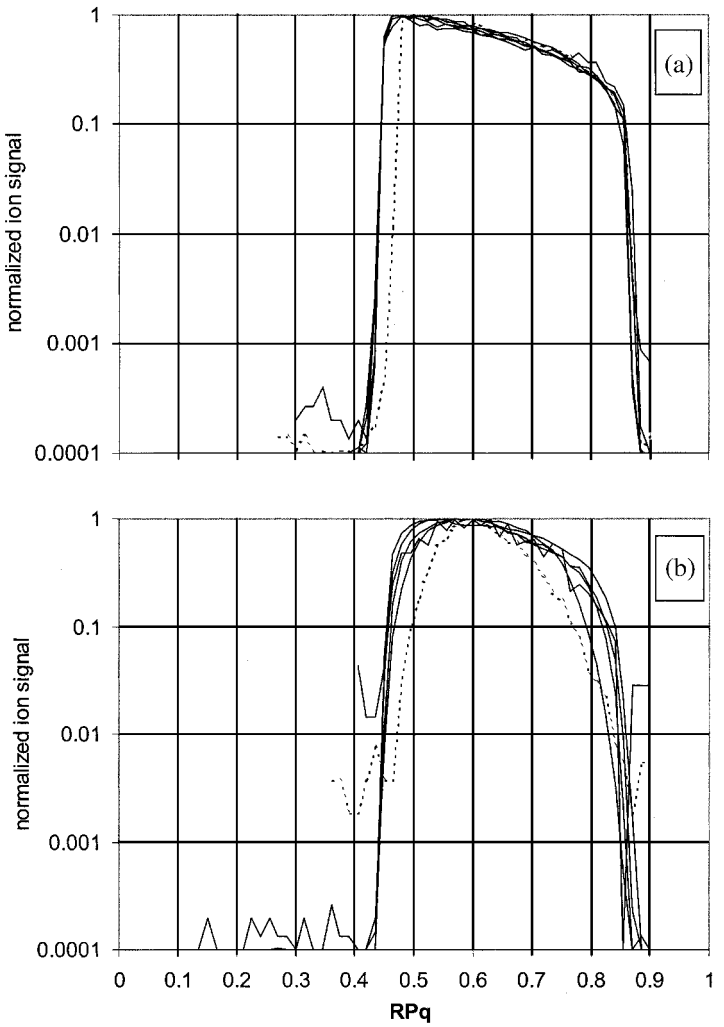

Fig. 12. Ion signals for $^{7}Li^{+}$, $^{24}Mg^{+}$, $^{59}Co^{+}$, $^{115}In^{+}$, $^{159}Tb^{+}$ and $^{238}U^{+}$ as a function of the RPq parameter obtained with RPa = 0.045 (RPq and RPa are proportional to the Mathieu parameters q and a). The $^{24}Mg^{+}$ signal behaves marginally differently than the other ion signals, and is shown in dashed lines (because the other ions behave nearly identically, they are all shown as solid lines). Data obtained under essentially collisionless conditions (reaction gas flow stopped and cell vented to mass analyzer chamber, $\approx 2\times10^{-5}$ torr) are given in (a), and for the cell pressurized with Neon (0.5 Ar-equivalent sccm = 0.525 sccm, $\approx$7 mtorr) in (b).

and it should be clear that high precision in construction (parallel, straight and uniform rods) is required in addition to stable and high precision voltage power supplies. Ion guides, on the other hand, are generally operated near the $a=0$ axis (r.f.-only) and typically at low $q<0.3$. Under this condition, the acceptance and ion transmission are relatively large. If the cell is pressurized, collisional focusing (discussed below) increases the transmission efficiency through a finite exit aperture and ion energies are damped, providing improved mass resolution for the downstream mass analyzer. If the pressurizing gas is reactive with one or more of the ions, the ion guide can also be used as a reaction cell to study ion–molecule chemistry, especially if operated at low q (adiabatic conditions), though a higher order multipole is more common for this application.

For various reasons, ion transmission efficiency is not independent of a and q. Fig. 12a shows the ion signals for several m/z ions as a function of the RPq parameter at RPa = 0.045, which are proportional to q and a respectively, for a quadrupole cell of length 12.5 cm having a tubular entrance aperture of 3.2 mm diameter and an exit aperture of 2 mm diameter, under near-collisionless conditions (pressure $\approx 2\times10^{-5}$ torr). For these data, RPq was adjusted by varying the frequency of the r.f. rather than the more common amplitude scanning. Mean ion energies in the quadrupole cell were mass-dependent and in the range of 4–11 eV (i.e. cell rod offset, CRO = 0 V) and were expected to have an energy distribution of approximately one-half the mean energy [90–92]. Under these conditions, periodic focusing effects are less evident [93,94]. As expected, the normalized signals as a function of RPq (q) are independent of the ion mass. Under r.f.-only ($a = 0$) conditions for a quadrupole, ions are normally stable in the range $0 < q < 0.908$; for $a = 0.0855$ (as appears to be equivalent to RPa = 0.045; see below), the stability range includes $0.42 < q < 0.84$. The presence of entrance and exit apertures, which provide boundary conditions of fringing fields, distorts these boundaries somewhat. The decay of the signals as RPq is increased from the maxima near RPq = 0.5 is believed to result principally from the relatively wide (3.2 mm diameter) ion beam entering the DRC and reflects the constriction of the acceptance ellipse of the quadrupole as RPq increases.

Fig. 12b provides similar data obtained with the cell pressurized to approximately 7 mtorr with Ne. Again, as expected, the dependence of the ion signals on the RPq (q) parameter are essentially independent of ion mass. The profiles are similar to those of Fig. 12a except for a relative suppression at the low and high RPq sides of the maximum peak (i.e. the profiles are more rounded). The reduced signals at low RPq are likely due to scattering losses because the restoring forces (potential well depth) are insufficient to refocus the ions back to the axis for transmission through the exit aperture. Relative suppression at high RPq is likely due to a different manifestation of scattering loss caused by the constriction of the acceptance of the quadrupole: there is a higher probability that after the collision (r, $\mathrm{d}r/\mathrm{d}t$) will be outside of the acceptance.

The data of Fig. 12a and b, and further data recorded at different values of the RPa parameter, may be converted to stability diagrams by making an arbitrary definition of 'stability': we have chosen to consider an ion stable if the ion signal is greater than 10 cps (i.e. RPq was scanned for a given RPa, and the stability boundary was defined as that value of RPq for which the ion signal was above or below 10 cps). These data appear as points in (a, q) space, and are overlaid on the conventional stability diagram defined by Eqs. (3.5) and (3.6) in Fig. 13. The measured stability points in (RPa, RPq) space have been converted to (a, q) space according to the (linear) empirical equations $q = 0.95\times\mathrm{RPq}$ and $a = 1.9\times\mathrm{RPa}$ in order to obtain congruence of the data with the theoretical values. These conversion factors are likely required as a result of capacitive losses inside the vacuum chamber, resulting in approximately 5% lower V_{rf} than expected, and the RPa conversion includes an additional factor of 2 (a simple scaling factor). With these corrections, the experimental points match the theoretical stability curves quite well for the instance of near collisionless conditions. More importantly, the concept of well-defined stability boundaries holds nearly equally for the pressurized condition, and this has important ramifications for the use of the stability characteristics of the quadrupole for the suppression of secondary chemistry in a reactive collision cell (Section 8.4). It appears that the stability boundaries are compressed for low mass ions under multiple collision conditions. This might be anticipated because of the more severe scattering for low values of the ratio $m_{\mathrm{ion}}/m_{\mathrm{neutral}}$. In some measure, it is also an artifact of using a 10 cps threshold for boundary determination, as the sensitivity, particularly for $^{7}\mathrm{Li}^{+}$, is severely diminished (mass ratio ~ 0.35) so that, for the 1 ppb concentration used in these experiments, the boundary threshold is passed 'early' (closer to the optimum value of q).

7.3. Higher order multipoles

The stability of ions in higher order multipoles

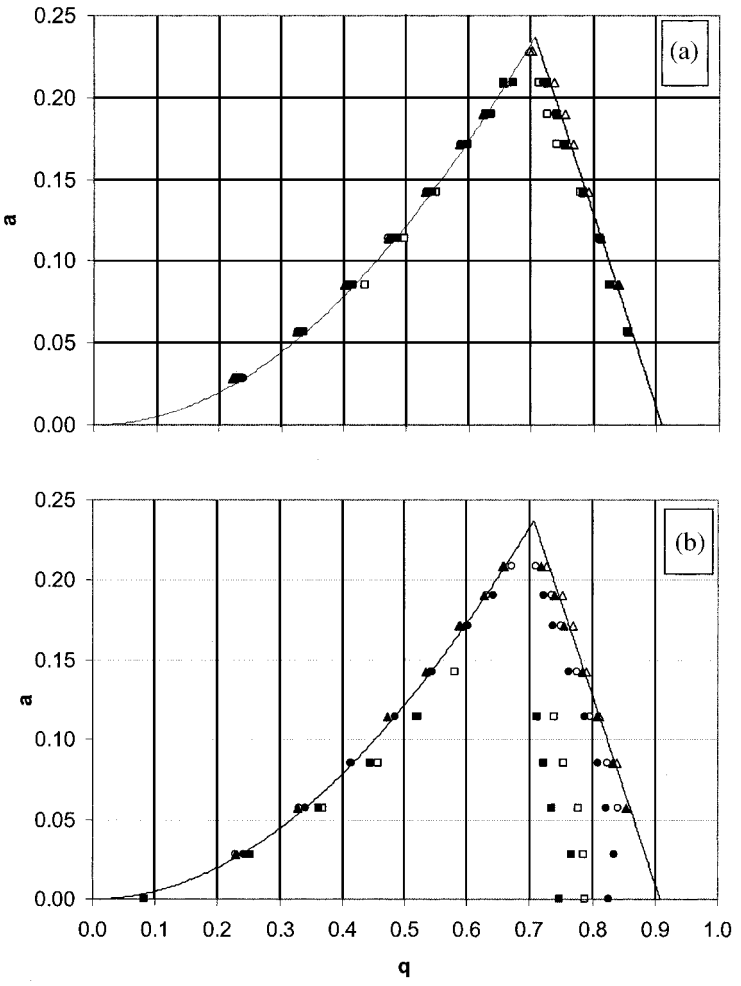

Fig. 13. Stability boundaries for the quadrupole reaction cell, defined as the point at which the absolute ion signal falls below 10 cps, measured for $^{7}Li^{+}$ (■), $^{24}Mg^{+}$ (□), $^{59}Co^{+}$ (●), $^{115}In^{+}$ (○), $^{159}Tb^{+}$ (▲) and $^{238}U^{+}$ (△) for data obtained in the manner of Fig. 12. The theoretical stability boundaries are given by the solid curves. The experimental parameters RPq and RPa were converted to the Mathieu parameters q and a according to the empirical equations $q=0.95\times$RPq and $a=1.9\times$RPa in order to obtain congruence of the data with the theoretical values. Data obtained under essentially collisionless conditions (reaction gas flow stopped and cell vented to mass analyzer chamber, $\approx 2\times10^{-5}$ torr) are given in (a), and for the cell pressurized with Neon (0.5 Ar-equivalent sccm = 0.525 sccm, $\approx$7 mtorr) in (b).

is a function of the position of the ion in the multipole, and ion motion is non-independent in the X and Y directions, as evident in Eqs. (7.4) and (7.5) for $n=3$ (hexapole), 4 (octapole), etc. The stability boundaries have been calculated by Hagg and Szabo for a hexapole [34] and an octapole [36] for different positions of injection into the multipole. Fig. 14 gives the resultant stability diagram for the hexapole for the introduction of ions into a non-pressurized hexapole at $r=0.1r_0$. Similar results are obtained for the octapole. In contrast to the quadrupole, for which corresponding calculations are given in Ref. [34], the higher order multipole lacks well-defined stability boundaries. Three conditions of stability are shown in Fig. 14: stable (I), partially stable (II) and unstable (III). Further, different stability characteristics are obtained for different positions of ion

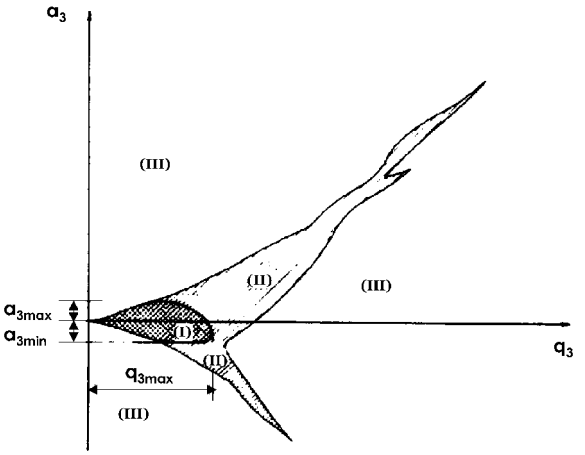

Fig. 14. Stability diagram for a hexapole for ions introduced at radial displacement $r=0.1r_0$, obtained by theoretical modeling. Three regions of relative stability are shown: stable (I), partial stability (II) and unstable (III). (From Ref. [34] with permission from Elsevier Science.)

injection. Accordingly, the higher order multipole has failed to find application as a mass filter.

These data have two important ramifications for the use of higher order multipoles. It is evident from Fig. 14 that the region of stability of the hexapole (and similarly for the octapole) is wider in (a, q) than for a quadrupole. This means that ions having a wider distribution of masses are simultaneously stable in the higher order multipole (i.e. the bandpass is wider, though less well-defined). Accordingly, the octapole in particular has found application in MS/MS, for which it provides a wider range of confinement of daughter ion masses than the quadrupole. This is desirable in the CID experiment, where the daughter ions are used for identification of the parent ion that was fragmented. It is not a desirable characteristic when a well-defined bandpass is desired for control of secondary chemistry (Section 8.4). The other ramification derives from the dependence of the stability on the position of the ion in the multipole. In the pressurized cell (collision or reaction cell), the ion must meet the acceptance and stability criteria following each collision. Accordingly, different conditions of stability and acceptance apply after each collision. While this complicates the modeling of the pressurized higher order multipole, the effect is offset by the wider stability, with the net result appearing to be somewhat higher efficiency of collection over a wider mass range of daughter/product ions.

The effective potential describes the time-averaged radial potential distribution in the multipole. For a multipole of order n ($2n$ poles), the effective potential, $V_{\text{eff}}(n)$, is given by [12]:

$$V_{\text{eff}}(n)=\frac{n^2}{16}\frac{e^2}{m\omega_0^2}\frac{V_{\text{rf}}^2}{r_0^2}\left(r/r_0\right)^{2n-2}+\frac{eV_{\text{dc}}}{2}\times\left(r/r_0\right)^n\cos n\varphi \qquad (7.11)$$

where the variables are defined as for Eqs. (3.5) and (3.6) (i.e. V_{rf} is the peak-to-peak voltage and V_{dc} is the DC potential between pole pairs). For multipoles operated in the r.f.-only mode, the second term is zero. Thus a higher order multipole has a wider valley plateau and steeper walls (near the rods). For the pressurized multipole, this means that there is a larger volume near the axis where the restoring forces are weak. Hence the higher order multipole finds value in applications where thermal conditions are desirable (e.g. for the study of thermal kinetics). On the other hand, the more narrow well of the quadrupole suggests that the ions will migrate closer to the axis so that collisional focusing (Section 8.2.1) should be more pronounced.

7.4. Prefilters

As discussed in Section 7.1.6, the fringing fields at the entrance and exit of the multipole are often defocusing. Brubaker [89] realized that the addition of an r.f.-only quadrupole at the entrance and exit of a quadrupole mass filter delays the onset of the instability because it delays the appearance of the DC field component. In addition, the acceptance of an r.f.-only quadrupole is larger than that of a mass filter. For both reasons, r.f.-only pre- and post-filters improve transmission of ions into and out of the mass filter. In practice, the post-filter has less benefit, particularly if an attractive extraction field (such as is common with a close-coupled detector) is present. It has become relatively common practice to include only a prefilter in commercial systems. Typically, the prefilter has

a length of $\sim 2r_0$. At least for organic mass spectrometers, it has become common to significantly extend the length of the prefilter and operate it at an elevated pressure in order to further increase the transmission efficiency into the mass filter through collisional focusing (Section 8.2.1). To date, it has not been common practice to include pre- and post-filters to a pressurized reaction/collision cell, probably because they are typically operated sufficiently far from the tip of the stability boundary (i.e. not as mass filters) that the benefit of delayed DC onset is less apparent.

7.5. Axial fields

Collisions in a pressurized multipole cause damping of the axial ion kinetic energy. If the energy is sufficiently damped, and ignoring the net drift of the gas, the ion motion approaches Brownian (essentially a random walk without preference for direction). If this condition applies, the transmission of ions out of the cell is expected to be reduced. If the gas (1 sccm) is introduced coaxially (annular area 0.06 cm^2) with the ion beam at the entrance of the cell (pressure ~ 20 mtorr), the gas will have a velocity at the entrance of the cell that is of the order of 10^4 cm/s. While the gas flow will also be damped in collisions, the impulse of the gas at the entrance of the cell induces a net drift velocity through the cell, and the ions will be carried with this gas flow. In this case, even thermalized ions are encouraged to transit the cell, typically in an average transit time of a few milliseconds. Hence, the flow of gas can provide an axial flow field that assists, at the least, with ion penetration into the cell.

Typically, ions are accelerated into the cell through an entrance aperture (or tube) at negative voltage relative to the source. The axial field downstream (within the cell) associated with this entrance potential is retarding, though its impact is marginal after a short penetration ($\approx r_0$) into the cell. Similarly, it is common to apply an extraction potential at the exit of the cell, usually by biasing of the exit aperture. This field accelerates the ions towards the exit aperture and is effective over an extraction length of, again, about r_0. Hence, there is a decelerating axial electric field at the entrance of the cell, which can be partially mitigated by an axial flow field, and an accelerating field at the exit of the cell. For the ICP-MS application, a large ion current is typically introduced into the cell, and the resultant charge density probably exceeds the space charge limit of the cell. Because of the combined effects of the fields at the entrance to the cell, it is expected that the maximum charge density occurs at a distance of approximately 1 to $2r_0$ into the cell. Upstream of this point, the ions are pushed by their residual entrance kinetic energy and the gas flow stream (if the gas is added coaxially at the entrance of the cell). Downstream of this point, the ions feel an accelerating axial field from the space charge field of the maximum ion density. Hence, the space charge within the cell may act to introduce an axial field gradient which assists with 'pushing' the ions through the cell.

Thermalization of the ions is associated with a broadening of the distribution of ion transit times through the cell, and hence a degree of homogenization of the ion beam takes place within a near-thermal pressurized cell. This has a significant benefit when the correlation of signals from a noisy ion source (such as the ICP) is desired, as is discussed later in Section 8.2.2. It also induces an effect known as cross-talk, which is related to the finite time required for the ion distribution to stabilize after a change in ion population. This is a well-known phenomenon in organic mass spectrometry, where the pressurized collision cell is typically capacitively coupled to a mass filter. When the mass filter is adjusted to a different mass, a certain time is required for the ions to redistribute within the collision cell, which causes a lag in the response. If the settling time of the mass filter/detector is too short, either or both of two observations might be made: the apparent ion signal corresponding to the new mass may be suppressed because these ions have not yet 'filled' the collision cell, or ions that were present in the prior state are still apparent. The matter has been discussed by several authors [95,96] for the organic MS/MS application.

Lock and Dyer [96] showed that a voltage gradient along the cell of only 1 V is sufficient to reduce the mean residence time to substantially

less than 1 ms, and this alleviates cross-talk. Several means to provide this axial field have been proposed and/or evaluated [60,96–99]. A proprietary electrode configuration for the cell, modeled after the configuration described by Loboda et al. [100] has recently been introduced under the name Axial Field Technology in a commercial ICP-MS instrument (the ELAN DRC^{Plus} from Perkin Elmer SCIEX). In this instance, the axial field is generated by the addition of electrodes, inserted between the active rods of the cell quadrupole, which produce an axial field gradient of approximately 0.2 V/cm when a DC potential of 200 V is applied to the electrodes. Under conditions where there is more than 1 collision/cm (i.e. typically >2 collisions/cm for near-thermal conditions), the field typically adds less than 0.1 eV to the collision energy, which corresponds to a temperature of less than 1000 K [101]. Accordingly, the axial field does not vigorously accelerate the ions through the cell; rather it 'herds' the slower ions towards the exit, thus compressing the arrival time distribution. While these additional electrodes might be expected to introduce an octapolar component to the r.f. field, the quadrupolar stability characteristics are dominant and the stability boundaries remain sharply defined, as shown in Fig. 15. The slight broadening of the apparent stability boundaries, compared to Fig. 13 likely stems from a possible approximately 5% imbalance in the applied axial field in the prototype instrument which increases (in the experimental configuration used) the value of the *a*-parameter.

The principal benefits of incorporating a DC axial field are obtained for a thermal (or near-thermal) cell and include: compression of the transit time distribution (allowing for more rapid scanning), increase of the space charge limit (alleviation of concomitant element effects), improved sensitivity (particularly with heavier reaction gases where the provision of a directed drift field helps to overcome scattering losses), and suppression of clustering reactions (because these reactions are very sensitive to the effective collision temperature) [102]. Hattendorf and Günther [79] showed, for a DRC cell not provided with an axial field, that the $^{24}Mg^+$ signal could be suppressed using short dwell times following a mass jump from $^{238}U^+$ when the bandpass for the latter does not include the lower mass ion, as shown in Fig. 16a. Increasing the dwell (measurement) time, which essentially allows longer time for stabilization of the ion distribution in the cell following the bandpass adjustment, eliminates the signal suppression. The same instrument was later operated with an axial field using the original short dwell times, and the need for additional recovery time following a bandpass jump from high mass was eliminated, as shown in Fig. 16b.

8. Ion chemistry in r.f. devices for analytical ICP-MS

8.1. Vacuum considerations

The gas dynamics of conventional ICP-MS are understood well enough for many instrument design purposes [68,92,103–106]. Flow through the sampler is characterized as continuum, and the central core of this expansion is skimmed at the skimmer. In the absence of distortions, which may be related to cone geometries, the flow downstream of the skimmer is supersonic, and the ions gain energy from the expansion that is proportional to their mass. This should yield an ion beam characterized by mass-dependent kinetic energies with a narrow energy distribution that differs in the axial and radial directions (high non-thermal energy, but relatively narrow distribution in the axial direction and low thermal distribution in the radial direction). Baranov and Tanner [107] have shown that the true axial energy distribution may be multimodal due to the effect of rarefaction waves downstream of the skimmer, and that the observation of these several energy distributions is a function of the plasma conditions and ion masses. Niu and Houk [68] have identified a disturbance at the skimmer that may be related to this. Olney et al. [106] have studied the beam dispersion downstream of the skimmer.

At least four configurations of the vacuum system for an ICP-MS instrument incorporating a collision/reaction cell may be envisaged:

1. the cell is entirely within the ion optics (first high vacuum) chamber;

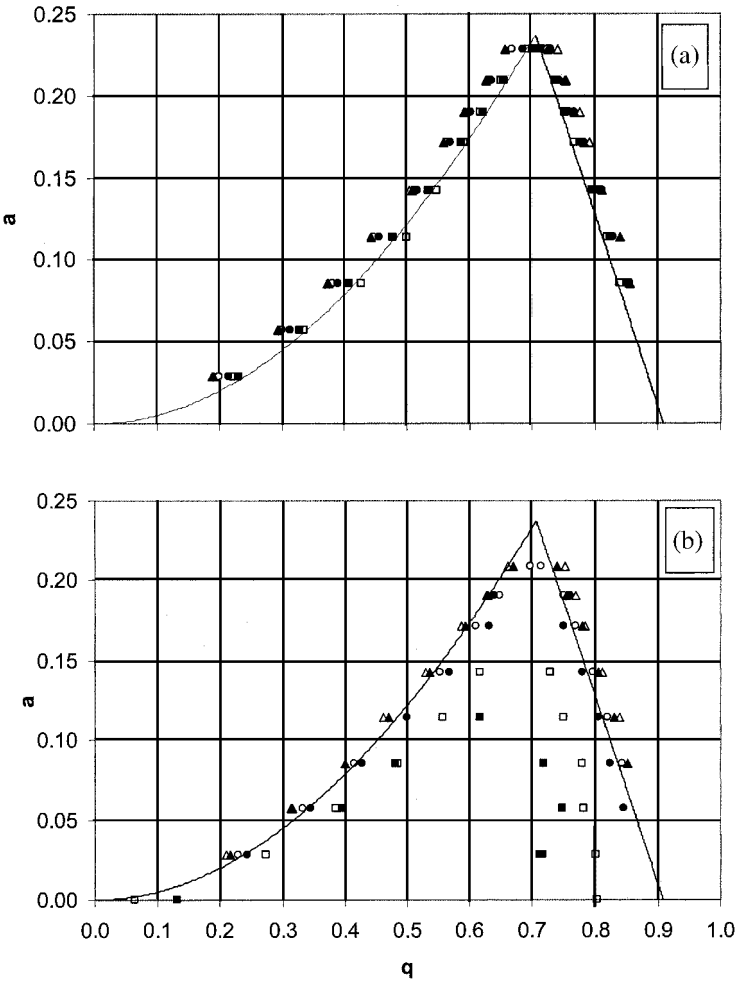

Fig. 15. Stability boundaries for the quadrupole reaction cell, defined as the point at which the absolute ion signal falls below 10 cps, measured for $^{7}Li^{+}$ (■), $^{24}Mg^{+}$ (□), $^{59}Co^{+}$ (●), $^{115}In^{+}$ (○), $^{159}Tb^{+}$ (▲) and $^{238}U^{+}$ (△) for data obtained and manipulated in the manner described for Fig. 13, with the exception that an axial field was established with the incorporation of shaped electrodes placed between the quadrupole rods. Data obtained under essentially collisionless conditions (reaction gas flow stopped and cell vented to mass analyzer chamber, $\approx 2\times10^{-5}$ torr) are given in (a), and for the cell pressurized with Neon (0.5 Ar-equivalent sccm = 0.525 sccm, $\approx$ 7 mtorr) in (b).

2. the cell is entirely within the mass analyzer (second high vacuum) chamber;
3. the cell is entirely within an additional vacuum chamber between the ion optics and mass analyzer chambers; and
4. the cell communicates between the ion optics and mass analyzer vacuum chambers.

Let us consider the vacuum pump requirements for a system that incorporates a conventional (sampler–skimmer) interface. The flow through the interface into the ion optics chamber is characterized as continuum and is proportional to the product of the squares of the diameters of the sampler and the skimmer and is inversely proportional to the square of the separation of the sampler and skimmer [103]. For a typical ICP-MS instrument (sampler diameter 1.14 mm, skimmer diam-

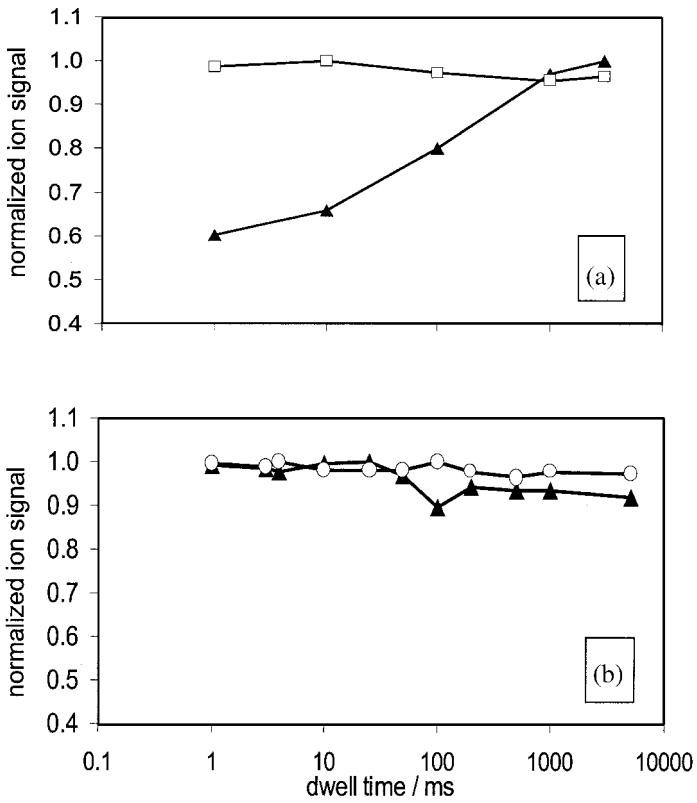

Fig. 16. Normalized ion signals for $^{24}Mg^+$ (▲) and $^{238}U^+$ (□) or $^{208}Pb^+$ (○) as a function of dwell (measurement) time in a pressurized cell. The ions were sequentially measured with a settling time of 3 ms with (RPa, RPq) = (0, 0.45). Accordingly, Mg^+ was rejected from the cell (outside of the bandpass) when the high mass ion was measured. (a) Without axial field, the Mg^+ signal is can be suppressed at short dwell times (insufficient time to re-establish the ion distribution within the cell). (b) With an axial field, the ion distribution within the cell is rapidly re-established and the measured signals are largely independent of the dwell time. ((a) Adapted from Ref. [79] with permission.)

eter 0.88 mm, sampler–skimmer separation 6.9 mm), the flow of source gas into the ion optics chamber is approximately 10^{19} atoms/s. It is generally desirable to provide conditions such that the ions suffer less than 1 collision with background gas in the ion optics chamber. The number of collisions that an ion suffers is the length that the ion travels in the chamber divided by the mean free path. For a collision cross-section of 50 Å^2 and a path length in the ion optics chamber of 5 cm, the required pressure is approximately 1.1 mtorr (4×10^{13} molecules/cm^3). A vacuum pump speed of approximately 250 l/s is required to provide this pressure. In the absence of a collision/reaction cell, the ion optics chamber usually communicates with the mass analyzer chamber via a differential pumping aperture. The type of flow through this aperture is determined by the Knudsen number, Kn, which is defined as the mean free path divided by the diameter of the aperture. Continuum flow is prescribed for $Kn < 0.01$, effusive flow for $Kn > 10$, and transition flow reigns between these limits. The pressure required of the mass analyzer chamber, in the instance that a quadrupole mass filter is used, is usually defined such that the mean free path is substantially greater than the path length of the ions within the quadrupole. Let us assume that the path length is of the order of 30 cm (for a 20-cm quadrupole, where the additional path length corresponds to the radial

excursions of the ions in the r.f. field). If we require fewer than 0.1 collisions per ion within the quadrupole, the required pressure is then of the order of 2×10^{-5} torr. If the differential pumping aperture has a diameter of 3 mm, then Kn = 17 and the effusive flow through this aperture is 2.7×10^{16} molecules/s. The required pump speed for the mass analyzer chamber is then 40 l/s. If a collision/reaction cell is present and gas is added to the cell, the pumping requirements are increased. While the actual pumping requirements are strongly dependent on the instrument configuration (aperture diameters, conductances, etc.), we estimate in Table 3 the pump speeds required for the four generic instrument configurations described above as a function of cell gas flow, where we have assumed for simplicity that the cell is enclosed and has entrance and exit aperture diameters of 2 mm.

The collision/reaction cell entrance is usually coaxially aligned with the ion source in order to optimize transmission of ions into the cell. If the source flow is not impeded, the pressure at the inlet is greater than the ambient pressure of the chamber with which it communicates. This is because the ion source is usually at higher pressure than the pressure of the chamber in front of the cell. The expansion of gas from the source imparts a directed flow which produces an impact pressure at the cell entrance. If the cell is exposed directly to the flow from the sampler and skimmer, the supersonic expansion generates an impact pressure of the order of 10–50 mtorr [106], though it could be as high as several torr [105] for a closely coupled cell. If the effective source is a blunt aperture downstream of the skimmer, the impact pressure at the cell entrance is a function of the flow characteristics emanating from the effective source, as described by Tanner et al. [104,105], and of the position of the cell relative to the aperture; accordingly, the impact pressure is expected to be about an order of magnitude less than for unimpeded flow, i.e. a few to a few 10s of mtorr [105,106]. Of course, the flow of source gas into the cell is a function of the cell pressure and of the impact pressure at the cell entrance. If the cell pressure is lower than the impact pressure (though it may be higher than the ambient pressure), source gas flows into the cell. This is particularly important as the ICP source gas may contain up to 17% H and O in the bulk Ar [68]. Accordingly, unimpeded exposure of the cell entrance to the directed flow of the source gas is a major source of contamination of the cell gas and causes unintentional chemical modification (e.g. oxidation) of the analyte ions in the cell. Further, substantial penetration of Ar can lead to increased scattering losses and energy damping (important if kinetic energy discrimination is used). Positioning of the cell at right angles to the expansion, or disruption of the directed flow by use of a photon stop, shadow stop or chicane lens in front of the cell, provided that a pressure differential across the latter is avoided, reduces the impact pressure to the ambient pressure and minimizes incursion of source gas into the cell (depending, of course, on the pressures of the cell and the chamber, and on the Knudsen number at the cell entrance).

The pressure within the cell is determined by the net flow into and out of the cell. This flow includes the intentional flow of collision/reaction gas, the flow of plasma gas into the cell through the entrance aperture (when the cell pressure is less than the impact pressure), and the flow of gas out of the cell through the exit aperture, the vent opening (if present and open) and the entrance aperture (if the cell pressure is greater than the source gas impact pressure). If the cell communicates between the ion optics chamber and the mass analyzer chamber, and no collision/reaction gas is introduced and a suitably large vent communicates between the cell and the high vacuum chamber, the pressure in the cell approaches the pressure of the mass analyzer chamber (for the ELAN DRC, the cell pressure in this mode is of the order of 2×10^{-5} torr). In this instance, the mean free path is of the order of 300 cm. At low r.f. amplitude and frequency and relatively high ion kinetic energy, the path length of the ion trajectory through the cell is approximately the length of the cell. If the cell is 12.5 cm long, the number of collisions suffered by an ion under the given conditions is approximately 0.04; that is, 1 ion in 25 suffers a single collision. Because the cell pressure is less than the ambient pressure, the gas composition of

Table 3
Estimated vacuum pump speeds for four generic cell configurations

Mass of cell gas (amu)	Flow of cell gas (sccm)	Cell pressure (mtorr)	Conventional (no cell)		Config. 1		Config. 2		Config. 3			Config. 4	
			Optics pump (l/s)	Analyzer pump (l/s)	Optics pump (l/s)	Analyzer pump (l/s)	Optics pump (l/s)	Analyzer pump (l/s)	Optics pump (l/s)	Intermed pump (l/s)	Analyzer pump (l/s)	Optics pump (l/s)	Analyzer pump (l/s)
	0	0.02	257	39									
2	0.1	0.5			259	39	257	146	257	50	9	258	54
2	0.3	1.4			263	39	257	360	257	50	23	260	161
2	0.5	2.4			267	39	257	574	257	50	36	262	268
2	1.0	4.7			277	40	257	1109	257	50	70	267	535
2	3.0	14.2			315	42	257	3250	257	50	205	286	1606
4	0.1	0.7			259	39	257	124	257	50	6	258	43
4	0.3	2.0			262	39	257	294	257	50	13	259	128
4	0.5	3.4			265	39	257	464	257	50	21	261	213
4	1.0	6.7			273	39	257	890	257	50	40	265	425
4	3.0	20.1			303	40	257	2592	257	50	115	280	1276
20	0.1	1.5			258	39	257	107	257	50	2	258	34
20	0.3	4.5			261	39	257	244	257	50	5	259	103
20	0.5	7.5			263	39	257	381	257	50	8	260	171
20	1.0	15.0			270	39	257	723	257	50	14	263	342
20	3.0	45.0			294	39	257	2092	257	50	42	276	1026

(1) The cell is entirely within the ion optics (first high vacuum) chamber. (2) The cell is entirely within the mass analyzer (second high vacuum) chamber. (3) The cell is entirely within an additional vacuum chamber between the ion optics and mass analyzer chambers. (4) The cell communicates between the ion optics and high vacuum chambers. These configurations do not represent any commercial instruments. *Assumes:* sampler diameter = 1.14 mm, skimmer diameter = 0.88 mm, sampler–skimmer spacing = 6.9 mm; cell is enclosed with 2 mm apertures at entrance and exit; all differential pumping apertures are 3 mm diameter; does not include entrainment of source gas into cell; pump efficiency relative to Argon: H_2 (0.62), He (0.78), Ne (0.97); backing pump speed is not a limitation; pressure requirements as given in text.

the cell is essentially the plasma gas composition or condensates thereof. Accordingly, the majority of the few collisions that occur are with Ar and do not result in a change in the ionic composition of the beam. If the plasma gas contains 8% O, as suggested as a maximum by Niu and Houk [68], 8% of the collisions, or 1 in 300 ions, suffers a collision with an oxygen atom. In the unlikely instance that every such collision results in the formation of an oxide ion (unlikely because such processes require a second collision to stabilize the product ion), the oxide ratio should increase by approximately 0.3%. Accordingly, the ion distribution should remain nearly identical to the plasma source distribution. (If all of the oxygen appears in polyatomic form, such as H_2O or OH, a stabilizing collision for the condensation product ion is not required and the prediction of $\approx 0.3\%$ increment in the oxide ratio is more justified.) The actual distance that an ion travels in its traverse of the cell is a function of the ion energy and of the r.f. amplitude and frequency, since the ion responds to the r.f. field. Assuming that the r.f. amplitude is relatively large so that the ion responds with a substantial displacement on each r.f. cycle, that the r.f. frequency is 1 MHz and that the ion energy is 20 eV (if there are few collisions, the ion energy is not efficiently damped), the ion experiences approximately 13 r.f. cycles. It might be reasonable to assume that the incremental path length during each r.f. cycle is of the order of 0.24 cm (this depends on the r.f. amplitude and the construction of the cell), so that the path length traversed by the ion increases to approximately 15 cm. The conclusion that the ion distribution is largely unperturbed from its source distribution remains valid. Accordingly, a vented reaction cell operating at approximately 2×10^{-5} torr emulates a conventional ICP-MS instrument.

If the cell is entirely within the ion optics chamber, the pressure in the cell will be at least the ambient pressure (and greater than this if the impact pressure is significant). Assuming that the cell pressure is then of the order of 1 mtorr, the mean free path decreases to 5.5 cm. Now, for a cell of length 12.5 cm, each ion suffers on average approximately 2 collisions (actually, more than this, because the ion energy is damped after each collision, so that the residence time increases and the number of r.f. cycles encountered increases with a concomitant increase in the path length traveled). In this instance, 1 in 6 ions will have a collision with an oxygen atom (if present as 8% of the gas in the cell), and since multiple collisions exist it is more probable that the resultant oxide ion will be stabilized. Accordingly, the ion distribution should shift significantly toward the formation of oxide ions (and other product ions, depending on the composition of the plasma gas entering the cell).

When the cell is operated as a collision/reaction cell, with the intentional addition of gas to the cell, the pressure is typically of the order of 1–30 mtorr. This pressure regime is difficult to measure reproducibly, since there are few types of gauges that will read in this range reliably, and those that do often suffer from hysteresis following a pressure pulse (for example, when the vacuum system is vented to atmosphere). Accordingly, it is common to infer the pressure of the cell from the knowledge of the flow rate of gases into and out of the cell. The flow regime at the entrance and exit lenses is likely in the transition regime between molecular (effusive) and viscous (continuum) flow, but a reasonable approximation of the flow through the cell apertures is to be had by assuming effusive flow. The equations appropriate for effusive flow are well known and may be found, e.g. in Ref. [92]. It should be recognized that the effusive flow rate is inversely proportional to the square root of the mass of the gas; thus a higher mass gas will yield a higher cell pressure because its flow out of the cell is less. This dependence is seen in Fig. 17, which approximates the cell pressure for an ELAN DRC as a function of the true flow of reaction gases of different masses.

The flow of collision/reaction gas into the cell may be controlled through a critical flow orifice or a needle valve, though it is probably most common to use a mass flow controller. It must be remembered that the calibration of a mass flow controller is dependent on the type of gas that is flowing. It is most common to calibrate the mass flow controller for either argon or nitrogen, and to make corrections based on the flow properties of the gas. Many such correction factors are available

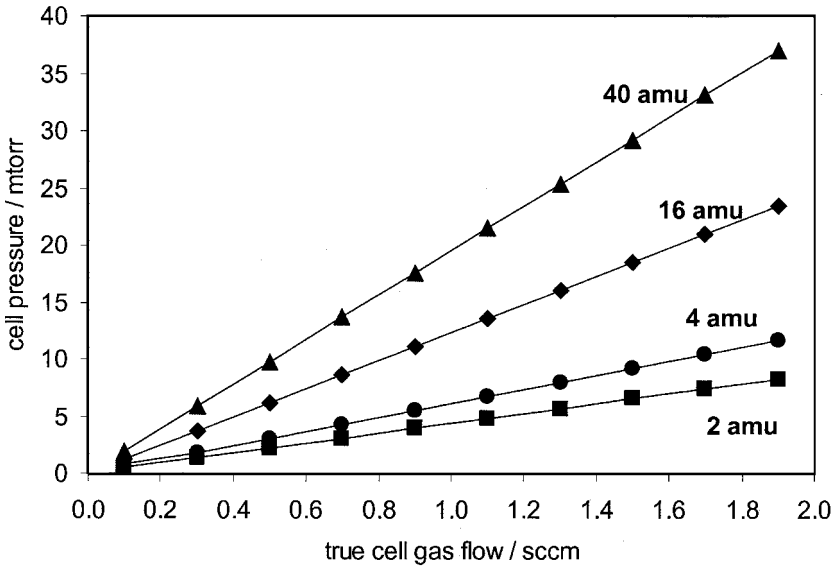

Fig. 17. Calculated pressure in a reaction cell as a function of flow rate of neutral gases having different molecular weights. Once sufficient gas is introduced into the cell to exceed the external (ion optics chamber) ambient pressure and the impact pressure at the entrance to the cell, the pressure may be estimated assuming effusive flow exiting through both the cell entrance and exit apertures. Effusive flow is proportional to the inverse square root of the molecular mass, and hence a higher mass gas establishes a higher pressure. In reality, the flow is at best transitional between effusive and continuum, and the model assumes thin plate apertures of diameter 2.0 and 2.2 mm. Hence, the model does not precisely describe the ELAN DRC, but the result is a reasonable approximation to expectation and experiment for this instrument.

or can be calculated, and those for some of the common gases used for the ICP-MS application are given in Table 4.

Once the true flow of the collision/reaction gas is known, and the flow into and out of the apertures of the cell are accounted for, the pressure within the cell can be approximated. When the cell pressure is less than the impact pressure, the cell gas must be contaminated by plasma gas. As the cell pressure increases, the incursion of plasma gas decreases until it is effectively excluded (other than for mixing in the aperture region; if the entrance aperture is tubular, the probability of source gas migrating against the pressure differential into the source is small). Now, if the cell is entirely within the ion optics chamber, the gas that subsequently enters the mass analyzer chamber is a mixture of the plasma gas and the collision/reaction gas, according to the relative flow rates of the two. The mass analyzer chamber pressure will increase only slowly with collision/reaction gas flow until the flow of cell gas is comparable to the flow of source gas into the optics chamber. If the cell communicates directly with the mass analyzer chamber (i.e. the only opening is the cell exit aperture), the gas that flows into the mass analyzer chamber is entirely cell gas, and the pressure of the mass analyzer chamber will change in proportion to the pressure of the cell. However, the pressure of the mass analyzer chamber is most often measured with a Bayert–Alpert type ionization gauge, which is sensitive to the composition of the gas. In the instance that the gas in the mass analyzer chamber is a pure gas, corrections factors are available. Assuming that the ionization gauge has been calibrated for N_2, the correction factors for some of the common gases for the present application are given in Table 4.

When the cell is pressurized above the impact pressure, a portion of the cell gas flows into the optics chamber through the cell entrance aperture. Then the gas within the ion optics chamber con-

Table 4
Gas correction factors for mass flow controller and for Bayert–Alpert gauge

Gas	MFC factor[a]	BAG factor[b]
Air	0.72	1.00
Ar	1.00	0.78
C_2H_6	0.36	0.38
C_3H_8	0.26	0.24
CH_3Cl	0.44	
CH_3F	0.40	
CH_4	0.52	0.71
CO	0.72	0.95
CO_2	0.50	0.70
D_2	0.72	2.86
H_2	0.70	2.17
H_2O		0.89
He	1.01	5.56
Kr	1.11	0.52
N_2	0.72	1.00
N_2O	0.51	
Ne	1.05	3.33
NH_3	0.53	0.81
NO	0.71	0.87
NO_2		
O_2	0.71	0.99
SF_6	0.19	0.45
Xe	0.95	0.35

[a] Assumes that MFC is calibrated for Ar; true flow = MFC reading × MFC factor.

[b] Assumes BAG is calibrated for N2; true pressure = BAG reading × BAG factor.

tains a fraction of cell gas in addition to the source gas. The fractional composition of the gas in the optics chamber is determined by the relative flow rates of the source gas (through the skimmer) and the cell gas (through the cell entrance aperture). For example, for the ELAN DRC pressurized to 20 mtorr with ammonia, the optics chamber pressure increases by approximately 5%. If the path length in the optics chamber (the distance between the skimmer tip and the cell entrance) is 5 cm, and the pressure in the optics chamber is of the order of 1 mtorr (so that the mean free path is ≈ 5 cm, and each ion suffers, on average, 1 collision), approximately 1 of each 20 ions will suffer a collision with an ammonia molecule during its transit between the skimmer and the cell. These collisions are generally non-thermal (the ions are extracted into the cell under a potential difference) and the reaction probability is consequently reduced, but the potential for a degree of pre-reaction exists, and these pre-reactions may support endothermic reaction channels.

The considerations given here suggest that if the cell pressure is less than the impact pressure at the cell entrance, the purity of the collision/reaction gas is a lesser concern since the cell must be contaminated with plasma gas regardless. If the cell pressure is substantially greater than the impact pressure, so that incursion of plasma gas into the cell is less probable, there is value in ensuring that high purity cell gases are used. This concept then allows an opportunity to dispel a misconception that is commonly held: that reactions of ions with the neutral products of prior reactions in the cell can be important. For example, it has been said that the O atoms produced in the dissociation/reaction of ArO^+ in the cell, or O atoms produced in the neutralization of O^+, might participate in further ion–molecule reactions. In fact, this is a very improbable occurrence. The total number of ions measured for a typical ICP-MS mass spectrum is of the order of 10^{11} cps. Assuming that the transmission efficiency of the mass analyzer is of the order of 10%, it may be concluded that the total number of ions entering the collision/reaction cell is of the order of 10^{12}/s. If every one of these ions contained an oxygen atom that was released as a neutral O atom following collision in the cell, the total 'flow' of O atoms into the cell through this route would be 10^{12}/s. A flow of reaction gas of 1 sccm contributes 4.5×10^{17} molecules/s. Therefore, the maximum partial pressure of the O atoms generated from reaction of ions within the cell is of the order of 2 ppm. That is, one of each 500 000 collisions may be with the product of a prior reaction. Even at the highest cell pressures, few ions experience more than 100 collisions. Therefore, even in the extreme case, only 1 of each 5000 ions can be expected to experience a collision with a neutral product of a prior reaction. Further, since most of the products of the prior reactions can be expected to be atomic, and the probability of formation of a stable condensation product ion resulting from reaction with an atom in a single collision is small (because a third body collision is then required to stabilize the product ion), the contribution of such reactions must be

small. Therefore, in most instances, reactions of ions with neutrals derived from source ions is inconsequential, and the observation of unexpected oxide ions most probably reflects contamination of the cell gas by other means. The exception is the instance when the precursor ion is abundant and the background at the product ion is low such that the maximum contribution of 0.02% of the precursor ion through this route might be observed.

8.2. Reaction energy

8.2.1. Thermalization and collisional focusing

Under usual operating conditions, ions must be accelerated (using an entrance aperture bias potential) through a counter flow of gas in order to enter the cell. In this instance, the ions enter the cell with a relatively large axial kinetic energy, and the initial collisions with the cell gas are energetic. If the energy in the center of mass (Section 5.2) exceeds the endothermicity of a feasible reaction channel, that reaction process may be enabled. This mechanism has been invoked by Douglas [20] to explain the relatively large loss cross-sections for small ions introduced into a collision cell at 50 eV (i.e. promotion of endothermic charge transfer).

In most collisions (Section 5.1), the ion transfers a fraction of its kinetic energy to the collision neutral, and the ion energy is damped. In the usual instance for ICP-MS, the axial kinetic energy of the ion is significantly greater than the radial energy, and the first step in the collisional damping of the ion's axial energy is transfer to (excitation of) the ion's radial energy. In an electrostatic collision cell (without r.f.), this radial excitation would likely lead to an increased probability of ion loss. This is one of the advantages of the r.f.-driven collision cell: the restoring force provided by the r.f. drives the radially excited ions back toward the cell axis. Transfer of energy from axial to radial excitation continues until the two modes approach equilibrium, and then both translational degrees of freedom relax together. Eventually, the axial energy should be completely relaxed to near-thermal, under which conditions the ion motion in the axial direction is close to Brownian. However, the radial energy does not completely relax, as it

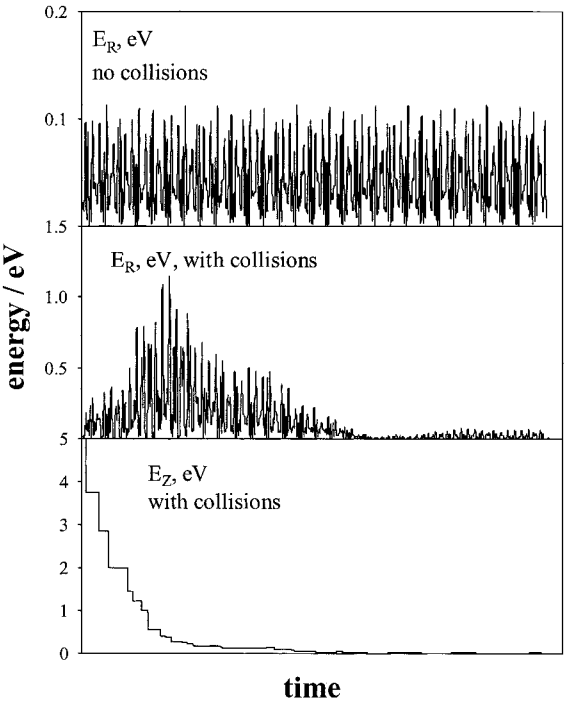

Fig. 18. Calculated radial and axial energy as a function of time for an ion in an r.f.-only quadrupole. The upper figure shows the radial energy in the absence of collisions. The middle figure shows the initial increase and then decay of radial energy resulting from conversion of axial energy to radial energy, followed by an approach to equilibrium, caused by collisions with the gas. The lower figure shows the decay of the axial energy caused by collisions with the gas. (From Ref. [28] with permission.)

continues to be excited to a degree by the r.f. field. At pseudo-equilibrium, the total ion energy is distributed between the radial, azimuthal and axial degrees of freedom, with radial being dominant due to the r.f. excitation. The magnitude of the total pseudo-equilibrium energy is a function of the operating parameters (a, q), and of the number of collisions per r.f. cycle (and is thus dependent on the pressure and r.f. frequency). For typical operating conditions ($q<0.6$), the total energy at pseudo-equilibrium may be of the order of 0.1 eV, which is near-thermal. A model describing the process of thermalization for the ICP-MS application has been reported [28]. Fig. 18 shows the energy transfer and relaxation due to collisions in an r.f. device.

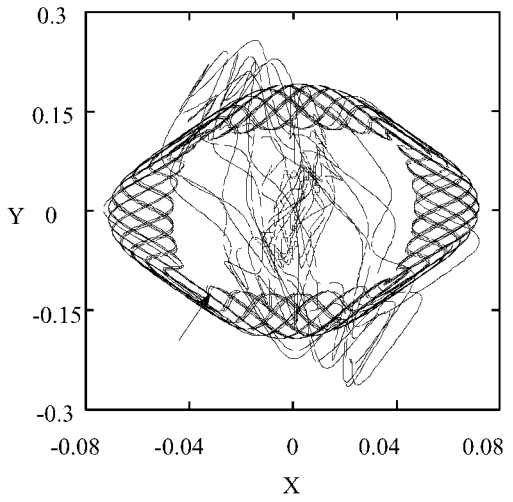

Fig. 19. Calculated trajectories with (lighter shaded) and without (darker shaded) collisions for an ion in a quadrupole r.f. field at $(a, q) = (0, 0.4)$. The same initial modeling conditions were used, and the initial displacement is indicated by the arrow. Without collisions, the ion trajectory is bound by an outside and an inside surface, as a result of the requirement for conservation of the total energy and the angular momentum, respectively. Collisions involve transfer of energy (axial to radial, and ion to neutral), and the ion displacement initially increases then collapses towards the quadrupole axis. (From Ref. [28] with permission.)

Fig. 9 showed an initial increase in ion signals at low flows of gas that was ascribed to collisional focusing [50,51]. The effect is significant for non-reactive ions ($k \ll k_L$). It is less pronounced for moderately reactive ions because the gain in sensitivity is offset by the reactive loss. For highly reactive ions ($k \geqslant k_L$), collisional focusing cannot occur because each collision is successful at converting the ion. The effect is intimately connected with energy damping and thermalization, where the reduction of ion energy causes the ions to migrate towards the minimum of the effective potential well (Section 7.3) near the multipole axis. The effect is shown by trajectory modeling in Fig. 19. Under collisionless and approximately adiabatic conditions, ion motion in the multipole is bound by the requirements for conservation of energy and momentum. Collisions, transferring axial energy into radial energy, first cause an increase in the magnitude of the radial excursions, and then the ions collapse towards the axis as the axial and radial energies relax together. Collisional focusing can be used in order to increase the analyte ion intensity by factors of 2–5. This increase directly improves the detection limit because the corresponding continuum (photon) background is not increased; even if the background is spectral, an improvement of the detection limit on the order of the square root of the intensity gain is obtained because of counting statistics (or more, if temporal homogenization is improved, as discussed in Section 8.2.2).

The benefits of collisional focusing are not yet widely adopted in the ICP-MS application partially due to the novelty of the technique and perhaps because of a perception that the reaction cell in the pressurized mode should be used only for interfered analytes. Several aspects should be considered if the benefits of collisional focusing are to be employed. To improve sensitivity, non-reactive gases ought to be carefully selected. The mass of the collision gas should be below that of the analyte ion in order to minimize scattering; the gas should be thoroughly dried to avoid any reactions with contaminant water vapors; and the gas flow control manifold should be sufficiently stable (with respect to flow and composition of the gas in the cell) to allow quantitative analysis on the top of the optimization mountain.

The thermalization of the ions has at least four important ramifications. (1) As the ion energies are relaxed, collisional focusing improves the transmission efficiency through an on-axis exit aperture of the cell. The improvement in sensitivity for non-reactive ions is a function of several parameters (number of degrees of freedom of ion and neutral, mass ratio, operating point, etc.). It is important also to determine that the background does not increase disproportionately, as in some instances new interferences may limit the improvement in analytical performance (Sections 8.3 and 8.4). (2) The collision cross-section increases with reduction of ion energy, leading to a higher number of collisions and, thus, a higher efficiency of reaction. At energies above approximately 1 eV, the interaction of the ion with the neutral is sufficiently short that polarization of the neutral does not occur to an appreciable extent. Under this

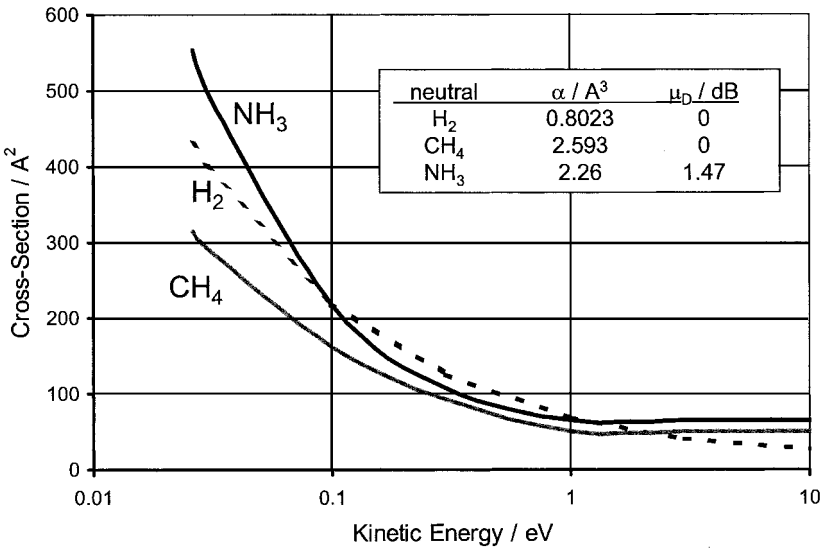

Fig. 20. Calculated collision cross-sections as a function of ion kinetic energy. Above approximately 1 eV, the cross-section is dominated by the 'hard sphere' physical sizes of the collision partners. Below approximately 0.5 eV, electrostatic interaction effects increase the cross-section. α is the neutral polarizability and μ_D is the permanent dipole moment of the neutral. (From Ref. [65] with permission, ©Springer-Verlag.)

condition, the collision cross-section is essentially the hard-sphere cross-section determined by the sum of the physical radii of the collision partners. As the ion energy approaches thermal, the cross-section increases due to interaction with the induced and permanent (if any) dipole moments of the neutral. Fig. 20 shows the calculated cross-sections for interaction of Ar^+ ions with neutrals having different polarizabilities and dipole moments. A lower mass collision gas is less effective at damping the axial energy, as implied by Eq. (5.1). Bandura et al. [65] have shown that, at relatively high energy, the number of collisions experienced by the ion increases only slowly (linearly) with cell pressure, reflecting the dominance of the (energy-independent) hard-sphere collision cross-section (see also Fig. 20). The number of collisions as a function of cell pressure increases rapidly at energies lower than 1 eV due to the significant increase in the collision cross-section. Since the extent of reaction is exponentially dependent on the number of reactive collisions (given by $k\Delta t$[B] in Eq. (6.21)), the efficiency of the cell increases dramatically when near-thermal conditions are obtained. (3) Under thermal conditions, the specificity inherent in thermal chemistry may be used to improve chemical resolution of isobars. (4) The selection of an appropriate reaction gas is immensely simplified by reference to the existing (and growing) database of thermal rate constants [10,75–77]. These rate constants, and the product branching ratios, have for the most part been measured under assiduously thermal conditions, using techniques such as the FA [74] and SIFT [11,66]. Provision of a controlled thermal environment in the reaction cell, achieved through collisional thermalization, allows direct application of these data in the development of new methods.

8.2.2. Temporal homogenization

Collisional focusing is also accompanied by collisional cooling, wherein substantial reduction of the average ion kinetic energy and of the width of the energy distribution is achieved. It can be expected that collisions in the pressurized device should also modify the arrival time distribution of ions. The fact that short transient signals are broadened in the pressurized multipole was recently used in a collisional damping ion transmission device for decoupling a pulsed MALDI ion source

from a continuous beam orthogonal-acceleration time-of-flight mass-analyzer, as described by Krutchinsky et al. [108]. Collisional broadening of the ion pulses allowed, in this case, the conversion of a pulsed ion beam into a quasi-continuous beam, with average arrival times for MALDI ions of Dalargin, Substance P, Melittin and Insulin ranging from 9 to 26 ms and half-width of the arrival time distributions of the same order. It was observed that the average arrival time depends on the pressure in the device [108] and on the DC potential difference between the entrance and exit aperture plates and the quadrupole rods [52]. Work performed in our laboratory for elemental ions from an ICP suggests that the degree of the collisional broadening in a pressurized r.f. quadrupole also depends on the target gas (dipole moment and polarizability, as well as the number of vibrational degrees of freedom) and on the Mathieu parameter q of the quadrupole [109]. Arrival time distribution profiles for $^{107}Ag^+$ ion pulses transmitted through a r.f.-only quadrupole pressurized with different gases is given in Fig. 1 of Ref. [109]. Polyatomic gases, even if lighter, produce more significant broadening. This can be attributed to more rapid thermalization of the ions due to a larger fraction of the translational energy being converted into internal energy of the polyatomic target, and also to the higher number of collisions with the polyatomic target gases due to their higher polarizability and thus higher (thermal) collisional cross-section. The dependence of the arrival time distribution on the operating parameter q is attributed to a combination of r.f.-heating, the depth of the pseudopotential well, and the dependence of the stability characteristics of the dominant ion population in the quadrupole on q. As plasma matrix ions enter the pressurized quadrupole at a rate of $\approx 10^{12}$ ions/s, the stability of the dominant ions and the development of a space-charge hill can play a major role in defining the residence time of other ions in the device.

Collisional damping has been used to homogenize the fluctuations of the ion beam extracted from an ICP [110] in order to improve the precision of the isotope ratios measured by a quadrupole analyzer. As collisional broadening occurs on a time scale of several milliseconds, fluctuations of the ion current at high and intermediate frequencies are smoothed, resulting in better correlation between sequentially sampled ion populations. It was shown that the collisional homogenization allows achievement of the counting statistics limit for the isotope ratio internal precision, with demonstrated precision of 0.02–0.03% R.S.D. for $^{107}Ag/^{109}Ag$, $^{207}Pb/^{206}Pb$ and $^{208}Pb/^{206}Pb$ ratios at sample concentrations of 40 ng/ml. Conventional methods for reduction of plasma noise, such as free sample aspiration or use of a torch bonnet, were not used. It was also shown that the external precision of Pb isotope ratios, measured for 7 samples at $n=9$ replicates per sample, was approximately $\sqrt{n}$ times lower than the internal precision, which indicated that the external precision was also defined by counting statistics only. When atomic gases are used for collisional homogenization, the number of collisions needed to achieve sufficient (on a millisecond scale) temporal homogenization can be enough to cause scattering losses of ion signal, so that the absolute value of ratio precision (for a given sample concentration), although being at its statistical limit, may not improve compared to non-pressurized cell operation. As polyatomic gases produce more significant damping of fast ion density fluctuations [108], a lesser number of collisions is required, and the absolute value of the ratio precision is improved. The most practical case of collisional homogenization is with use of a polyatomic gas for chemical resolution of isobaric interferences. Use of a reactive gas such as NH_3 allows simultaneous reactive removal of isobaric interferences and collisional homogenization of the analyte ion populations. It has been shown [109] that the ratios of the normally interfered isotopes ^{54}Fe, ^{56}Fe and ^{57}Fe can be measured by quadrupole ICP-MS at the counting statistics limited internal precision of 0.05–0.1% for a sample concentration of 50 ng/ml.

8.2.3. r.f. contribution to reaction energy

It should be evident that the r.f. contributes to the reaction energy through the radial excitation of the ions. The energy contributed in this fashion is essentially the pseudo-equilibrium energy discussed above. Accordingly, a higher reaction ener-

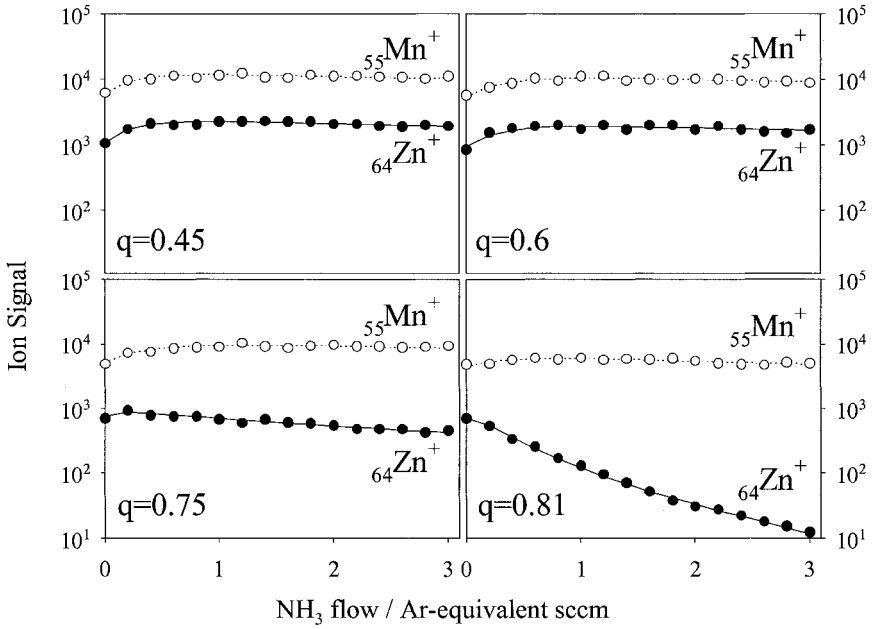

Fig. 21. Ion signals for Mn^+ and Zn^+ as a function of ammonia gas flow at several operating points, q, in the quadrupole stability diagram. Both ions are unreactive (or slowly reactive, perhaps scattered) at low and mid values of q. Reaction is promoted for Zn^+ at high q, while Mn^+ remains unreactive. Charge transfer for Zn^+ and Mn^+ with ammonia is endothermic (at room temperature) by 0.8 and 2.8 eV, respectively. The results suggest that the ion energies are less than 0.8 eV at low and mid values of q, but are above 0.8 eV due to the r.f. contribution to the ion energy under non-adiabatic conditions at high q. (From Ref. [28] with permission.)

gy is provided by a higher r.f. amplitude or by fewer collisions per r.f. cycle (i.e. a lower pressure or higher frequency). Competing with the latter is the breakdown of the adiabatic approximation at higher q, which appears to dominate. For example, Mn has an IP of 7.4 eV and Mn^+ is unreactive with NH_3 since charge transfer is 2.76 eV endothermic. Zn^+ is endothermic for charge transfer with NH_3 by only 0.78 eV. As shown in Fig. 21, neither Mn^+ nor Zn^+ are seen to react with ammonia at $q<0.7$. However, as q is further increased (by reducing the r.f. frequency; the r.f. amplitude was constant through this experiment), reaction of Zn^+ is facilitated, presumably by charge transfer, while Mn^+ remains unreactive (and serves as a normalizing signal to correct for potential scattering losses). It is concluded that the reaction cell employed contributes less than 0.8 eV to the reaction energy at $q<0.7$, but that the r.f. contribution to the reaction energy can be adjusted through the operating parameter q.

8.2.4. Transferability of methods

If methods are to be transferable from one instrument to another, and the methods take advantage of near-thermal chemistry, the instruments must provide similar thermal environments and a method must be available to validate this assumption. One means to determine the thermal characteristics of a reaction cell is to establish a thermodynamic ladder of reactions. A proposal for such a scheme has been made [28], and is given in Table 5. It is proposed that these reactions be investigated by measuring the reactant ion signal as a function of reactant neutral flow, in order to determine the lower limit of endothermicity supported by the instrument. For example, the reaction of Se^+ with NH_3 is observed to proceed (though the product ion was not observed, it is presumed to react by charge transfer) over a wide range of the operating parameter q [28] with an ELAN DRC. As noted above, the reaction of Zn^+ with NH_3 is observed only at $q>0.7$. Therefore, a lower

Table 5
Proposed reactions for thermodynamic evaluation of a reaction cell for ICP-MS

Ion		Reaction gas		Products			ΔH (kcal/mol)	ΔH (eV/mol)
Ce^+	+	O_2	→	CeO^+	+	O	−70.8	−3.1
Xe^+	+	O_2	→	O_2^+	+	Xe	1	0.058
Se^+	+	NH_3	→	NH_3^+	+	Se	9.3	0.4
Zn^+	+	NH_3	→	NH_3^+	+	Zn	18	0.78
I^+	+	O_2	→	O_2^+	+	I	36	1.6
Se^+	+	N_2	→	N_2^+	+	Se	133	5.8
CeO^+	+	H_2	→	Ce^+	+	H_2O	188.2	8.2

limit for the r.f.-field contribution to the reaction energy for this instrument is determined as <0.4 eV at low and mid values of q (consistent with the estimation given in Section 8.2.1), and this contribution increases at high values of q. It would be valuable to determine the consistency of these observations on different instruments of the same manufacture, and also across platform designs, in order to validate the concept that developed methods are transferable between instruments.

8.3. Sequential chemistry

The gas that fills the cell is usually reactive with at least some of the ions. Even if an intentionally non-reactive gas is used, reactive contaminants are commonly present either as an impurity or from entrainment of plasma gas into the cell. As long as ions and reactive gas components are in the cell, reactions may take place resulting in the formation of new ions that may be isobaric with an analyte of interest. If multiple collision conditions are provided, as required for efficient suppression of plasma-based interference ions, secondary reactions that may produce a ubiquitous chemical background are promoted.

For example, if a cell of length 12.5 cm is operated at a pressure of approximately 10 mtorr, the average ion experiences some 20 collisions. If an ion reacts on its first collision, the product ion on average may suffer a further 19 collisions. In this instance, there are some 20 banked levels of sequential chemistry. Because the ion flux into the cell is large (which distinguishes the ICP-MS applications from other mass spectrometries), even a gas contaminant at trace levels can produce significant levels of new interferences.

As an example, consider a subset of the reactions that can occur using methane as a reaction gas. It is known [10] that Ar^+ reacts with methane via dissociative charge transfer according to:

$$Ar^+ + CH_4 \rightarrow CH_4^+ + Ar \quad (8.1)$$

$$\rightarrow CH_3^+ + Ar + H \quad (8.2)$$

$$\rightarrow CH_2^+ + Ar + H_2 \quad (8.3)$$

The products of this reaction, if retained in the cell, react further. For instance, the CH_3^+ ion reacts with methane by condensation according to:

$$CH_3^+ + CH_4 \rightarrow C_2H_5^+ + H_2 \quad (8.4)$$

and the product ion of this reacts further according to:

$$C_2H_5^+ + CH_4 \rightarrow C_3H_7^+ + H_2 \quad (8.5)$$

In general, condensation and dissociative proton transfer reactions will generate a rich array of hydrocarbon ions:

$$C_nH_x^+ + CH_4 \rightarrow C_mH_y^+ + (\text{neutral products}) \quad (8.6)$$

with $m=1, 2,\ldots, n+1$ and $y=0, 1, 2,\ldots, x+4$.

Further, if a trace of water is in the cell, ions of the form $C_mH_yO^+$ are to be expected (in addition to oxide and hydroxide ions of elements in the sample).

Accordingly, a reaction cell operated at several mtorr methane, and which is not operated in a

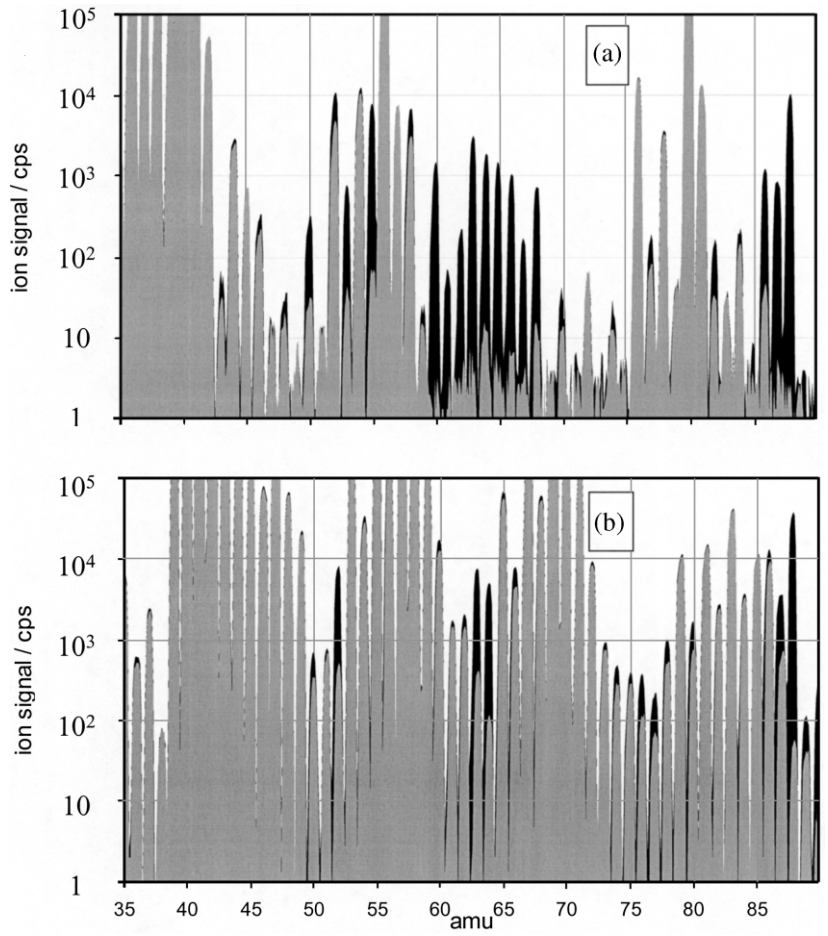

Fig. 22. Spectra obtained using an ELAN DRC^{Plus} with an axial field applied, for high purity water (grey) and a solution containing 1 ppb each of K, Ca, Cr, Mn, Fe, Ni, Cu, Zn, Se and Sr (black). (a) Standard mode (no gas added to cell, cell vented to mass analyzer vacuum chamber), with (RPa, RPq) = (0, 0.2), CPV (entrance and exit lenses of cell) = −16, CRO (cell rod offset) = −12 and QRO (mass analyzer quad rod offset) = +2. (b) DRC mode with CH_4 reaction gas flow = 0.92 Ar-equivalent sccm (0.48 sccm, ≈6 mtorr), with (RPa, RPq) = (0, 0.15), CPV = −18, CRO = −1 and QRO = −3.

manner to suppress either the formation or transmission of product ions, should be expected to show an elevated spectral background at many masses. Fig. 22a shows overlaid mass spectra for a DIW blank and a mixture of analyte elements each at 1 ppb recorded without reaction gas in the cell (i.e. 'standard mode' to emulate conventional ICP-MS). The relatively low spectral background in important regions of the spectrum allows sensitive determination of many elements (e.g. Ni (as $^{60}Ni^+$), Cu, Zn and Sr are readily observed), while K, Ca, Cr, Mn, Fe, ^{58}Ni and Se are obfuscated by argide ions (ArH^+, Ar^+, ArC^+, ArN^+, ArO^+, $Ar^{18}O^+$ and Ar_2^+, respectively). By contrast, the same spectra are shown in Fig. 22b with methane as a reaction gas under conditions where a broad range of ion masses are simultaneously stable in the cell. While some of the argide ion signals are substantially reduced in intensity, as a result of reaction with CH_4, a generally elevated spectral background is observed. This background is principally the hydrocarbon ions produced in sequential reactions, as discussed above. The resultant detection power of the instrument for elements

that are not normally interfered is seriously degraded by the secondary chemistry.

It should be evident that a reaction cell can be operated in a manner to efficiently reactively remove plasma-based interference ions (e.g. though the scales used make it less evident, the $^{40}Ar^+$ and $^{40}Ar_2^+$ signals in Fig. 22b are reduced by nearly 4 orders of magnitude relative to Fig. 22a), but this improvement is more than offset by the formation of new interferences at many masses. This then raises the issue of the three forms of efficiency that are required of the reaction cell: (1) efficient removal of plasma-based interference ions, (2) efficient transmission of analyte ions of interest, and (3) efficient suppression of the appearance of new interference ions produced in secondary chemistry in the reaction cell. As we have discussed above, the first two efficiencies are addressed by the selection of the reaction gas (reactive with one of the interference or the analyte) and the pressure of the gas (gas thickness) in the cell, and may be influenced also by electrical conditions under which the cell is operated (e.g. the end cap voltages and the r.f. amplitude). We now must address means of achieving the third dimension of efficiency: suppression of unwanted new ions produced in the cell. To make things more difficult, there are also instances in which it may be desirable to determine an analyte at a different mass, as the product of an atom transfer reaction; examples, including oxidation of V, hydroxylation of Sr and fluorination of Sr, are given in Section 8.4.3. When this is desired, it is also desirable to suppress the formation of other ions that might interfere at the same mass. Hence, a degree of selectability in the promotion and suppression of product ions in the cell would be valuable.

8.4. Secondary chemistry control

There are a number of possible means to control the appearance of secondary reaction product ions in the mass spectrum. Two of these dominate in today's instruments. Kinetic energy discrimination after the cell allows operation of the cell as a passive device (in the sense that the chemistry is allowed to proceed unhindered). In this method, resolution of the plasma ions from cell-produced ions is based on the kinetic energy difference between them. A potential energy barrier is established downstream of the cell and provides a degree of resolution of plasma polyatomic ions from atomic ions. Alternatively, the cell may be operated in a bandpass mode to establish a window of ion masses that are simultaneously stable within the cell and that rapidly ejects ions from the cell that are outside of this window in order to restrict the occurrence of secondary chemistry within the cell itself.

8.4.1. Post-cell kinetic energy discrimination

We earlier noted that ions are generally introduced into the cell with excess axial energy. This is because the cell is typically operated at higher pressure than the optics chamber that precedes it; therefore, the ions must be accelerated through the counterflow of gas emanating from the cell entrance aperture. Under conditions of high collision number, the ion loses axial kinetic energy sequentially in subsequent collisions until a near-thermal distribution of energies is obtained. The gas can be considered as essentially stagnant in these collisions. If the ion is substantially more heavy than the gas molecule and reacts with the gas by small charged particle transfer (an electron or proton), the resultant product ion remains nearly as stagnant as the reactant gas molecule was (essentially, E'_2 in Eq. (5.2)). Reaction of an ion by transfer of a heavy atom (e.g. O) also leads to a product ion having a lower kinetic energy, in part because at least a part of the product ion is derived from the stagnant neutral and, perhaps more importantly, because such reactions typically require a relatively long interaction time between the ion and neutral during which the kinetic energy of the partners is redistributed. Polyatomic ions, either as the reactant ion (perhaps sampled from the ion source) or as the product ion, present a special case. In this instance, some of the energy that is delivered to the collision complex from the ion's pre-collision kinetic energy can be redistributed into the internal degrees of freedom of the product (or original ion that has undergone collision without reaction) polyatomic ion. As a result, its post-collision kinetic energy can be lower than

the kinetic energy of an atomic ion of the same mass-to-charge ratio. Moreover, the polyatomic ions, due to their relatively large size, may have significantly larger hard-sphere collision cross-sections than those of atomic ions. As a result, at collision energies above approximately 1 eV, they experience a larger number of collisions and thus lose more kinetic energy per unit path length than atomic ions do. The difference in collision cross-sections generally diminishes at lower energies, as they are then defined principally by the ion–dipole interaction (which is a function of the neutral and not substantially of the ion).

Therefore, prior to thermalization of the incident plasma ions, the product ions might be discriminated from the plasma ions on the basis of their kinetic energy. Placement of a potential barrier downstream of the cell (e.g. an aperture lens or the mass analyzer quadrupole bias voltage at a potential more positive than the cell pole bias potential) discriminates against ions that have energies less than the barrier potential. If the barrier height is between the axial energies of the plasma ions and the energies of ions that are produced within the cell, a degree of discrimination against the latter is afforded. If the energy distributions of the plasma ions and cell-formed ions overlap, the potential barrier cannot be used efficiently and the transmission of both analyte and interference ions is suppressed.

As noted in Section 5.1, the rate of energy damping is proportional to the ratio of the mass of the ion to the mass of the gas molecule. Fig. 23 gives the results of calculations of energy damping as a function of ion and neutral mass assuming elastic (no internal excitation) interaction. As assumed for the fragmentation calculations of Section 5.2, the ion energy at the entrance of the cell is taken as 8 eV. Relatively realistic cases are considered, though the ions and neutrals are treated as elastic particles and hence we disregard vibrational modes of energy damping and ignore ion–dipole interactions (i.e. we consider the hard sphere case). To a first approximation the examples could be considered to represent the collision of Ar_2^+ with H_2 ($m_{ion}/m_{neutral}=40$), Ar^+ with He ($m_{ion}/m_{neutral}=10$) and Ar^+ with CH_4 ($m_{ion}/m_{neutral}=2.5$). The cell pressure is assumed to be 20 mtorr and r.f. effects are ignored. Fig. 23a gives the residual ion energy as a function of the number of collisions suffered. Clearly, a higher mass ratio is less efficient at damping the ion energy; after a given number of collisions, the ion retains more of its initial energy, and hence is more easily distinguished from ions produced within the cell on the basis of the kinetic energy difference. As an example, we have indicated a horizontal line at 1.6 eV which is intended to represent the kinetic energy barrier height that might be used. On average, a collision pair having a high mass ratio (e.g. $Ar_2^+/H_2=40$) allows discrimination (assuming the unrealistically favorable case that the ion energy distributions are extremely narrow) up to 35 collisions, whereas the lower mass ratio pairs become indistinguishable (on the basis of kinetic energy alone) at as few as 3 collisions. These data are displayed differently in Fig. 23b, where the abscissas axis has been converted to distance traveled through the cell. Because the higher mass ratio case leaves the ion with greater residual energy after each collision, that ion also travels the furthest for a given number of collisions. Since the energy discrimination device is applied at or downstream of the exit of the cell, the ions must transit the cell retaining sufficient energy to surmount the potential energy barrier. Therefore, the maximum pressure (which is interchangeable with distance in this example) that allows for kinetic energy discrimination is proportional to the ion/neutral mass ratio.

As has been emphasized earlier, the efficiency of removing the plasma-based interference ion is exponentially dependent on the number of reactive collisions. If each collision considered in Fig. 23 is effective at reacting the isobar, the efficiency of the cell as a function of ion/mass ratio can be inferred from the data given. However, conditions must be applied that ensure that the majority of ions retain an energy above the potential barrier height, and thus these ion–molecule collisions are energetic (non-thermal). As shown earlier, the rate of reaction typically decreases as energy (temperature) increases, and so it may be concluded that these energetic collisions may be less effective in leading to reaction, resulting in lesser efficiency of isobar removal than the number of collisions

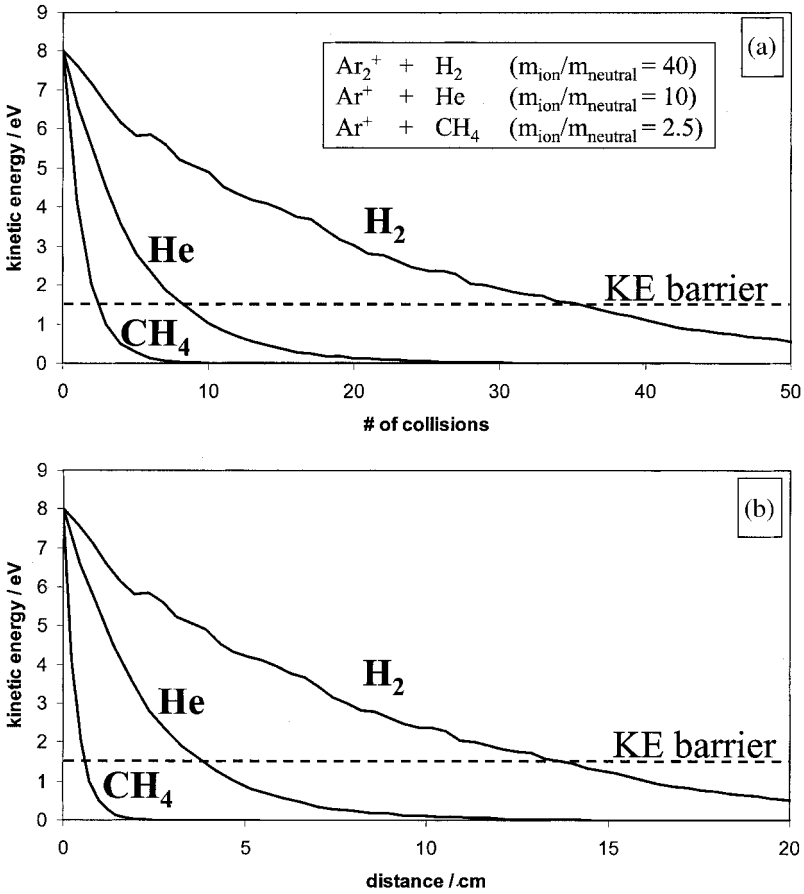

Fig. 23. Calculated residual kinetic energy as a function of the number of collisions (a) or distance traveled through the cell (b) for an ion (Ar_2^+ or Ar^+) with H_2, He or CH_4, corresponding to ion/neutral mass ratios of 40, 10 and 2.5. The horizontal dashed line is intended to indicate the height of a possible kinetic energy barrier placed downstream of the cell: ions that have energies above the barrier height may be transmitted to the mass analyzer, while ions having energies below the barrier height are discriminated against.

alone implies. Further, because the ion kinetic energy adds to the reaction energy, endothermic processes are facilitated and may diminish the specificity provided by thermal chemistry by promoting unwanted reaction of the analyte ion or allowing alternate reaction channels yielding unexpected product ions.

The kinetic energy barrier may be applied as a relatively repulsive ion optic component downstream of the cell (e.g. an aperture lens), or even at the exit end cap of the cell. It is more common to discriminate the ions using the rod offset of the mass analyzing filter (or, equivalently, the bias potential of the cell rods). Under thermalized conditions, the ion energy is defined by the cell bias potential, as the ions 'forget' the energy that they had at the ion source. If the mass analyzer rod offset (QRO in the instance of the ELAN DRC) is more negative than the CRO, exiting ions are accelerated and energy discrimination is not applied; energy discrimination may be effected when QRO is more positive than CRO provided that the ion energies are thermalized to near CRO. Fig. 24 shows the ion signals for three analyte ions (Na^+, Cu^+ and Pb^+) and an ion that is principally formed in the cell (m/z=45, not iden-

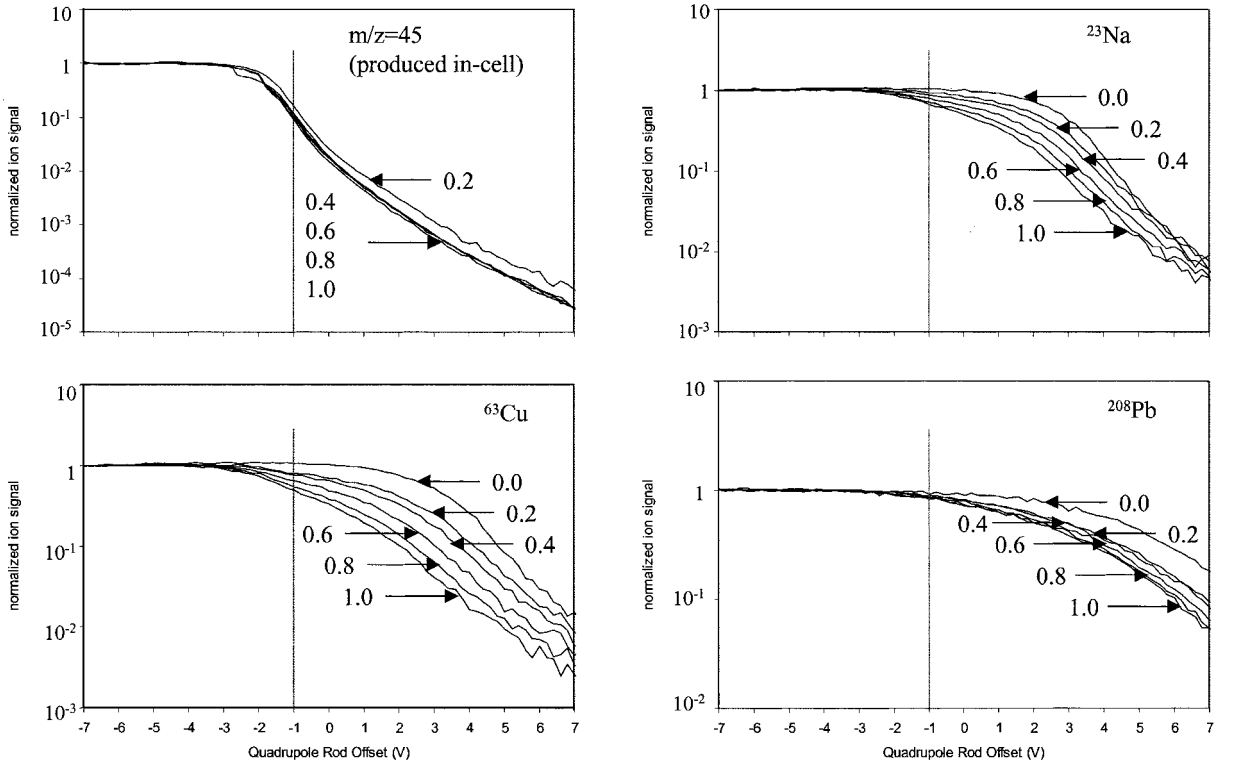

Fig. 24. Ion signals for several ions as a function of quadrupole rod offset potential for various H_2 gas flows. The gas flow, in Ar-equivalent sccm (1 unit = 0.7 sccm H_2), is given beside the arrows. The CRO was −1.0 V (indicated by the grey vertical line). The ion at $m/z = 45$ (not identified) is primarily produced within the cell. Ion energies tend towards the in-cell ion energy (near the CRO potential) at higher H_2 flows and lower ion masses. Note that the vertical scales differ.

tified) as a function of the mass analyzer rod offset potential (QRO) and as a function of the flow of H_2 into the cell. For these experiments, the CRO was −1.0 V. The pressure within the cell is not directly monitored for logistical reasons; provided that the flow of the gas and the conductance of the cell apertures is known, the cell pressure can be calculated with reasonable accuracy. Our best attempt at these calculations for our instrument was given in Fig. 17, where the flow of Hydrogen (2 amu) is corrected according to the factors given in Table 4. Because the ion transmission efficiency through the mass filter is a function of the ion energy in the mass filter, which discriminates against low energy ions, these 'stopping curves' may not be directly interpreted as ion kinetic energy curves (though these are related, and we will discuss them as though they reflect the ion energy distribution). If there were no bias in the energy filtering, the stopping curves could be differentiated to yield ion energy distributions. There are two important characteristics of the energy distribution that the stopping curve provides: the 'most probable energy' and the energy distribution width. These may be interpreted to describe a stream having a flow velocity corresponding to the most probable energy and an effective temperature given by the width of the energy distribution. If the energy distribution is approximately thermal, the 'most probable energy' typically falls near the point where the normalized stopping curve falls below $1/e$; we will use this 'definition' as a marker for ion energy. Secondly, it should be clear that a steeper slope corresponds to a lower 'temperature' and a broader slope to a higher 'temperature'. We will use this interpreta-

tion to compare sets of data below. The zero point of the energy is approximately the energy with which the ions leave the vacuum interface (plasma potential plus the energy corresponding to the expansion velocity plus the interface potential if it is positive) at low cell pressure and shifts to the cell bias potential (CRO) when many collisions thermalize the ions. In fact, prior to thermalization, the flow velocity may have a wide distribution (poorly defined most probable energy) and two or more simultaneous temperature distributions.

When no gas is added to the cell (and in this instance the cell is vented to the high vacuum chamber so that the mean free path is very long), the stopping curves reflect the energies that the ions gain in the supersonic expansion to vacuum. When gas is added to the cell, the most probable energies of the source-derived analyte ions (Na^+, Cu^+ and Pb^+) decrease, but notably the temperature of these ions increase. This is completely in accord with the description given in Section 8.2.1, whereby the axial kinetic energy of the ions is first converted into radial excitation and then both the axial and radial energies (temperatures) relax together towards an asymptotic temperature distribution. Before relaxation is complete, the temperature gradient (i.e. the rate of change of the width of the energy distribution) can be quite dramatic, and different ions can demonstrate different 'temperatures'. In the data shown here, the Na^+ and Cu^+ ions relax somewhat more than do the higher mass Pb^+ ions, though all of these source-derived ions remain well above room temperature even at the highest H_2 flow. Clearly, H_2 is ineffective at thermalizing the ions, though the temperature and most probable energy of the ions is inversely proportional to the ion/neutral mass ratio. On the other hand, the $m/z=45$ ions are cool relative to the atomic analyte ions, reflecting their formation within the cell (evidenced by nearly 4 orders of magnitude increase in signal intensity with addition of H_2 to the cell).

On the other hand, the use of a heavier and polyatomic gas such as methane induces a rapid cooling of the ions and reduction of the flow velocity, as seen in Fig. 25. At a flow of 0.2 Ar-equivalent sccm (0.10 sccm, $\approx$2 mtorr, estimated), the most probable energy has decreased significantly and the 'temperatures' of many of the ions has increased somewhat. With 0.4 Ar-equivalent sccm flow (0.21 sccm, $\approx$3 mtorr), the flow velocity is quite low (the most probable energy for most of the ions is near the CRO = −1.0 V) and the majority of the ions have a relatively low temperature. Further increases in methane flow tend to thermalize the ions in the tail of the energy distribution.

Kinetic energy discrimination nearly equally discriminates against desired product ions (e.g. oxidation or fluorination, in the instances where these are promoted for analytical benefit) and the unwanted product ions of the sequential secondary chemistry. That is, kinetic energy discrimination does not facilitate measurement of an analyte shifted in mass by the intentional addition of an atom while simultaneously suppressing the appearance of background ions produced in the cell in the sequential chemistry.

In order to properly demonstrate the efficiency of the cell at improving the signal/background ratio by plotting reaction profiles either as a function of reaction gas flow or potential barrier height, it is necessary to show data for both a matrix blank and an analyte sample. Measurement of the ion signal as a function of the kinetic energy discrimination barrier height measures two phenomena simultaneously: ion loss due to scattering, reaction or fragmentation, and signal loss due to energy damping (the ion energies shift below the barrier height). Only the former results in an improvement in the signal/background ratio unless there is a substantial difference in the rate of energy loss of the isobaric ions. Because of their additional degrees of freedom in which collision energy can be deposited, polyatomic ions lose energy somewhat more rapidly than do atomic ions. Therefore, kinetic energy discrimination provides a degree of resolution of atomic (analyte) ions from polyatomic (plasma-based interference) ions, but this distinction is generally small and is achieved through differential signal loss (i.e. both the atomic ion and polyatomic ion signals are reduced, with the latter somewhat more significantly). Therefore, observation of suppression of a plasma-based interference ion using kinetic energy discrimination (either by scanning the height

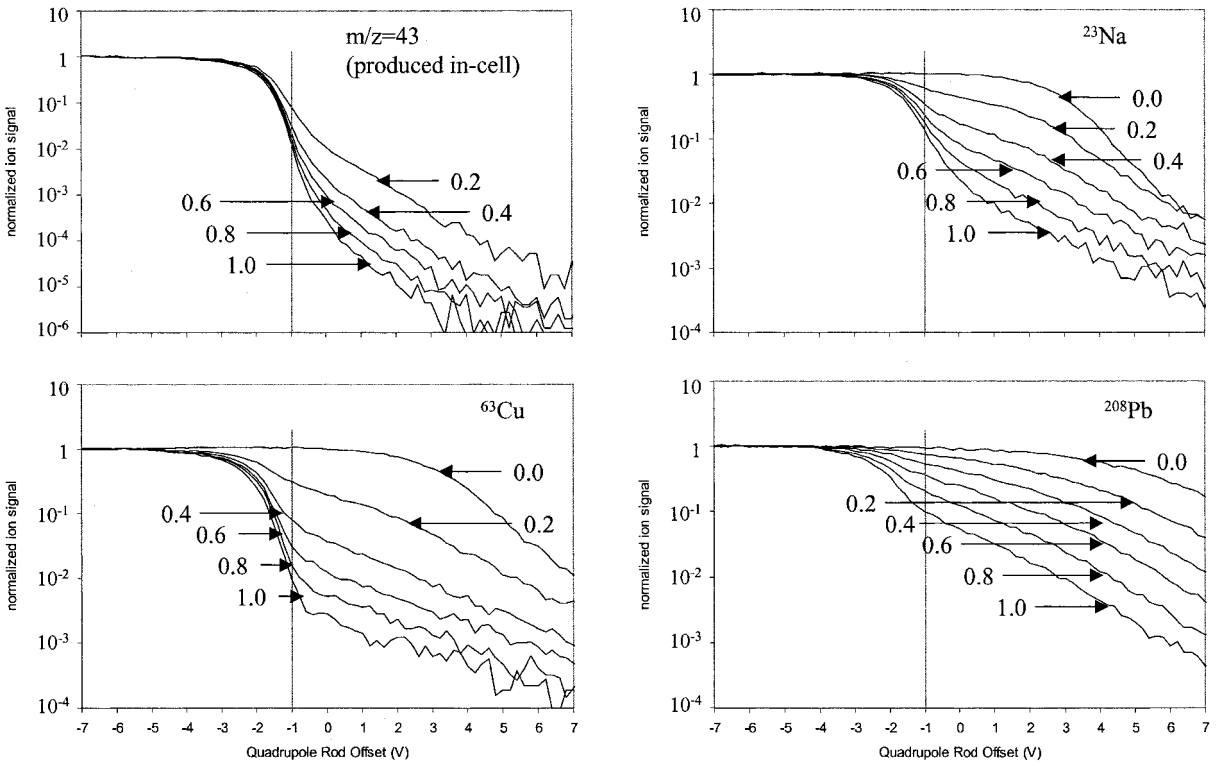

Fig. 25. Ion signals for several ions as a function of quadrupole rod offset potential for various CH_4 gas flows. The gas flow, in Ar-equivalent sccm (1 unit = 0.52 sccm CH_4), is given beside the arrows. The CRO was −1.0 V (indicated by the grey vertical line). The ion at $m/z = 43$ (not identified) is primarily produced within the cell. Ion energies tend towards the in-cell ion energy (near the CRO potential) at higher CH_4 flows and lower ion masses. Note that the vertical scales differ.

of the barrier or by varying the gas density at a given barrier height) might infer a concomitant improvement in analyte signal-to-background, but this must be confirmed by similar measurement of the analyte ion signal. For example, Boulyga and Becker [111] have reported that the Ar_2^+ signal can be suppressed by 5 orders of magnitude using H_2/He and a potential barrier height of 1.6 eV (the difference between the Hexapole Pole Bias and the mass analyzer pole bias), but only by 2 orders of magnitude with the barrier removed. At the same time, they report that the ratio of the Se^+ ion signal to background (Ar_2^+) signal, measured with the potential barrier, improves only by 2 orders of magnitude. The implication is that 3 of the 5 orders of magnitude suppression of Ar_2^+ results from damping the ion energy below the barrier height, and that Se^+ is similarly suppressed.

To select an appropriate set of cell conditions to demonstrate the efficacy of post-cell kinetic energy discrimination, we recorded reaction profiles (ion signal vs. gas flow) at various barrier heights (applied as the mass filter rod offset, QRO, relative to the CRO). As will become evident shortly, we were unable to select a m/z for an analyte ion that was interfered by a cell-formed ion for which the interference ion could be efficiently removed by reaction and for which energy discrimination provided a substantial improvement in detectability. Therefore, despite the paragraph above, we recorded reaction profile data for several generally-not-interfered analyte ions and several ions that appeared to be formed within the cell. The selection of the 'optimum' kinetic energy barrier height (QRO) was taken from the data of Figs. 24 and 25, where the ratio of the $^{63}Cu^+$ signal to an

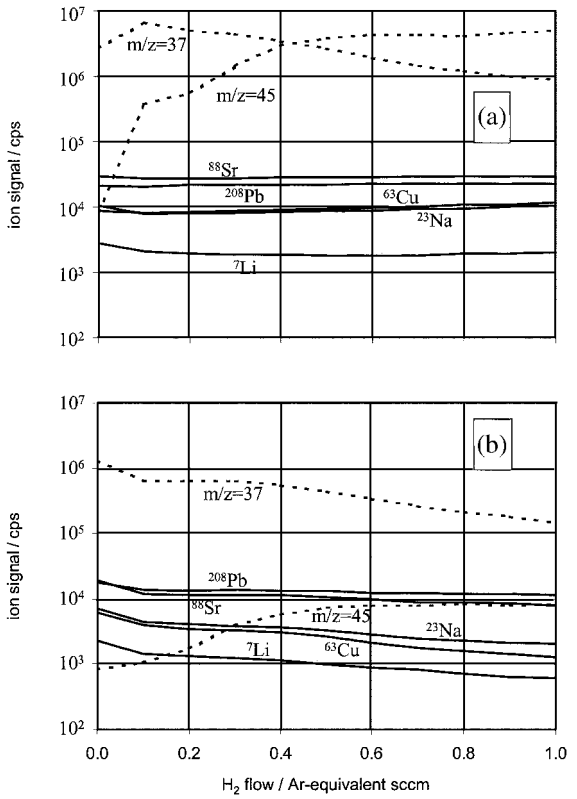

Fig. 26. Reaction profiles of analyte ions (solid lines) and unidentified ions produced within the cell (dashed lines) as a function of H_2 reaction gas flow (1 Ar-equivalent sccm = 0.7 sccm). (a) Without post-cell energy discrimination (quadrupole rod offset is −3 V, 2 V more negative than CRO). (b) With post-cell energy discrimination (quadrupole rod offset is +2 V, 3 V more positive than CRO).

'interference ion' ($m/z=45$ for H_2, $m/z=43$ for CH_4) was near maximum and the analyte signal intensity was simultaneously as large as possible (i.e. on the basis of background equivalent concentration, BEC). Accordingly, data were recorded for QRO = −3 (non-discriminating) and QRO = +2 (energy discriminating).

Reaction profiles for H_2 as the reaction gas and with/without energy discrimination are given in Fig. 26. In the absence of energy discrimination, analyte ion signals are insensitive to the H_2 flow. On the other hand, the dramatic (orders of magnitude) increases in the not-identified ion signals at $m/z=37$ and 45 evidences their formation by reaction within the cell. When kinetic energy discrimination is applied, only a slight loss of the analyte signals is obtained, corresponding to the fraction of these ions that have been cooled below the barrier height. However, the 'interference ions' (e.g. $m/z=45$) are suppressed by up to 3 orders of magnitude (relative to the non-discriminating case). As much as these 'interference ions' (albeit at a different m/z than the analyte ions) reflect the behavior of same-mass interference ions, the resultant improvement in the signal-to-background is approximately 2 orders of magnitude.

It is important to realize that the application of the kinetic energy barrier does not affect the formation of the 'interference ions' within the cell: they are formed at the same rate independent of the QRO voltage. Only the transmission of these ions through the mass filter, and hence their detection, is affected by the energy barrier: this reduces the interference by 1–2 orders of magnitude.

Reaction profiles for CH_4 as the reaction gas, obtained under similar conditions, are given in Fig. 27. In the instance where energy discrimination is not applied, the analyte ion signals other than $^7Li^+$ actually increase with methane flow, presumably a result of collisional focusing which is more effective for the heavier, polyatomic collision/reaction gas. The production of new 'interference ions' (e.g. $m/z=43$) is again evidenced by a 3 order of magnitude increase of these signals. However, the application of an energy barrier causes a substantial loss of analyte signal. This reflects the more efficient cooling of the ions by the more heavy, polyatomic reaction gas, so that the energies of a large fraction of the analyte ions fall below the barrier. It could be noted, then, that collisional focusing is not commensurate with energy discrimination: the increase in signals due to collisional focusing is coincident with the reduction of their ion energies, and these lower energy ions are those that are discriminated against by the energy barrier. Accordingly, the ions that are detected tend to be those that have had the fewest collisions, and these have consequently not been focused to the axis of the cell. Even more so than in the instance of H_2, the 'interference ions' are highly discriminated against, by up to 5 orders of

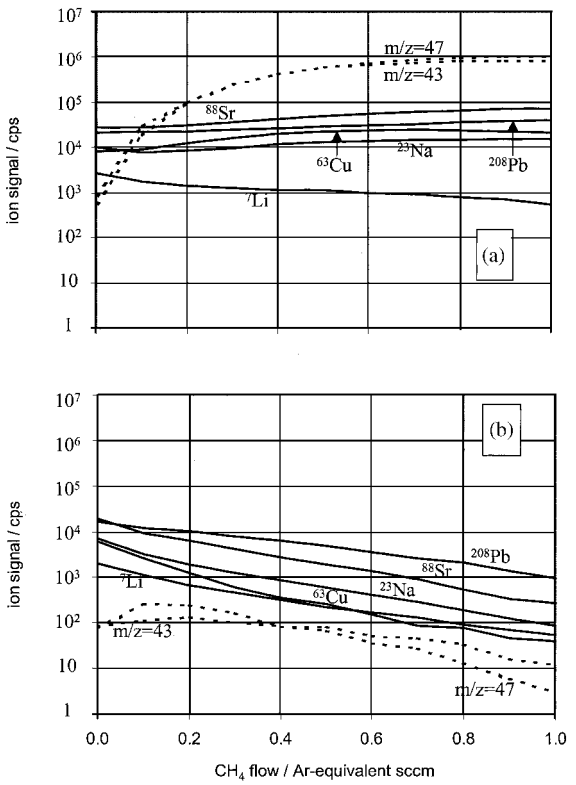

Fig. 27. Reaction profiles of analyte ions (solid lines) and unidentified ions produced within the cell (dashed lines) as a function of CH_4 reaction gas flow (1 Ar-equivalent sccm = 0.52 sccm). (a) Without post-cell energy discrimination (quadrupole rod offset is −3 V, 2 V more negative than CRO). (b) With post-cell energy discrimination (quadrupole rod offset is +2 V, 3 V more positive than CRO).

magnitude relative to the non-discriminating case. However, in this instance, the analyte ions are correspondingly suppressed by up to 2 orders of magnitude, which mitigates the improvement in signal-to-background to some 2–3 orders of magnitude.

The data of Fig. 24 through Fig. 27 were used to determine 'optimum' analytical conditions of reaction gas flow and energy barrier height. In fact, in all instances, the 'optimum' conditions were provided at zero flow and no energy discrimination; that is, conventional ICP-MS conditions. However, a local optimum was obtained near a flow of 0.4 Ar-equivalent sccm for either gas and the energy barrier height discussed above. It is appropriate to remind once again that the efficiency of reaction in the cell is exponentially dependent on the pressure of the reaction gas (gas thickness), but energy discrimination requires that the ions not be thermalized; this imposes a limitation on the efficiency that can be obtained.

Spectra obtained with and without energy discrimination, using H_2 as the reaction gas, are shown in Fig. 28. Great care was taken to ensure that the cell gas was as pure as possible; this included the use of 99.999% H_2 and substantial purging of the gas system. Before the gas line was purged, addition of gas to the cell caused a substantial change in the mass spectra obtained. After purging, little spectral improvement was observed (other than the increase in certain discrete ions, such as those shown in Fig. 26). This was then taken as evidence of sufficient purging: analyte and cell-formed ion signals were monitored (without energy discrimination) until the signals no longer changed with time.

For the most part, when H_2 is used as the reaction gas, energy discrimination has little impact on spectral regions of typical interest. Certain ion signals were dramatically suppressed by the barrier; these include the ions at $m/z=43$, 44 and 45, as well as $m/z=55$ ($H_3O^+ \cdot 2H_2O$?) and the m/z region 68–72. However, comparison with the conventional ICP-MS spectra (Fig. 22a) shows little, if any, improvement due to the addition of H_2 reaction gas. It is therefore our conclusion that, under the conditions used in our work, H_2 is a rather ineffective reaction gas, at least for general purposes of multi-element determinations. This is consistent with the database of thermal rate constants for reactions of ICP ions with H_2 [10], and with the interpretation that the ions retain a substantial fraction of their source energy (when energy discrimination may be applied) so that relatively few reactive collisions are obtained. Accordingly, it is our interpretation that other reports of the efficacy of hydrogen as a reaction gas [27,62,63,112] principally reflect one or more of four enabling conditions: (1) the ions are introduced with higher energy, so that the collision energy exceeds the endothermicity of normally disallowed reactions, (2) contaminants in the cell

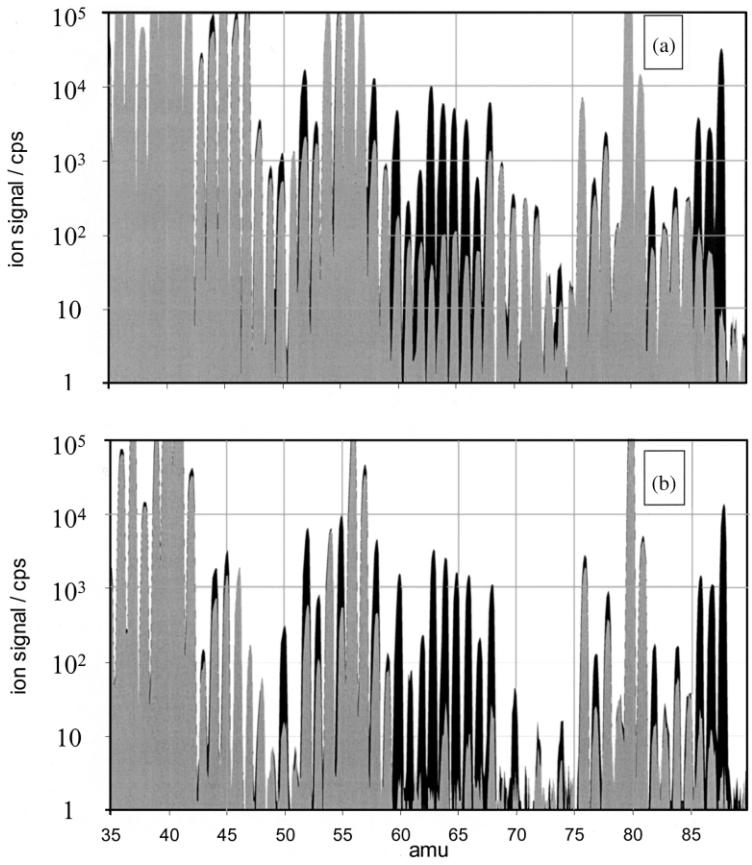

Fig. 28. Mass spectra for high purity water (grey) and a solution containing 1 ppb each of K, Ca, Cr, Mn, Fe, Ni, Cu, Zn, Se and Sr (black), with H_2 as reaction gas at a flow of 0.4 Ar-equivalent sccm (0.28 sccm) and the cell operated with a wide transmission bandpass (RPa, RPq) = (0, 0.15). (a) Without post-cell energy discrimination (QRO = −3, CRO = −1). (b) With post-cell energy discrimination (QRO = +2, CRO = −1).

gas, introduced either with the gas or inadvertently from the external vacuum chamber or plasma gas entrainment, are the effective reaction neutrals, (3) in some instances (notably Se^+/Ar_2^+), differential energy loss rates may allow a degree of energy discrimination against the polyatomic ion, (4) some collisional fragmentation of weakly bound polyatomic ions (e.g. Ar_2^+) occurs.

Fig. 29 provides spectra using methane as the reaction gas with and without energy discrimination. In this instance, the methane substantially reduces the argide interferences on $^{80}Se^+$, $^{56}Fe^+$ and $^{52}Cr^+$, but introduces a number of new and significant interference ions (especially at m/z = 43–48, 53–55, 57 and 60–75) when energy discrimination is not applied. These new interferences are dramatically suppressed with energy discrimination, but, as noted above, the analyte signals are also substantially reduced. Accordingly, it is evident that CH_4 has some desirable characteristics as a reaction gas in removing certain argide interferences, but the efficiency of cooling the ions means that low pressures are necessary for energy discrimination, with concomitant reduction in reaction efficiency. Because of these antagonistic characteristics, methane is not viable as a reaction gas when energy discrimination is required, and this can almost certainly be projected to also include other relatively heavy and polyatomic reaction gases.

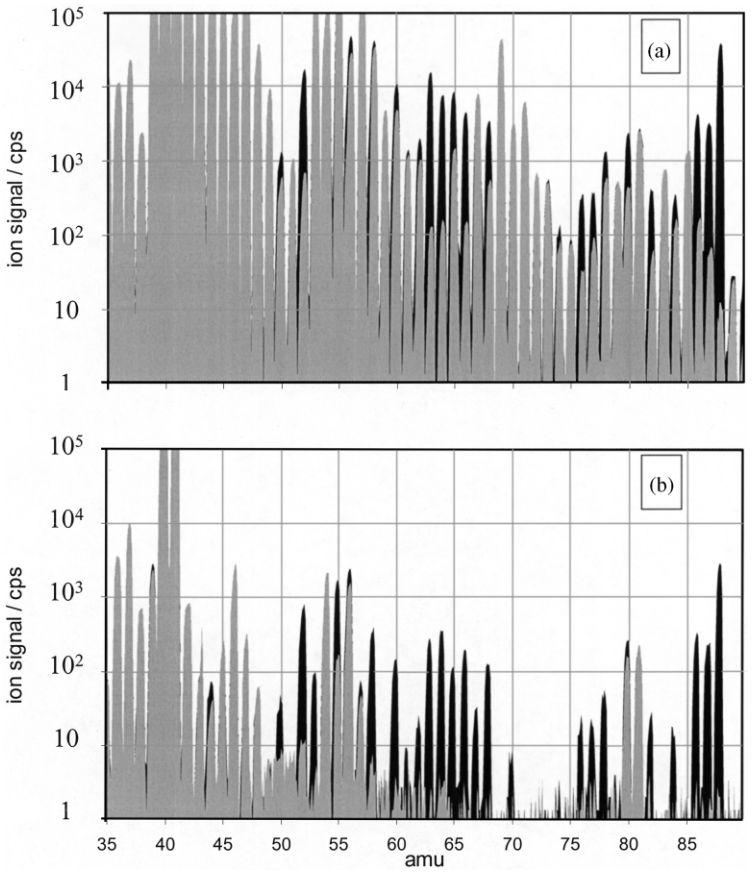

Fig. 29. Mass spectra for high purity water (grey) and a solution containing 1 ppb each of K, Ca, Cr, Mn, Fe, Ni, Cu, Zn, Se and Sr (black), with CH_4 as reaction gas at a flow of 0.4 Ar-equivalent sccm (0.21 sccm) and the cell operated with a wide transmission bandpass (RPa, RPq) = (0, 0.15). (a) Without post-cell energy discrimination (QRO = −3, CRO = −1). (b) With post-cell energy discrimination (QRO = +2, CRO = −1).

8.4.2. Bandpass control of secondary chemistry

Section 8.3 gave an example of a series of sequential reactions that lead to potential new isobaric interference. In almost all instances, the sequential reactions involve either a primary (plasma-based) reactant ion or an intermediate product ion that has a mass that is significantly different from the analyte ion. Ejection from the cell of any one of these intermediate ions aborts the remainder of the reaction chain and eliminates the formation of the new interference.

A quadrupole finds application as a mass filter because it has well-defined stability boundaries that are independent of the position of the ion within the quadrupole field (Section 7.2). Perhaps surprisingly, the stability boundaries remain reasonably well-defined even when the quadrupole is pressurized (Fig. 13). The latter experimental observation suggests that a quadrupole reaction cell can be operated in a bandpass mode in which the low mass and high mass cut-offs are determined principally by the amplitude and frequency of the r.f. (the Mathieu parameter q) and the amplitude of the DC applied between pole pairs (the Mathieu parameter a). When pressurized above a few mtorr, the quadrupole is unlikely to be suitable as a mass filter, at least with mass resolution that would have analytical merit in the

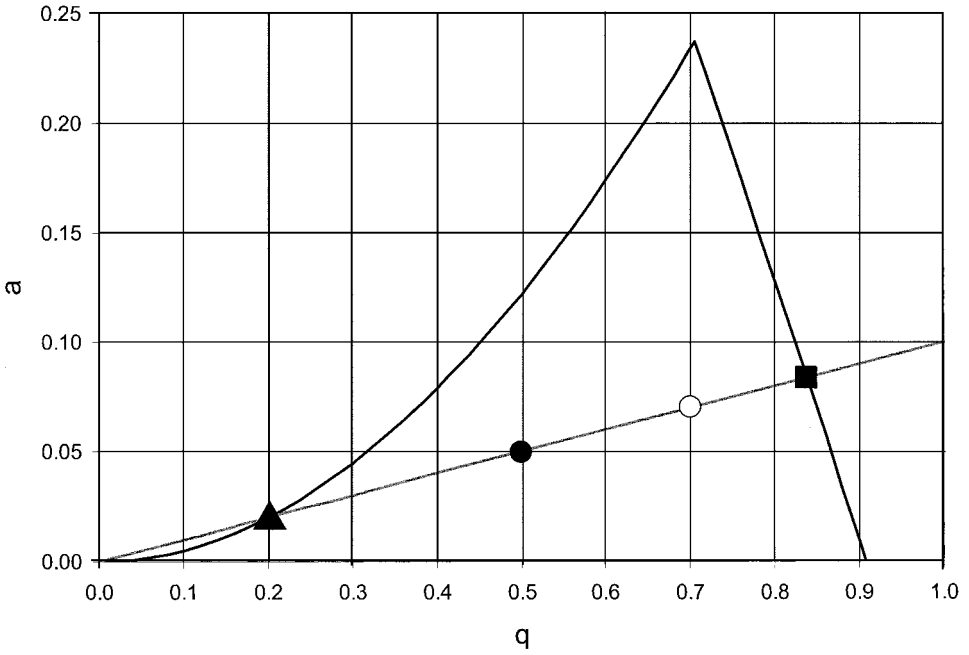

Fig. 30. Quadrupole stability diagram with hypothetical scan line. (▲) Denotes the high mass cut-off, and (■) denotes the low mass cut-off. The bandpass includes a lower mass range when operated at (●) than at (○), and this can affect the formation of secondary interferences if the precursor ion is included/excluded under these conditions.

ICP-MS application. However, even a relatively wide bandpass (a few amu to 10s of amu) can dramatically suppress the secondary chemistry. In the instance where it is desired to remove an existing isobaric interference, the bandpass is established in order to make the analyte ion (and the isobaric interference) stable. This provides a condition for efficient transmission of the analyte ion and an environment which permits the isobar to react with the reaction gas. Provided that the bandpass excludes at least one of the intermediate product ions of the sequential chemistry that would otherwise create a new interference, that sequential chemistry is aborted and the new interference is not formed.

The position of the stability boundary relative to the analyte ion is conveniently selected by adjustment of either the r.f. voltage, as is typical for the mass filter, or the frequency of operation. Because the r.f. contribution to the reaction energy, which is important in the establishment of thermal conditions, is a strong function of the r.f. amplitude, it is convenient to use the frequency for this purpose in the reaction cell. The impact of the selection of the operating point (a, q) on the bandpass mass limits is considered in reference to Fig. 30. In this figure, the low mass cut-off is indicated by the solid square and the high mass cut-off by the solid triangle, and either of two operating points is indicated by the circles. The solid circle indicates an operating point of $(a, q) = (0.05, 0.5)$. If the analyte mass is 56 amu, the bandpass extends from approximately 33 to 147 amu (calculated for an ideal quadrupole under collisionless conditions). If, instead, the operating point was chosen as indicated by the open circle $(a, q) = (0.07, 0.7)$, the bandpass would include approximately 47–205 amu. In both instances, the analyte ion (e.g. Fe^+) is within the stability bandpass and is expected to be retained and transmitted. An isobaric plasma-based ion (e.g. ArO^+) is stable with respect to the quadrupole field, but may be reactively removed if the reaction gas is appropriately chosen. For the sake of argument,

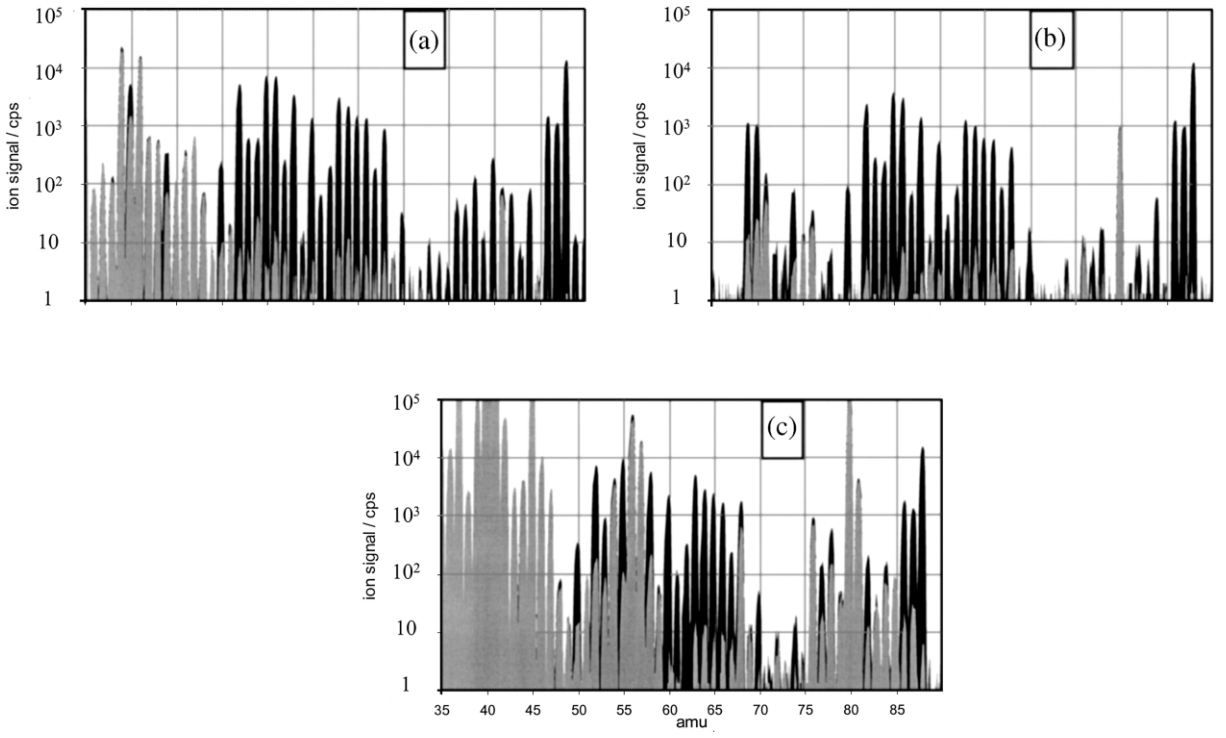

Fig. 31. Mass spectra for high purity water (grey) and a solution containing 1 ppb each of K, Ca, Cr, Mn, Fe, Ni, Cu, Zn, Se and Sr (black). The cell is operated at (RPa, RPq) = (0, 0.7), such that the low mass cut-off is approximately 78% of the analytical mass and without post-cell energy discrimination (QRO = −3, CRO = −1). (a) With CH_4 as reaction gas at a flow of 0.92 Ar-equivalent sccm (0.48 sccm). (b) With NH_3 as reaction gas at a flow of 0.9 Ar-equivalent sccm (0.48 sccm). (c) With H_2 as reaction gas at a flow of 0.8 Ar-equivalent sccm (0.56 sccm).

consider that an ion of $m/z = 40$ (perhaps Ar^+, as a primary ion derived from the plasma, or some intermediate reaction product ion) could react with the reaction gas to form a new ion at $m/z = 56$ (i.e. formation of a new isobaric interference for Fe^+ within the cell). If the first operating point (solid circle) were adopted, the $m/z = 40$ ion would be retained in the cell, and it could therefore react to form the new isobaric interference. However, if the second operating point (open circle) were adopted, the $m/z = 40$ ion would be outside of the stability bandpass and would be rapidly ejected from the cell; as a result the new isobaric interference would not form.

We saw in Section 8.3 that pressurizing the reaction/collision cell with a reactive gas (e.g. CH_4) and operating with a wide bandpass gives rise to a more complex spectral background than if the cell were not pressurized (cf. Fig. 22a and b). The spectra of Fig. 31a were obtained with the bandpass of the cell shifted to higher mass (larger q). The increase in the low mass cut-off clarifies the mass spectrum. The sensitivity for the analyte ions remains comparable to that of Fig. 22a and b. The reduction of plasma-derived interference ions is obtained through reaction with the cell gas. The appearance of new interference ions produced within the cell is suppressed, apparently as a result of the rejection of lower mass ions that otherwise would react in secondary processes to produce the ubiquitous background seen in Fig. 22b.

The bandpass approach does not rely on differences in ion energies between desired and undesired ions. Hence, the cell may be operated at higher pressure (gas thickness), providing more collisions which help to thermalize the ions (allowing rea-

gent selection on the basis of the thermal database and providing the specificity of the thermal chemistry) and improve the efficiency of the reactive removal of plasma-based interference ions. This is evident in a comparison of Fig. 29 with Fig. 31a. The former data were obtained with a methane flow of 0.4 Ar-equivalent sccm (0.21 sccm, ≈3 mtorr) whereas the latter were obtained at 0.92 Ar-equivalent sccm (0.48 sccm, ≈6 mtorr). A dramatic reduction in the signal intensities of the plasma-based argide interference ions (e.g. Ar^+, ArH^+, ArC^+, ArO^+ and Ar_2^+) is obtained, a direct result of the exponential dependence of the efficiency of these reactions on the reaction gas pressure, and the formation of new interferences in the cell (most of the ions in the DIW spectrum of Fig. 29) are suppressed by the application of the bandpass. It should be recognized that, whereas post-cell energy discrimination allows the secondary chemistry to proceed and discriminates the ions downstream of the cell, the bandpass approach suppresses the secondary chemistry as it occurs through removal of the precursor ions. It should also be noted that the bandpass of the DRC cell is adjusted in concert with the m/z set for the downstream mass analyzer; the bandpass is thus dynamically adjusted as opposed to being static at a given r.f. amplitude and frequency.

The effect of the bandpass on the secondary chemistry, and some insight into the sequence of the chemistry, can be obtained by recording the ion signal as a function of the bandpass parameters. Fig. 32a shows the ion signals for $^{63}Cu^+$ and several not-identified ions that are formed within the cell with methane as the reaction gas as a function of the RPq parameter (the Mathieu q parameter) in r.f.-only mode. If all of these ions were derived from the plasma, they should show a similar dependence on RPq, as shown in Fig. 12b. Clearly this is not the case, and the implication is that the not-identified ions are created inside the cell; this also agrees with the increasing signals for these ions as the methane flow is increased (the $m/z=47$ profile is seen in Fig. 27). While it is preferred, in order to determine the optimum value of RPq, to measure the RPq-profiles at the same m/z for a standard and a blank, the present result suggests that operation at RPq > 0.6 should

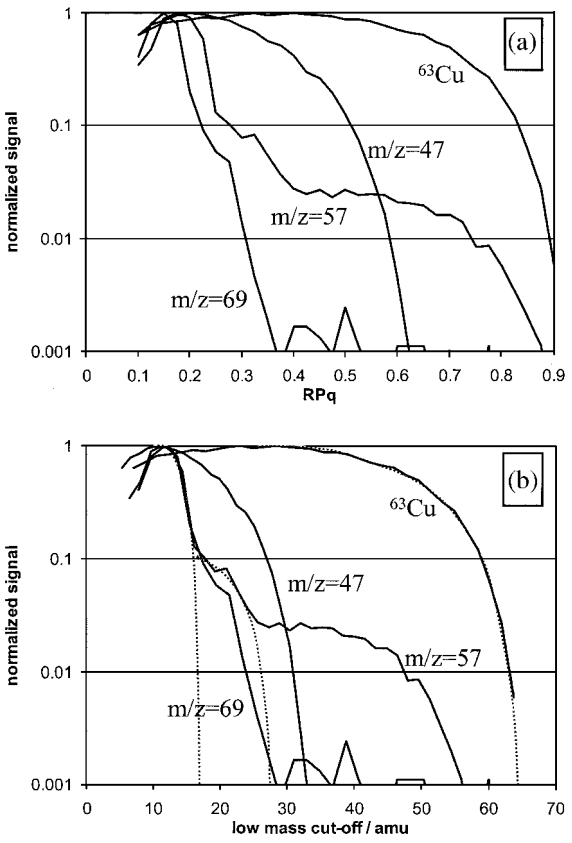

Fig. 32. (a) Optimization of the RPq parameter for $^{63}Cu^+$ as an analyte ion and three unidentified ions that are produced within the cell. CH_4 was used as reaction gas at 0.92 Ar-equivalent sccm (0.48 sccm), and post-cell energy discrimination was not employed (QRO = −3, CRO = −1). (b) The same data is presented as a function of the low mass cut-off, assuming a cut-off near RPq = 0.89. In the latter case, extrapolation of the decay of the signal with increasing cut-off mass (shown by the dashed lines) corresponds roughly to the mass of the precursor ion that gives rise to the observed signal. Two such precursor ions are evident for the $m/z=57$ ion.

alleviate many interferences. Of course, a different value of RPq may be optimum for each mass and for each gas and pressure, but the data presented suggests that a reasonable compromise can be adopted for multi-element measurement.

As noted earlier (Section 7.2), the experimental definition of the stability boundary is a matter of interpretation. If we now accept that the RPq-profile for $^{63}Cu^+$ is representative of a non-reactive ion, and define that this ion becomes unstable

when its signal falls below 1% of its maximum, near RPq = 0.89 = RPq_{max} (recall that $q = 0.908$ is the theoretical r.f.-only stability boundary for an infinitely long and accurate quadrupole), the RPq scale of Fig. 32a can be converted to a low mass cut-off scale (using Eq. (6.32) with q_1 and m_1 referring to the RPq and mass of the monitored ion, $q_2 = RPq_{max} = 0.89$ and m_2 being the cut-off mass), as in Fig. 32b. Here, the sequential nature of the chemistry leading to the formation of the $m/z = 47$, 57 and 69 is evident. Both the $m/z = 57$ and 69 ions apparently derive from sequential chemistry involving a precursor ion having a m/z of approximately 17 amu (probably CH_x^+, where extrapolation of the first decay region to 1% suggests that x is probably 5), and a second precursor in the vicinity of $m/z = 27$ (either $C_2H_3^+$ or $C_2H_5^+$, by the same logic and on the basis of the known chemistry of hydrocarbon ions with methane). Therefore, the chemistry forming these ions involves at least three steps: formation of CH_x^+, which reacts to form $C_2H_x^+$, which subsequently reacts either directly or indirectly to form the ions at $m/z = 57$ and 69. It will be recognized that there are at least two ions having $m/z = 57$ in this example. The chemistry leading to the dominant ion has just been described, and accounts for the RPq-profile below approximately RPq = 0.4 (low mass cut-off = 27 amu). However, either Fig. 32a or b show that there is also a relatively stable ion at $m/z = 57$. This is evident from the recognizable RPq-dependence of the signal above RPq = 0.4, which emulates that of the $^{63}Cu^+$ ion. Indeed, these data were recorded for a sample that contained Fe, and the high-RPq contribution comes from the unreactive $^{57}Fe^+$ isotope. The $m/z = 47$ ion has a different chemistry than the others. Clearly, it is not a primary stable ion derived from the plasma (it is suppressed at too low a RPq value for this to be true). Also, it does not appear to be a pure hydrocarbon ion, as it does not involve intermediates of the 'normal' hydrocarbon ions $C_nH_x^+$. Rather, it appears to derive from reaction of an ion having a m/z of approximately 31. It may well be a methane cluster of HNO^+, known to be a prominent ICP ion in aqueous sampling.

The important point to note is that at low q (RPq), the secondary chemistry is enabled because the precursor ions are stable, and the product ions appear in the mass spectrum. In most instances, this is undesirable; the exception is discussed in Section 8.4.3. When it is desired to suppress the appearance of these ions, a higher operating point (larger RPq) may be sufficient. If the chemistry rather derives from a higher mass ion (fragmentation or dissociative reaction), a non-zero value for the Mathieu a parameter (RPa in the ELAN DRC) may be effective, as this institutes a high mass cut-off; an example of this for an interference for $^{27}Al^+$ was shown in our early work with 'unclean' hydrogen [29] but has not been published elsewhere. In addition, there is some evidence that a non-zero value for the Mathieu a parameter provides more sharply defined stability boundaries (for both the low- and high-mass) in the pressurized quadrupole, and this will be the subject of continuing investigation.

For the mass range below 100 amu, methane appears to be a generally suitable reaction gas. A few atomic ions, including As^+ and Ti^+ react with methane, perhaps making it not a universal selection for ultratrace multi-element determinations including these ions (though it will be shown in Section 8.4.3 that there is a solution for these as well). However, CH_4 reacts too slowly with Ar^+ and ArH^+ to allow ppt determinations of K and Ca. An alternate gas of relatively general utility, but that is particularly well suited for the determination of K, Ca and Fe, is ammonia. Spectra similar to those shown for H_2 and CH_4 above, using NH_3 as the reaction gas, are given in Fig. 31b. The NH_3 gas flow used to obtain these spectra was on the high side of common usage, and was selected to optimize determination of Ca^+ at $m/z = 40$. Such a high pressure promotes the reaction of even slowly reacting atomic ions, and hence the signature isotopes of Se^+ are missing (the products have not yet been determined; it is possible that charge transfer, endothermic by 0.4 eV, may be promoted at the relatively high RPq used for these data). Simply to provide a reference for other workers, we include the corresponding spectra using H_2 as the reaction gas in Fig. 31c. As noted earlier, these data were obtained under

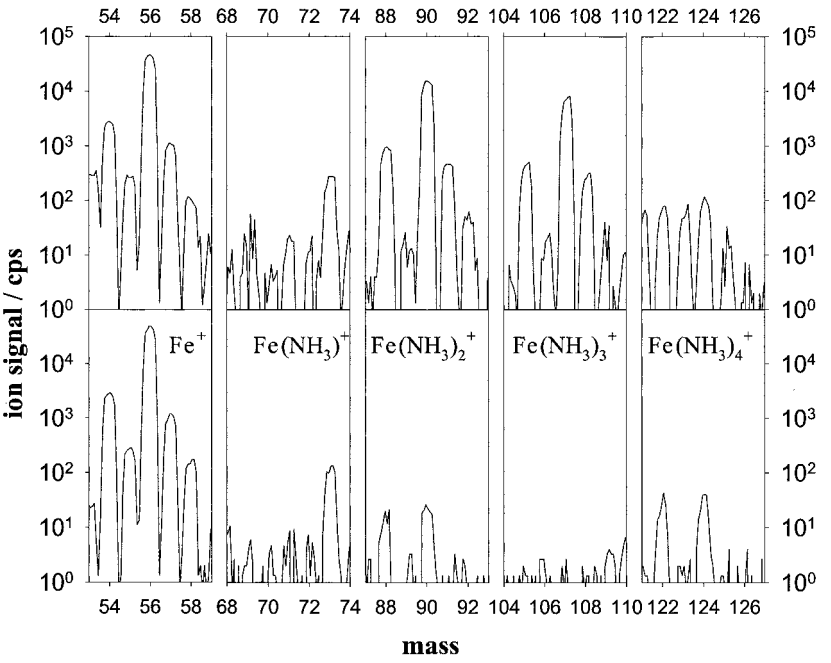

Fig. 33. Mass spectra in the vicinity of Fe^+ and its ammonia clusters, recorded with an NH_3 flow of 1.5 Ar-equivalent sccm (0.8 sccm). The upper spectra were recorded at low q (RPa, RPq) = (0, 0.2), and the lower spectra at higher q (RPa, RPq) = (0, 0.5). Cluster ions of Fe^+ are observed when the low mass cut-off is below the mass of Fe^+ (so that the 'naked' ion and its clusters are simultaneously stable). Notably, the first cluster is relatively absent, reflecting its fast rate of adding a second ammonia cluster. When the bandpass is set to exclude Fe^+ when determining masses corresponding to the higher cluster ions, the clusters are virtually absent, because they cannot be formed when the precursor ion is removed early in the cell.

as clean conditions as possible, and little difference from the conventional spectra of Fig. 22a is to be seen (other than increased background signals at $m/z = 43$, 45, 46, 47 and 69).

We were not able to observe the products of the Ca^+ and K^+ ion–molecule reactions with ammonia. Although the Fe^+ decay is just slightly faster (Table 2), the products of the ion–molecule reaction can be observed under conditions where both the Fe^+ ion and its product ions are stable (Fig. 33).

It has been observed that Fe^+ reacts with ammonia by termolecular association and sequentially forms the ligated cations $Fe(NH_3)_x^+$, where $x = 1$–4:

$$Fe(NH_3)_{x-1}^+ + NH_3 \rightarrow Fe(NH_3)_x^+ \qquad (8.7)$$

These reactions have been observed by others in thermalized systems [113,114]. NH_3 plays the role of a stabilizing third body. Mass spectra of the mass region including the product ions are presented in Fig. 33 for $q = 0.2$ and 0.5 ($a = 0$ in both cases), where it is seen that the cluster ions are present at low q but are largely absent at high q. The progress of the reaction is apparent from the sequence of the intermediate product ions.

The ability to support several consecutive steps of ion–molecule reactions is related to the number of reactive and scattering collisions and to the confinement properties of the r.f.-field. Reflecting the conditions that allow production and confinement of product ions in a quadrupole cell, it was observed that every consecutive step of ion–molecule reaction is discriminated with respect to the precursor ion. Assuming that all reaction channels and product ions have been monitored, it is feasible to correct the product ion intensities in order to conserve the overall charge, but we will not do so here.

Selection of suitable ligands and operation at relatively high pressure is very important to enable the utilization of ternary association reactions for the potential determination of an analyte as its cluster ion. For example, M^+–O_2 or M^+–N_2 bond-dissociation energies are perhaps large enough to expect observable addition, but the lifetime of the intermediate complex involving diatomic ligands is relatively short because of the small number of internal degrees of freedom expected to be effective in the energy dispersal. Hence, these cluster ions are unlikely to be prominent. In contrast, ammonia is a good electron donor ligand and has accessible internal degrees of freedom for energy dispersal, so that at higher pressures its collision complex may have a sufficiently long lifetime to allow collisional stabilization. In some instances, its cluster ions might have analytical value. This type of reaction rarely proceeds at the collision rate. Most often, the intermediate ligated ion must be collisionally stabilized before unimolecular decomposition back to the separated reactants. A higher pressure provides a higher probability of a stabilizing collision.

The chemical stability of products must be accompanied by the stability of their trajectories in the DRC. In Fig. 33, it is apparent that operating at high q suppresses the appearance of cluster ions nearly completely. The most important reason for this is the rejection of the parent ions in the quadrupole field due to their instability simultaneously with the product ions. A lesser contributing cause is that a higher value of q provides a larger contribution to the thermal energy, thereby promoting the unimolecular decomposition of the collision complex and interrupting the chain of successive reactions. The rate of formation of the first adduct, in particular, depends on the operating point because it has a limited number of degrees of freedom. Successive clustering has a distinctive feature: on every reaction step the product ion has a higher mass-to-charge ratio than the precursor ion. In our experimental arrangement, the DRC is interposed between the ICP ion source and quadrupole mass analyzer. The DRC has dynamic low- and high-mass cut-offs, which are adjusted in concert with the analyzed mass and the requested q and a at that mass. Therefore, considering this tandem arrangement, the products of the addition reaction between Fe^+ and ammonia are dynamically scanned. Under the DRC operating conditions, parent and daughter ions are always positioned in different places on the stability diagram. For example, when the third adduct is analyzed at $(a, q) = (0, 0.5)$, the parent Fe^+ is at $(a, q) = (0, 0.96)$, which is in the unstable region of the stability diagram, and is rejected from the cell before it can react. In order to see the third adduct, all of the precursor ions throughout the chain of successive reactions must be stable in the cell. Therefore, favorable and unfavorable conditions for clustering of many plasma ions can be chosen in the DRC by selecting the appropriate stability boundaries of the r.f.-field.

8.4.3. Promotion of secondary chemistry

It was noted in Section 8.3 that the reaction cell should be efficient both at removing the isobaric interference ion and at suppressing the secondary chemistry that would otherwise create new interferences. However, there are instances in which it is more convenient to react the analyte ion (generally by transfer of an atom) than to reactively remove the interference ion. Most often, this situation will arise when the thermochemistry is unfavorable for charge transfer (i.e. the interference ion has a similar or lower IP than the analyte). Such an instance arises when it is desired to chemically resolve certain isobaric atomic ions (e.g. ^{87}Rb and ^{87}Sr). If heavy atom transfer (e.g. oxidation) is to be a viable option, the product ion m/z should be relatively free of interference, or the interference should also react at a sufficient rate that it no longer interferes with determination of the analyte as the MX^+ ion. If this is the case, the efficiency required of the reaction chemistry need not be exceptional: it may be sufficient to convert only a fraction of the atomic analyte ion to achieve a substantial improvement in detection ability. Also, it is clearly necessary to enable the secondary chemistry. Therefore, kinetic energy discrimination is of little value, as this would discriminate against the desired product analyte ion. If the bandpass approach to secondary chemistry control is used, the bandpass must include both the reacting (atomic) analyte ion and the product (molec-

ular) ion. If the bandpass is established with reference to the product ion m/z, the favorable values of (a, q) will be less than for an atomic (not transformed) ion. If the atomic analyte ion has a $m/z=m_1$ and the product ion has $m/z=m_2$, then the product ion will be observed only for:

$$q_{m_2} \prec \left(\frac{m_1}{m_2}\right) 0.908 \tag{8.8}$$

More typically, if the ion signal maximizes at $q=q_{\text{opt}}$ (typically ~ 0.5) under pressurized conditions, the approximately optimum value of q for m_2, will be:

$$q_{m_2} = \frac{(m_1+m_2)}{2m_2} q_{\text{opt}} \tag{8.9}$$

For example, in chloride matrices V^+ is interfered by ClO^+. ClO^+ should be expected to react with ammonia by charge transfer (0.79 eV exothermic). It was originally reported [76] that reaction does not occur, but reexamination [115] confirms the relatively fast charge transfer reaction rate constant of 6×10^{-10} cm^3/s. V^+ reacts slowly to form VNH^+ ($k=2.2\times10^{-12}$ cm^3/s) [10]. The 300-fold difference in reaction rate should make NH_3 an attractive reaction gas for this application. However, at low values of RPq ammonia is observed to be ineffective at resolving V^+ from ClO^+ [116]. This appears to be due to a minor reaction channel of Cl^+ forming NH_2Cl^+ (exothermic by 25 kcal/mol) at the same m/z, which is consistent with unreported work from our laboratory with ND_3 as a reaction gas indicating the formation of both ND_2Cl^+ and $Cl^+\cdot ND_3$ at low RPq. For the production of the NH_2Cl^+ ion to be suppressed, q_{m_2} must be greater than the value calculated according to Eq. (8.8), or $35/51\times0.908=0.62$. Indeed, it is observed that the interference at $m/z=51$ in 1% HCl solution is reduced to 3 ppt BEC [116] or to the instrument background level [117] for operation at RPq = 0.65 or higher.

An alternative approach is to oxidize the V^+ to VO^+ ($m/z=67$) using N_2O as the reaction gas. Unfortunately, ClO^+ also reacts, albeit slowly, to form ClO_2^+ at the same m/z. However, VO^+ can be readily further oxidized to VO_2^+ ($m/z=83$) whereas ClO_2^+ does not. Observation of V as VO_2^+ requires that V^+, VO^+ and the final product VO_2^+ be simultaneously stable, and according to Eq. (8.9) the optimum should occur near $q_{m_2}=(51+83)/(2\times83)\times0.5=0.4$. Results presented by Bandura et al. [65] show that the operating point is optimized as predicted.

It is well known that Se^+ is interfered in conventional ICP-MS by the argon dimer ion, and As^+ is interfered by $ArCl^+$ in samples containing chlorine. H_2 has been used to allow the determination of As in Cl matrices [30,118–121], but is ineffective for the determination of Se at trace levels (Fig. 31c). On the other hand, CH_4 is effective for the determination of Se (Fig. 31a, and Sloth and Larsen [122]), but As^+ reacts to form $AsCH_2^+$ (at $m/z=89$). It is often of interest to determine As and Se nearly simultaneously, e.g. in LC-ICP-MS where the time resolution of the As and Se species are not sufficient to allow change of the reaction gas. In the absence of ^{89}Y in the sample, methane may be used for the simultaneous determination of Se and As, where Se is measured as the atomic ion and As as the product ion, as shown in Fig. 34.

Beta decay of ^{87}Rb to ^{87}Sr allows age determination of rocks through the isochrone obtained by the measurement of the $^{87}Sr/^{86}Sr$ isotope ratio together with the Rb/Sr element ratio [118,123,124]. Because of the overlap of the $m/z=87$ isobars, chemical separation is usually required before analytical measurement. However, Sr^+ is readily oxidized (by N_2O) whereas Rb^+ is not; if this reaction could be efficiently promoted, chemical separation could be performed in situ in the reaction cell, with measurement of the Sr isotope ratio as the oxide ions, eliminating the risk of contamination and ratio distortion in an additional separation step. The reaction profiles for Sr^+ and Rb^+ with N_2O are given by Bandura et al. [65]. While it is clear that the concept has merit, the experimental observation was that the product ion SrO^+ reacted further with an unknown impurity (water in the N_2O?) to form $SrOH^+$, and the partitioning between the oxide and the hydroxide complicates the measurement of the Sr isotope ratio. However, it was also shown that SrO^+ reacts rapidly with methane to form the hydroxide, and

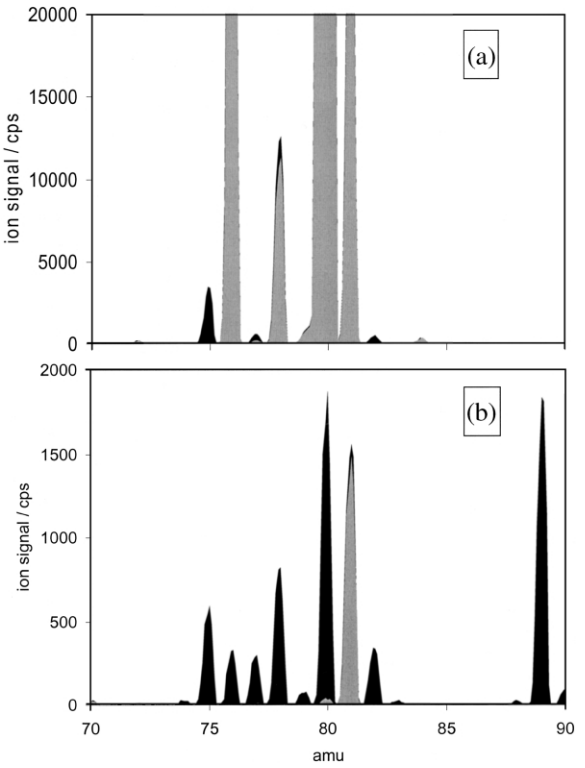

Fig. 34. Mass spectra for a high purity water (grey) and a solution containing 1 ppb of As and Se (black). (a) Standard conditions (no reaction gas, cell vented to mass analyzer chamber). As^+ is observed at its atomic mass (the solution did not contain chloride), and Se^+ is largely hidden by the Ar_2^+ background. (b) Cell pressurized with CH_4 at a flow of 0.7 Ar-equivalent sccm (0.36 sccm), and operated at (RPa, RPq) = (0, 0.5). Approximately 80% of the As^+ is reacted to $AsCH_2^+$ at $m/z=89$, and the Se^+ isotopes are readily apparent at their atomic masses.

this can be used to force the secondary reaction (forming the hydroxide) to near completion. Consequently, a mixed reaction gas of N_2O and CH_4 (which must be mixed in the low-pressure gas manifold, because they are combustible at higher pressure) allows rapid sequential oxidation and hydroxylation with high efficiency. This was our first experience with the promotion of sequential chemistry using two reaction gases.

Superior results for the geochronological application have been reported by Moens et al. [118] using CH_3F in a Ne buffer. Sr^+ reacts with methyl fluoride by F-atom transfer, forming SrF^+, and Rb is unreactive. An advantage is had using this chemistry because F is monoisotopic and hence measurement of the Sr isotope ratios is not convoluted by further corrections. Fig. 35 provides a superimposition of spectra for two solutions, one containing Rb and the other Sr, so that the separate contributions to the combined mass spectrum can be observed. The Sr^+ signal is largely shifted to SrF^+, and the Rb^+ signal is obtained at its atomic mass. It might be noted, as mentioned earlier, that exceptional efficiency of conversion of the Sr isotopes is not required for this application, as the $m/z=85$ corresponds only to Rb and can be used for the construction of the isochrone. Neon buffer was used to homogenize the ion temporal distribution (Section 8.2.2), and yielded isotope and element ratios that approximated the counting statistics limit. The resultant isochrone, expressed in the usual isotope configuration, is shown in Fig. 36, where the ICP-DRC-MS result using in situ chemical element resolution compared very favorably with the accepted TIMS result that used prior chemical separation [118].

9. Applications

In the 5 years since their first commercial implementation, publications relating to the use of

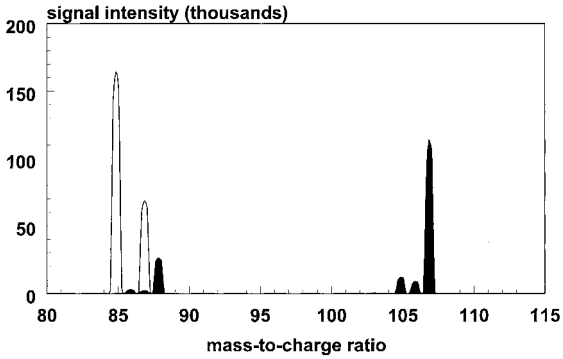

Fig. 35. Mass spectra for 50 ppb Rb and Sr, measured separately and overlaid to show the contributions of the isotopes to the combined spectrum, with CH_3F as reaction gas. Sr^+ reacts to form SrF^+ (F is monoisotopic, so that the isotope ratio of SrF^+ reflects the isotope ratio of Sr^+), and Rb^+ is unreactive. (From Ref. [118] with permission of The Royal Society of Chemistry.)

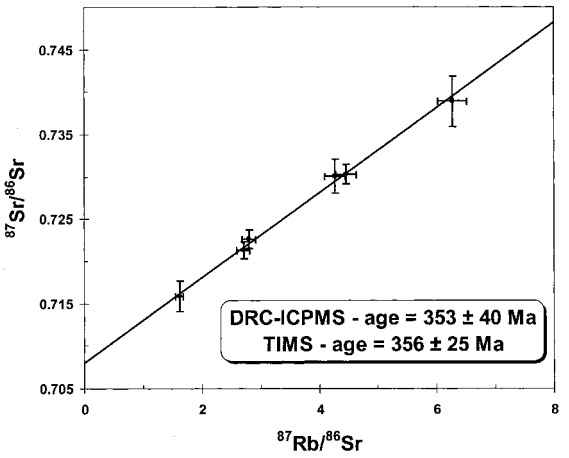

Fig. 36. Sr/Rb isochrone for an intrusive rock formation, obtained by dissolution and direct nebulization without element separation, using CH_3F to convert the Sr^+ to SrF^+, with Neon buffer to improve temporal homogenization. The derived age of the rock is in agreement with the TIMS result [161] and has comparable precision. (From Ref. [118] with permission of The Royal Society of Chemistry.)

collision/reaction cells in ICP-MS have been dominated by fundamental studies and phenomenological characterization rather than practical application. It should be expected, and recent trends justify this, that acceptance of the technique has begun an explosion in the number of publications dealing with the solution of real analytical challenges. We review here the reports of applications of which we were aware as of September 2001.

The 3D ion trap inherently lends itself to operation as a collision/reaction cell device. Variable storage/reaction time can be optimized for speed of analysis or efficiency of reaction, and extends the dynamic range of the instrument which is otherwise severely limited by the space charge of the accumulated ions. It has historically been operated in a bandpass mode (even single amu) using filtered waveforms or broadband excitation, principally to allow for sensitivity enhancement by selective ion trapping, and this capability can be used to suppress the appearance of secondary reactions, though at the expense of duty cycle. Some applications of the ion trap were reviewed in Section 4.3 and are not repeated here. We refer to the paper of Eiden et al. [26] for a summary of the performance characteristics of the ion trap that make it attractive for elemental analysis.

Though a collision/reaction cell appears to offer significant advantage for sector-based ICP-MS, and principally for multicollector detection, adoption in this configuration has been slow. The Micromass IsoProbe has been available for some time, and takes advantage of collisional energy damping to eliminate the need for an electrostatic sector, and the Thermo Elemental Axiom (having both magnetic and electrostatic sectors) has been offered in a cell-configuration (but is no longer). Both of these instruments are (were) available with multicollector detection, and should allow the determination of isotope ratios of interfered elements. An early report [125] indicates that high precision isotope ratios of Fe are indeed possible, but also that the use of H_2 (or impurity H_2O) as the reaction gas can lead to the formation of hydroxides such as $ArOH^+$ that may lead to inaccurate (though precise) results.

Guzowski and Hieftje [126] have suggested the potential analytical benefits of incorporating a collision/reaction cell in an orthogonal Time-of-Flight ICP-MS, including the improvement of resolution and sensitivity as a result of the narrowing of the ion energy distribution before acceleration. While significant improvement in the determination of elements interfered by the argide ions is obtained, it seems that further work is necessary to realize the TOF-specific advantages. Perhaps a notable exception is the reduction of continuum background, probably resulting from more efficient exclusion of argon from the flight tube with a corresponding reduction in the production of argon metastables that may, in part, be responsible for this background. Further, it was shown that the resolution is sufficiently improved to allow spectral discrimination of hydrocarbon ions produced in unwanted secondary reactions. Similar conclusions are reported by Leach and Hieftje [127] for an axial-acceleration ICP-TOF-MS.

By far, the most common application of collision/reaction cells has been in quadrupole mass filter instruments. Of course, this is partly a result of the general acceptance of these instruments in the conventional ICP-MS configuration because of

their relative ease of use, but it is also a reflection that the cell offers relief of the principal disadvantage of the low (unit mass) resolution of the quadrupole. The sequential scanning characteristic of the quadrupole is also compatible with bandpass operation of the cell. Further, the quadrupole has less-demanding vacuum requirements than either a sector or TOF, and so the cell may be operated at higher pressures (higher reaction efficiency), higher conductance to the mass analyzer, and/or with less expensive vacuum pumping.

9.1. Method development

It is convenient if the instrument may be operated either with or without collision/reaction gas. Operation as a conventional ICP-MS allows optimization of the sample introduction, plasma and ion optics in the familiar manner and permits approximately independent optimization of the cell parameters (recognizing that certain parameters, such as cell and analyzer rod offsets, are mode-dependent). This recognizes that, for the most part, operation of the cell is independent of the plasma and sampling characteristics. The latter statement is not entirely true, but simplifies the first-order optimization of the instrument. Of course, different 'interfering' plasma ions, or the intensities of these ions, are obtained under different sampling and plasma conditions, and the operating conditions of the cell should be adjusted to account for this (i.e. higher or lower efficiency depending on the relative intensities of the analyte and interference, which prescribes the type or pressure of gas to be used in the cell). Where satisfactory performance is obtained using conventional (non-pressurized cell) conditions, this is almost certainly preferred. Of course, an experienced user will realize that improved sensitivity (detection limit) can be obtained by taking advantage of collisional focusing with a pressurized cell (even for a non-interfered ion, where a non-reactive gas may be preferred) [111,112,128,129]. However, where this additional performance is not required for the application at hand, it seems propitious to take advantage of the familiar convenience of this mode.

Where an application requires the use of a cell to improve the performance, it is very important to understand the analytical objectives and the constraints that these impose. Where an increase in sensitivity by as much as a factor or 5 or 10 is the principal goal, collisional focusing with a non-reactive gas may be sufficient [111,112,128]. The gas should have a mass that is a significant fraction of the mass of the analyte ions of interest, and/or the cell should be operated at relatively high pressure. It is important that the gas be as pure as possible and that other gases (plasma or ion optics chamber gases) are excluded as much as possible to minimize reaction. Where collisional focusing is obtained, a significant improvement in abundance sensitivity may also be achieved because of the concomitant narrowing of the ion energy distribution which improves the resolution of the downstream quadrupole mass filter [27,53]. Concomitantly, such conditions lead to temporal homogenization of rapid variations of ion flux, such as high frequency plasma source noise. If the mass filter is scanned sufficiently rapidly to account for low frequency fluctuations, the collisional broadening within the cell (on the order of 5 ms, or homogenization of fluctuations faster than 200 Hz) leads to improved signal correlation and precision of isotope ratios [109].

Where suppression of a background interference is required, a reactive gas is prescribed. It is important to recognize whether the application is specific to a few elements or is generic for a wide range of elements. In general, a multi-element method requires some compromise of performance relative to a specific method. In this instance, a less reactive gas, such as H_2, may be appropriate, as few of the atomic analyte ions react. However, our experience has been that high purity hydrogen does not provide high efficiency of argide ion suppression (cf. Fig. 31c). This is in contrast to the conclusions of other reports [27,79,121] but is consistent with the TOF results of the Hieftje group [126,127]. Careful review of the results reported by Feldmann et al., [62,63] and Boulyga and Becker [112] indicates that, while improvements in signal-to-background (or BEC) of 2–4 orders of magnitude are obtained for some of the argide ions, the background is far from eliminated

(which requires improvements of up to 9 orders of magnitude). Further study to determine the reasons for the disparate results reported for H_2 as a reaction gas are required and should probably focus on the role of impurities in the chemistry or the importance of concomitant damping gases [30,79] to facilitate thermalization of the ions. Other gases, such as methane, ethane, ethylene, or even ammonia may be more effective 'general purpose' gases, though reaction of some analyte ions with the gas (such as As^+ with CH_4 or NH_3) must be accounted for (and in these instances, it may be appropriate to determine these reactive ions at the masses of their product ions).

Where the analytical challenge is limited to a few elements, exceedingly high efficiency of improvement in the BEC can be obtained with appropriate choice of the reaction gas. Kinetic [10] and thermochemical [9] databases provide the basis for selection of the appropriate gas. Optimization of the cell pressure (flow rate of gas) and means of suppression of the secondary chemistry (kinetic energy discrimination or bandpass parameters) should be performed by comparison of a method blank and a spiked sample. Where a true blank is available (most environmental, clinical, geological samples), the criterion of optimization might be the achievable detection limit. Where temporal homogenization leads to background signal noise that is characterized by counting statistics, it is convenient to determine the 'estimated detection limit' defined as 3 times the square root of the blank signal divided by the net sensitivity (for optimization purposes it is not essential to define the measurement time). Many elements will optimize at similar cell pressure, though some (especially $^{40}Ca^+$) will optimize at a higher pressure because of the higher efficiency required. Some compromise for this parameter may then be required, but this usually results in detection limits that are within a factor of a few of the ultimate element-specific values. Where a true blank is not available (e.g. for semiconductor pure water or high purity acid analyses), it is our contention that a preferred basis of optimization is the BEC, as the blank itself in this instance is also the sample, and the minimum BEC must correspond to the upper limit concentration of the analyte in the sample.

To be of greatest value, a method should be transferable between instruments and laboratories. Certainly, variations in achievable results will be inevitable due to differences in skill levels in sample preparation (notably in contamination), but the method itself should be applicable with as little variation as possible. This is possible where the different instruments provide comparable thermal characteristics, consistent ion optic optimization, and uniform gas flow calibration. Indeed, it is to be expected that the majority of practitioners will operate under the conditions of methods developed in other laboratories, and that 'cookbook' recipes will be provided for many common applications. Nonetheless, the development of specific applications can be a challenging exercise, and will be facilitated with the promulgation of a generic, knowledge-based approach to method development.

9.2. Developed methods

9.2.1. High purity water and process chemicals (semiconductor)

Because reaction cell methods provide a rather simple and effective means of suppressing Ar^+ and argide polyatomic interferences on Ca^+, K^+ and Fe^+, principally because the argide ions have relatively high electron affinities (the corresponding neutrals have high IPs) and hence react by charge transfer with a variety of neutral gases and produce few secondary interferences, initial attention focused on its use as an alternative to cool plasma methods [130,131]. In general, comparable results are obtained for high purity water analysis, but the reaction cell approach has an advantage for the analysis of high purity acids and other complex samples where the cool plasma approach suffers from concomitant element effects (easily ionized element effects) in the plasma which diminish sensitivity [131]. Even for the high purity water application, the reaction cell approach has an advantage in that the method allows identification of the residual argide signal through the element-specific slope of the reaction profile [30],

whereas this contribution to the signal in the cool plasma method may be uncertain and variable.

The suppression of the argide ions was clearly shown in the early work of Rowan and Houk [21] and the ion trap results of Koppenaal et al. [22–26], though the application to semiconductor materials analysis was not explicitly noted. While Turner et al. [27] claimed high efficiency for H_2 as a collision gas, the role of impurities was not recognized and the quantitative benefits were not obvious. Feldmann et al. [63] showed low-ppt detection limits, using H_2 as a reaction gas, though several of the important analyte elements (Ca, Fe, Ni) were detectable at levels higher than required for the semiconductor application, and a value for K was notably absent. Boulyga and Becker [111] showed that up to 5 orders of magnitude suppression of Ar^+, ArO^+ and Ar_2^+ could be obtained with H_2 using kinetic energy discrimination, with a concomitant, though lesser, effect on the sensitivity to atomic analyte ions. Tanner et al. [30,119,132] showed greater than 8 orders of magnitude suppression of Ar^+, while retaining the sensitivity to Ca^+, using NH_3 as a reaction gas, providing sub-ppt detection limits for a suite of elements including Ca, K and Fe in high purity water. It was also shown that As^+ reacts with NH_3, not recognizing the potential for determination of As as $AsNH_2^+$, and that satisfactory results for As were obtained using H_2 in a buffer gas of Ar. The NH_3 results are consistent with those reported by Bollinger and Schleisman [133,134]. The latter work also showed the notable potential for determination of As as AsO^+, though the mechanism of this conversion was not clearly proven and appeared to be a result of reaction with adventitious contaminants. Olesik et al. [135] showed oxidation of As^+ with O_2, and corresponding oxidation of Se^+. Recent work by Bandura et al. [65,80] has shown the efficacy of oxidation using O_2 as the reaction gas; results given in Fig. 34 demonstrate a similar potential for determination of As as $AsCH_2^+$ with CH_4 reaction gas. Table 6 summarizes the reported detection limits in high purity water.

Vollkopf et al. [136] met semiconductor guidelines requiring $\pm 25\%$ recovery at the 10 ppt level in 31% hydrogen peroxide, even for ^{56}Fe which was determined at 3.3 ppt in repetitive analyses over a 5 day period with 95% mean spike (11.25 ppt) recovery. Bollinger and Schleisman [133] report detection limits for 41 elements in high purity water, nitric acid and hydrochloric acid.

Kishi and Kawabata [137] show that the efficiency of chemical resolution in a reaction cell allows the determinations to be conducted under robust plasma conditions where even relatively concentrated acids (nitric and sulfuric) do not cause plasma suppression effects; exemplary data comparing the sensitivity for K^+ as a function of nitric acid concentration and plasma power are given in Fig. 37. Table 7 gives the results of Porche et al. [138] showing spike recoveries of better than $\pm 20\%$ for a suite elements in 2000 ppm Si and determination of these at the low ppt level.

9.2.2. Environmental

Environmental samples present a spectrum of challenges: high salt content requires a rugged interface and optics, high concentrations of concomitant elements present spectral interferences, and in some instances exceptional detection limits are required (e.g. determination of actinide contamination). The first of these presents a particular challenge for cell-based instruments, as it is to be expected that direct exposure of the cell to the plasma source risks contamination of the cell with the major elements of the sample both through deposition of atomic ions (which can be expected to 'stick' once neutralized on a surface) and by direct impact of incompletely vaporized particles. Contamination of the cell can lead to memory effects, as deposited material can be sputtered and reionized within the cell, and can cause surface charging of sensitive optical components (particularly the multipole rods) resulting in unstable signals. Common high concentration elements, such as Na, form argides readily; fortunately, most of the argide ions, including the metal argides, have relatively high electron affinities (the corresponding neutrals have high IPs) and can be chemically resolved in a manner entirely analogous to that for ArO^+, ArH^+, etc. Hence, these historically challenging interferences, that have limited the application of ICP-MS for seawater analysis

Table 6
Detection limits (ppt) in high purity water

Element	Isotope	Feldmann et al. [63][a]	Tanner et al. [30][b]	
	(amu)	(DL/ppt)	(DL/ppt)	(BEC/ppt)
Li	7		0.08	0.06
Be	9	7.7	0.6	
B	11		1	6.3
Na	23		0.3	0.7
Mg	24	28	0.35	0.22
Al	27		0.07	0.13 (NH_3)
K	39		0.35	0.68 (NH_3)
Ca	40	70	0.4	0.62 (NH_3)
V	51	0.9	0.3	(NH_3)
Cr	52	0.7	0.25	0.98 (NH_3)
Mn	55	1.7	0.09	0.11 (NH_3)
Fe	56	17	0.15	1.63 (NH_3)
Co	59	0.7	0.07	
Ni	60	16	0.4	0.76
Cu	63	3		0.75
Zn	64		0.6	1.84
Zn	68	8		
As	75		0.6	(H_2/Ar)
Se	80		0.7	(CH_4)
Sr	88	0.3	0.02	0.01
Rh	103		0.01	
Ag	107	0.3		
Cd	114	0.4	0.08	0.04 (NH_3)
In	115		0.01	
Sb	121		0.06	
Te	128	9		
Cs	133		0.03	
Ba	138	0.2	0.04	0.01 (NH_3)
Pb	208	0.7	0.03	0.01
Bi	209	0.5		
U	238	0.1	0.01	

[a] These data appear to have been obtained under compromise conditions appropriate for the entire suite of elements, using H_2/He as the collision/reaction gas. The high purity water may have been acidified.

[b] These data were obtained under cell conditions that were approximately optimum for each element. Some of these data were obtained in a round-robin test, for which the indicated BECs were obtained at the same time as the DLs. The type of reaction gas used (if any) is given in parentheses. Water was obtained from a Millipore Elix/Gradient water system.

for instance, are rather trivial challenges for collision/reaction cell instruments. More challenging, because of their thermochemical properties that resist charge transfer and other convenient reactions, are certain oxide ions such as MoO^+ and CaO^+ that interfere with the determination of Cd and Fe, Ni, Co, etc., respectively.

Godfrey et al. [139] described the analysis of potable water containing Na, K and Ca at high ppm levels and As, Cd and Se at ppb levels using the PQ ExCell. On-line sample dilution, with standard addition in the diluent, was used. Both standard and Collision Cell Technology (CCT) modes were used, with notable improvement observed principally for Fe and Se due to attenuation of argide interferences and the consequent availability of more abundant isotopes for analysis. As these results were obtained for He as the collision gas, and since we have shown that collisional fragmentation must be inefficient (Section

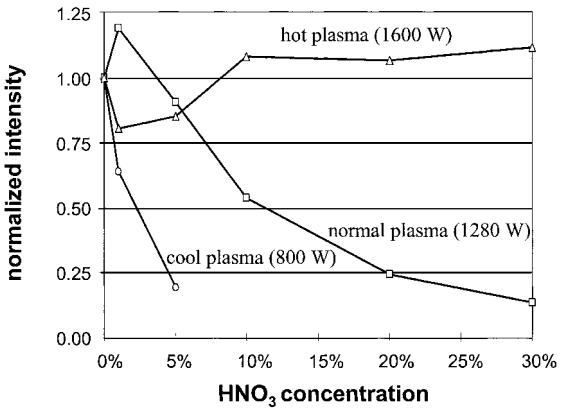

Fig. 37. Potassium ion signal ($^{39}K^+$), normalized to the signal for pure water, as a function of nitric acid concentration at three plasma powers. Under cool plasma conditions (800 W), the acid causes matrix suppression of the K^+ signal. The suppression is less severe under 'normal' (1280 W) plasma conditions, but is still substantial. Little dependence on the nitric acid concentration is observed under 'hot' plasma conditions (1600 W). Data were obtained using ammonia reaction gas to remove the ArH^+ interference. (From Ref. [137] with permission.)

5.2), it must be concluded that the beneficial effects result from contaminants derived either from the gas (the purity was not indicated) or, more likely, from incursion of plasma gases into the cell.

Leonhard et al. [121] provide the first report using the Octapole Reaction System with the Agilent 7500c, showing multi-element determination in 1:10 diluted seawater and in 0.3% NaCl solution. Three modes of analysis are described: standard (no cell gas), H_2-mode and He-mode. A lesser abundant isotope of Se was used for analysis, though dramatic improvement in the determination of Fe is shown at its major isotope at $m/z=56$. The $ArCl^+$ interference on As^+ is reportedly resolved in He-mode, though the authors note that the role of contaminants in the gas is unknown. Reaction profiles are provided showing more rapid suppression of argide and oxide interferences than of analyte ion signals, where the latter appears to be ascribed to energy discrimination as the cell pressure is increased. The result, nonetheless, is a substantial improvement of more than 2 orders of magnitude in BECs for Cr, Fe, Co, Cu and As. Detection limits for a suite of elements are sufficient for multi-element determination in diluted seawater, though half of the elements are determined at or near their detection limits. No mention is made of means to

Table 7
Spike recovery and determination in 2000 ppm Si (from Ref. [138])

Element	m/z	Unspiked sample measured concentration (ppb)	Spike amount (ppb)	Spiked sample measured concentration (ppb)	Spike recovery (%)	DL (ppt)
B	11	1.311	4.85	5.232	80.8	6.9
Na	23	1.055	4.85	5.696	95.7	1.9
Mg	24	0.045	4.85	4.675	95.5	1.1
Al	27	0.846	4.85	5.261	91	3.4
K	39	0.264	4.85	5.138	100.5	1.9
Ca	40	0.214	4.85	5.3	104.9	1.11
V	51	0.001	4.85	4.896	100.9	0.84
Cr	52	0.052	4.85	4.869	99.3	2.7
Mn	55	0.001	4.85	4.723	97.4	0.67
Fe	56	0.018	4.85	4.56	93.7	3.6
Ni	58	0.017	4.85	4.265	87.6	3
Co	59	0.003	4.85	4.414	90.9	0.72
Cu	65	0.034	4.85	4.351	89	5.1
Zn	66	0.048	4.85	4.38	89.3	7.7
Mo	98	0.005	4.85	4.385	90.3	2
Cd	114	0.001	4.85	3.938	81.2	0.98

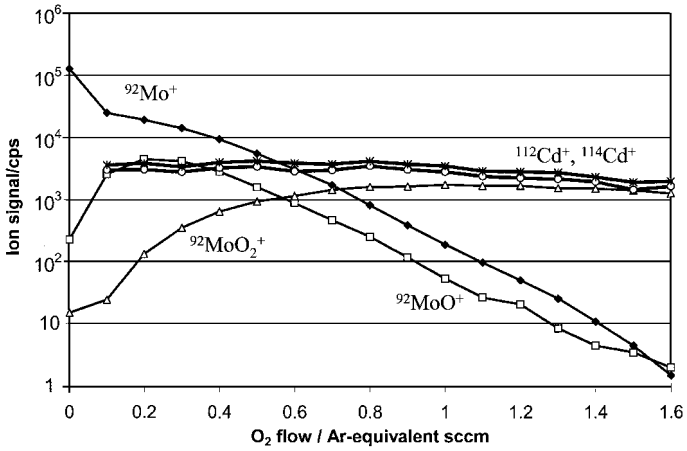

Fig. 38. Reaction profiles for Mo^+, MoO^+ and Cd^+ with O_2 reaction gas, obtained for a solution containing 20 ppb Mo and 2 ppb Cd, at the operating point (RPa, RPq) = (0, 0.75) with a high accelerating field. Mo^+ is sequentially oxidized to MoO^+ and MoO_2^+. Operation with a high low mass cut-off (high q) minimizes formation of MoO^+ within the cell by rejecting the precursor Mo^+, which in turn facilitates quantitative conversion of the monoxide ion to the dioxide ion.

account for the difficult oxide interferences CaO^+ and MoO^+ on Fe and Cd, respectively.

Bandura et al. [65,80] investigated ion–molecule chemistries that may be of value for the determination of Fe in high Ca matrices, for which the interference imposed by CaO^+ is a significant challenge. Because of its high thermodynamic stability (low corresponding IP and O-atom affinity), the CaO^+ is resistant to many convenient reaction gases. Two potential strategies were presented: oxidation of Fe^+ with N_2O to remove the analyte ion to FeO^+ for mass analysis at $m/z = 72$ (further oxidation of CaO^+ is slow), or O-atom abstraction from CaO^+ to CO (Fe^+ is non-reactive with CO). Neither approach will eliminate the interference at very high Ca/Fe ratios, but the latter in particular offers the potential for an order-of-magnitude improvement in the BEC for Fe (perhaps limited by concomitant re-oxidation of Ca^+ by impurities in the gas).

Recent unreported work from our laboratory suggests that the MoO^+ interference on Cd^+ might be resolved by promotion of oxidation with O_2 as the reaction gas. The O-atom affinity of Cd^+ is not known (but reaction with O_2 is apparently endothermic) while oxidation of Mo^+ to MoO^+ is nearly thermoneutral (according to the NIST database of Ref. [9], the reaction is exothermic by 2.7 kcal/mol, which is consistent with the observation that the reaction is observed to proceed, albeit slowly, in the SIFT apparatus [140], as is the subsequent oxidation to MoO_2^+). For this scheme to be effective, relatively high O_2 pressures are required, since it is necessary to achieve quantitative conversion of plasma-produced MoO^+ to its dioxide. The formation of MoO^+ in the cell, which would exacerbate the challenge, is suppressed by operation at relatively high q (to remove the precursor Mo^+ from the cell). Provision of an axial field within the cell to promote transport of the ions through the relatively heavy and high-pressure gas is essential. Reaction profiles for Mo^+, MoO^+ and Cd^+ are given in Fig. 38. The increment of the MoO^+ interference on Cd^+ at low flow is a result of the primary oxidation of Mo^+, but at higher O_2 flows the monoxide is nearly quantitatively converted to MoO_2^+. Concurrently, Cd^+ is transported without reaction. Spectra of 10 ppb Mo in high purity water with and without 10 ppt Cd are given in Fig. 39 under conditions optimized for Cd determination in a Mo-matrix.

Exceptional sensitivity is required for the analysis of actinides in the environment, such as the determination of uranium isotope ratios for identification of spent fuels. Boulyga et al. [128]

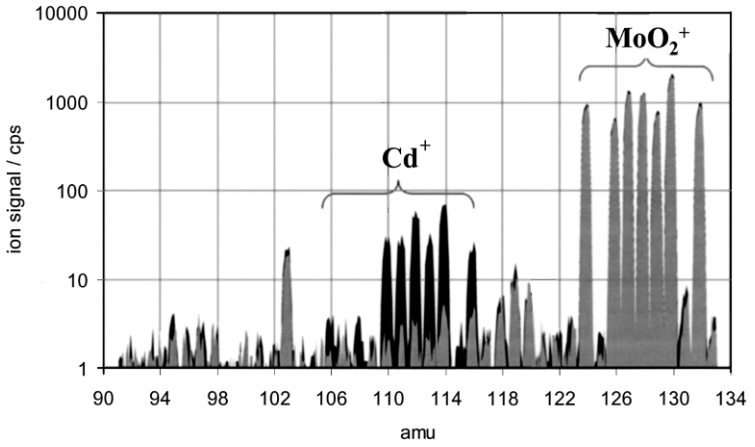

Fig. 39. Mass spectrum of a solution containing 10 ppb Mo with (black) and without (grey) 10 ppt Cd, obtained with O_2 reaction gas (1.6 Ar-equivalent sccm = 1.14 sccm), (RPa, RPq) = (0, 0.75). Oxidation of MoO^+ to MoO_2^+ relieves the interference of the monoxide ion on Cd^+.

analyzed soils in the vicinity of the Chernobyl incident, and were able to identify fallout from the accident through the unnatural abundance of $^{235}U/^{238}U$ and $^{236}U/^{238}U$ ratios. Combination of ultrasonic nebulization with collisional focusing provided by He in the collision cell of the Platform provided astounding sensitivity of up to 27 GHz/ppm, though it is not clear how the analog output of the Daly detector is converted to ion count rate. Nonetheless, the sensitivity was sufficient to provide for single digit ppq detection of ^{236}U, and to identify the unnatural isotope distribution in the soil samples. Because of the relative abundance of the isotopes, care was required to minimize formation of hydrides, and a membrane desolvator was effective in this regard though at the cost of some sensitivity.

9.2.3. REE and actinide oxide and hydroxide ions

The atomic ions of the rare earth elements (REEs) have relatively high O-atom affinities. Several REE-oxide ions persist even at the plasma temperature at levels sufficient to convolute the determination of the suite of REEs. Du and Houk [141] have shown that the collision/reaction gases He/H_2 significantly reduce the signals for metal oxide ions relative to atomic ions. The effect is observed only when the mass analyzer bias potential is positive with respect to the collision cell bias potential (i.e. when kinetic energy discrimination is employed). A reaction mechanism for the relative suppression of the oxide ions is not obvious. A reasonable interpretation is that the oxide ions are discriminated against relative to the corresponding atomic ions on the basis of their post-collision kinetic energies. If a substantial fraction of the oxide ions observed were in fact produced within the cell, due to reaction with impurities introduced either with the gas or by entrainment of plasma gas, the product ions would have lower kinetic energy than the atomic ions since the product ion of the reaction is retarded somewhat by addition of the oxygen atom from the relatively stagnant gas. In addition, polyatomic ions have larger collision cross-sections than the corresponding atomic ions and, hence, will suffer more collisions with resultant increased energy damping. Finally, the polyatomic ions have additional internal degrees of freedom in which to dissipate the collision energy, so that the post-collision translational energy is, on average, less than for a corresponding atomic ion. Together, these effects suggest that the metal oxide ions will have a lower average kinetic energy than the atomic ions, and hence are more efficiently discriminated against by the potential barrier established at the mass filter. This mechanism does not account for the observed element-specific variation

of the efficiency of oxide-suppression noted by Du and Houk, unless there are differences in the proportion of the oxides that are formed within the cell, the cross-sections are substantially different, or the efficiencies of energy conversion into internal excitation differ because of the different bond strengths.

As an aside, Du and Houk [141] present an expression for the mean free path in a collision cell, $\lambda = (\sqrt{2}\pi\sigma n)^{-1}$, that differs from that used to describe the mean free path in, for instance, the ion optics, $\lambda = (\sigma n)^{-1}$. The $\sqrt{2}$ term is properly used when the ion velocity is comparable to the neutral velocity; that is, for a thermalized condition, appropriate for a thermalized cell. When the ion velocity is substantially greater than the neutral velocity, as in the ion optics or in a cell prior to thermalization, the $\sqrt{2}$ term is omitted. However, the π term is appropriate only when the cross-section, σ, is given as the square of the impact parameter. As used by Du and Houk, and used here, the cross-section is given as the integral area of interaction (i.e. $\pi(r_1 + r_2)^2$ for the hard sphere case), in which case the π term is inherently included. Accordingly, Du and Houk have underestimated the mean free path, and over-estimated the number of collisions, by approximately a factor of 3.

Simpson et al. [142] propose the use of O_2 as a reaction gas to suppress the appearance of oxide ions that interfere with the determination of the noble metals. The noble metals are relatively resistant to oxidation, whereas potential interferences (such as the oxides of Zr, Nb and Hf) appear to react with O_2, presumably by further oxidation. The result is that the noble metals can be determined with much reduced (or eliminated) interference. Two mechanisms are suggested for this observation. The first is that the oxide ions, or their further oxidation products, are more efficiently scattered from the cell due to their more efficient thermalization with the gas. However, relatively high flow rates of O_2 were used, implying a relatively large number of collisions, and the gas itself is relatively heavy. Hence, it is expected that all of the ions are nearly uniformly thermalized, so that scattering losses of the polyatomic and atomic ions should be comparable. The alternative suggestion is that the refractory interferences are sequentially oxidized to high levels (e.g. HfO_4^+) which removes the interfering ions from the spectral region of interest. These higher oxides (and hydroxides, presumably derived from reaction with impurity water in the gas) were observed for Hf, and it is suggested that yet further oxidation removes the interfering ions completely beyond the mass range of the instrument. A further possibility might be that sequential oxidation eventually leads to an ion that might be unstable (i.e. that eliminates O_x^+ as a product ion), in a manner analogous to NO^+ that hydrates three times ($NO^+(H_2O)_3$) before subsequently producing $H_3O^+(H_2O)_2$ [143], hence removing the interference ion and product ions which include it from the spectrum.

Though CO is an effective reductant (its O-atom affinity is sufficiently large to extract an O atom from CaO^+, as discussed above), CO_2 will donate an oxygen atom to most of the REE ions (except Eu^+ and Yb^+). As shown by Baranov et al. [144], CO_2 as a reaction gas nearly quantitatively converts most of the REE ions to their oxides. While there are stronger oxidant reaction gases that will allow oxidation of all of the lanthanide ions, the advantage of CO_2 is that the O-atom affinities of most of the REE-oxide ions appear to be less than that of CO, so that the oxides do not further oxidize to the dioxide. Hence, the REE pattern is simply reproduced 16 amu higher than the atomic spectrum (with the addition of the ^{18}O contribution, which can be corrected for using the natural abundance of the oxygen isotopes), alleviating the spectral overlap of the oxides.

Hattendorf and Günther [145] used a reaction cell in an innovative study of the formation of doubly charged oxide and hydroxide ions of Th. These ThO^{2+} and $ThOH^{2+}$ are typically present (in various ICP-MS instruments) at approximately 1% of the Th^{2+} signal level, which is itself 1–3% of the singly charged Th^+ signal. All of the doubly charged ions optimize in a similar manner with respect to the plasma conditions, which distinguishes them from ThO^+ which optimizes under cooler plasma conditions. They studied the relative oxidation and hydroxylation rates of the doubly

charged Th^{2+} ion in the reaction cell, showing that doubly charged ion reaction rates are typically greater than those of the corresponding singly charged ions. This allowed the preliminary conclusion that the doubly charged oxides and hydroxides are likely formed in reactive collisions with O-containing species either in the expansion through the interface or within the ion optics chamber, while singly charged polyatomics are more probably characteristic of the plasma source itself. Interestingly, the reaction study was performed with high purity neon as the reaction gas, taking advantage of the oxide impurities in the gas (which was used directly and not processed through a getter).

The doubly charged ion reactivity report allows comment on an interesting but separate issue. The present authors originally expected that the use of a reaction cell should cause the doubly charged ions to be under-represented in the spectrum. This was based on the recognition that the second IP of most species is relatively large, so that charge transfer is in many instances exothermic, and that the collision rate should be larger than for singly charged ions because of the enhanced charge-induced-dipole potential, leading to more collisions and hence higher reaction efficiency. The effect is generally not observed, at least for atomic neutral reactants. This is a result of the surprisingly low rate constant (efficiency) for charge transfer reactions of many doubly charged atomic ions with atomic neutral species [146]. The interaction of a doubly charged ion and a neutral is attractive at large internuclear separation and repulsive at small separation, but the products are two singly charged ions that are mutually repulsive. It might be simplistically viewed that the repulsion of the product ions causes separation of the transition state before the electron is completely transferred. In fact, there is a 'reaction window' based on the energetics of the reaction (for $\Delta H_r \sim -4 \pm 1$ eV) for which the reaction typically proceeds with rates comparable to efficient singly charged ion–molecule reactions [146–148], which makes this type of reaction unique in being 'thermodynamically driven' (the rate constant depends on the heat of reaction) [148]. In many reactions with molecular neutrals, but not all, the multitude of electronic and vibrational states cause curve crossings in the reaction coordinate system that facilitate fast (frequently dissociative) charge transfer reaction [146].

It may be opportune here to dispel yet a further frequent misunderstanding. It is common to determine the 'oxide ratio', as a significant performance characteristic for conventional ICP-MS, through measurement of the CeO^+/Ce^+ ratio. The present authors have often been told that this ratio is dramatically increased when NH_3 is used as a reaction gas, with the interpretation that the oxide ratio is increased, presumably resulting from reaction with impurities in the gas. However, Ce^+ reacts with ammonia forming $CeNH^+$ and $CeNH_2^+$, the latter being isobaric with CeO^+, and the increase in this measured ratio simply reflects the reaction efficiency. Spectra are given in Fig. 40 for reaction of Ce^+ with NH_3 and ND_3. Deuterated ammonia causes a shift of the product ion masses that is consistent with the formation of $CeNH^+$ and $CeNH_2^+$, with little, if any, evidence for concomitant formation of an oxide ion (though the spectra require correction for the contributions of the Ce isotopes, for the D/H purity of the ND_3, indicated by the manufacturer to be 99%, and for the possible persistence of the $\approx 3\%$ CeO^+ that derives from the plasma as its reactivity with NH_3 is not known). If it is desired to know the oxide ratio as an indication of plasma conditions, it should be measured without gas in the cell. If it is necessary to use a pressurized cell, the plasma conditions are reflected only if an element whose atomic and oxide ions are either non-reactive (a possibility may be Ba^+/BaO^+, for which at least the atomic ion appears to be unreactive with NH_3) or similarly reactive; otherwise the observed ratio is reflective of the relative reactivity within the cell, even with high purity inert gases, as shown by Hattendorf and Günther [145].

9.2.4. Geological

Alleviation of the interferences caused by REE oxides, discussed above, is probably most relevant to geological applications. Other applications of collision/reaction cells in this area include the resolution of interelement isobaric interferences, improvement of isotope ratio precision through

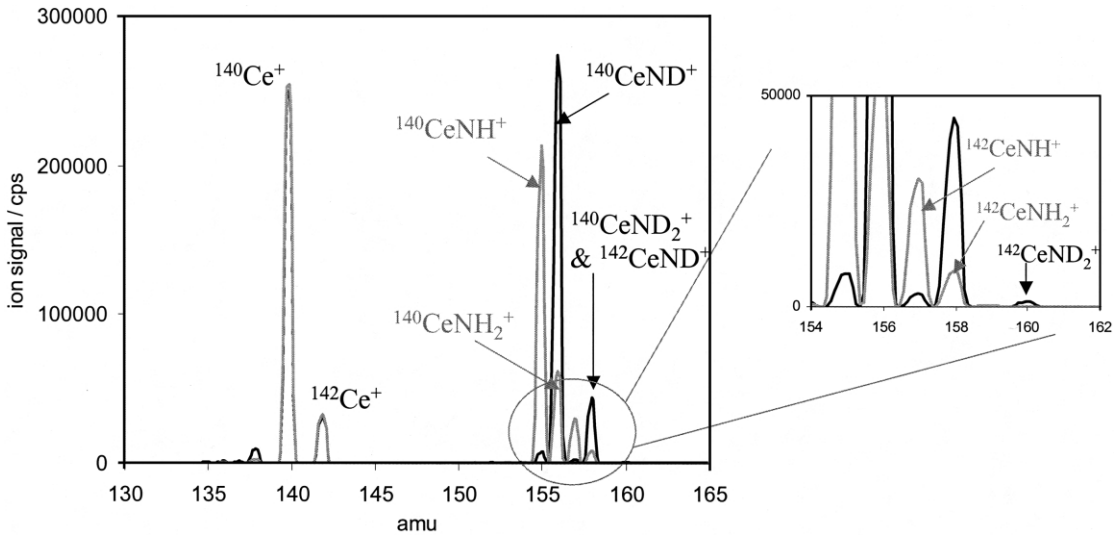

Fig. 40. Mass spectra obtained for a solution containing 5 ppb Ce, using NH_3 (grey) or ND_3 (black) as reaction gas. Reaction gas flow was 0.3 Ar-equivalent sccm (0.16 sccm) yielding approximately 50% reaction of the Ce^+, and the operating point was (RPa, RPq) = (0, 0.5). The principal reaction product ion is $CeNH^+$ ($CeND^+$), with a minor ($\approx$20%) reaction channel leading to $CeNH_2^+$ ($CeND_2^+$). (Ion signals below 140 amu are dominated by washout of Ba from an earlier experiment: the ND_3 experiment was performed first, so the Ba^+ signals appear enhanced but these are artefactual.)

collisional homogenization, and laser ablation of inhomogeneous materials.

Mason [149] has recently reviewed the use of collision and reaction cells for laser ablation. A description of available instrumentation is given, together with a brief review of some of the relevant fundamentals. Applications for the analysis of a variety of geological matrices, including chromite, carbonate and carbon-rich minerals, inclusions and sulphides are reviewed, and the potential for biogeochemical determinations is suggested. It is noted that the 'dry' plasma typically used in this application is characterized by different polyatomic interferences than are encountered during solution nebulization. Notably, the oxides are less of a challenge because the oxygen content of the plasma is less; the problem does not disappear, but is reduced in magnitude. The argide ions cause the most interference, including the argide ions of concomitant elements (ArC^+, $ArNa^+$, $ArCr^+$, etc.). Fortunately, as noted earlier, these argide ions have high electron affinities and are normally resolved through using the same chemistries as appropriate for Ar^+, ArH^+, ArO^+, etc. Multi-element conditions, which may require a degree of compromise in the overall chemistry, is particularly important for transient samples, such as raster scanning of inhomogeneous materials, or the analysis of fluid inclusions. Mason's identification of a potential problem in rapid scanning over a transient has been discussed in Section 7.5, where it is shown that an axial field minimizes the settling time for ion signal stabilization.

Hattendorf and Günther [79], however, note that this is not the only deficiency of using a reactive gas, such as ammonia, for multi-element determination. While noting the limitation of the ion transit time for the original DRC instrument, they also note that certain important elements are reactive with ammonia and hence are suppressed due to their conversion to other species. While it may be possible to determine these elements at their product ions, this may not be consistent with full-elemental coverage, as there may be a concomitant need to suppress the observation of condensation products that are interferences and to promote similar processes for the measurement of the reactive ions. That is, a gas is not appropriate if it

reacts with an element in the sample to form an interference for another element if the product ion cannot be, or is desired not to be, suppressed. In this instance, the efficiency of the chemistry must be compromised by selection of a less reactive gas. The latter work compared the efficiency of H_2 and NH_3 for the suppression of common interferences, noting that the latter is approximately 1 order of magnitude favored, consistent with literature values of the reaction rate constants. Addition of a relatively heavy buffer gas, such as Ne or Xe, enhances the thermalization of the ions and improves the efficiency of H_2 as a reaction gas, allowing 3 orders of magnitude suppression of the $^{40}Ar^+$ signal (by contrast, buffering with He provided only approx. 1 order of magnitude reaction). It was found that buffered H_2 was sufficient for the analytical purpose, consistent with the precept noted in Section 9.1 that the reaction gas is to be selected on the basis of the analytical objectives and the constraints that these impose. Ca was determined in high purity quartz using the most abundant $m/z=40$ isotope, providing an improvement in detection limit of 2 orders of magnitude over prior work (≈ 1 μg/g in the glass). It was also shown that the $ArCr^+$ interference on Nb and Zr could also be relieved, allowing the determination of these elements in pure chromium metal. In related work using solution nebulization, Hattendorf et al. [150] determined Zr and Nb in chromium matrix solutions. Suppression of the $ArCr^+$ interference was obtained as above, but a new interference related to the use of solution nebulization, formation of CrO_x^+, was observed. These ions apparently derive from reactions of Cr^+ with oxygen species in the cell and are suppressed by operating with a bandpass having a relatively high low mass cut-off (RPq = 0.7). The detection limits obtained for Nb and Zr, estimated to be 2 and 5 ng/g, respectively, in the pure Cr metal, appear to be limited by Nb and Zr contamination in the Cr stock solution (as determined by the terminal slope of the reaction profile, as discussed in Section 6.2.3.3).

Günther et al. [151] show equivalence of the standard mode (unpressurized) and DRC mode (pressurized with H_2/Ne) for major, minor and trace element determinations in fluid inclusions by LA-ICP-MS, concluding that the reaction cell is well-suited for fast transient multi-element analysis. They note that most (uninterfered) elements are unaffected by the reaction cell conditions employed (though the sensitivity for the refractory elements Ce and Th is reduced due to oxidation with impurities in the gas), and that substantial improvement in detectability for normally interfered elements (a factor of 250 in detection limit for Ca and 20 for Fe) is obtained. They also show that the temporal response for fast transients (on the order of a second) is unaffected by pressurizing the cell, which is consistent with a temporal homogenization period on the millisecond timescale.

Isotope ratio measurements are of particular importance in some geological applications. Sector instruments equipped with multicollector detectors provide excellent ratio precision, and the incorporation of a collision/reaction cell should allow accurate measurements for normally interfered elements [125]. Feldmann et al. [63] report Pb isotope ratios, measured with a quadrupole (sequential scanning) equipped with hexapole collision cell, with precisions better than 0.1%. The measurement of U isotope ratios in contaminated soils [128] has been discussed earlier, and measurement of the $^{235}U/^{238}U$ ratio at 0.07% R.S.D. has been reported [129]. Measurement of the Pb and U ratios are not usually convoluted by spectral interferences requiring chemical resolution, but use of the collision cell to provide enhanced sensitivity through collisional focusing is advantageous. Boulyga and Becker [111] discuss the use of a collision cell for the measurement of isotope ratios of Ca, Fe and Se where a hydrogen/helium mixture is used to eliminate the common spectral interferences that hitherto have prevented accurate measurements at low (sub-ppm) concentrations. Optimization results with respect to helium flow (providing collisional focusing), hydrogen flow (providing chemical resolution) and hexapole bias (kinetic energy discrimination) are provided. Mass discrimination factors across the mass range are determined and compare favorably to conventional quadrupole instruments. Combined uncertainty for the Ca and Fe (10 ppb) and Se (100 ppb) isotopes is generally better than 0.7%, and the accuracy is

generally better than 1%. Improved precision of isotope ratio measurements have also been reported by Bandura et al. [109,110], as discussed in Section 7.5, and by Moens et al. [118], as discussed in Section 8.4.3.

Mason et al. [67] have discussed optimization for the determination of $^{34}S/^{32}S$ ratios in lake water which is affected by biogenic redox reactions. The interference of O_2^+ on sulfur is shown to be reduced by reaction with Xe (with He buffer and enhanced with the addition of H_2) in a collision/reaction cell. The BEC is reduced by about an order of magnitude to approximately 1 ppm, which is sufficient for the application at hand (determination of S isotope ratios at 10–50 ppm), and detection limits in the range 20–50 ppb are shown. Precision in the isotope ratio measurements (for 10–50 ppm S in water and acidic solutions) approaches the counting statistics limit (≈0.2–0.4% R.S.D.). The method is applied to the determination of sulfur concentration and isotope ratios in crater-lake acid water and spring water and is in good agreement with other measurements.

9.2.5. Biological

We consider biological applications in the wider sense to include speciated determination of drugs, nutrients and poisons and their metabolites, clinical diagnostics and proteomic/genomic analyses. With particular reference to the latter, Jakubowski [152] has said 'in the new millennium, the largest impact on organic mass spectrometry will be from inorganic mass spectrometry'. While this may have been made as a provocative statement, we concur that ICP-MS will make important contributions to proteomic applications, wherein the particular advantages of the method over organic MS methods (relative independence of sensitivity on species and sample matrix, large dynamic range, low detection limits, accurate quantitation) will be capitalized despite the lack of specific mass spectral identification of the species.

Sloth and Larsen [122] showed effective suppression of the Ar_2^+ interference on Se isotopes using CH_4 as a reaction gas, and then used this to speciate selenoamino acids using cation exchange chromatography. Detection limits for these species on the order of 20 pg/ml (as selenium) is said to allow determination at physiologically significant levels. Because of the removal of the argide interference, isotopic ratio determination allows confirmation of the presence of Se, although it was shown that a correction for the formation of SeH^+ (at ≈9.6%) is necessary. Interestingly, experiments with deuterated methane indicate that the hydride does not derive from the reaction gas, suggesting the role of contaminants in the cell.

A thorough comparison of different nebulizers (Meinhard, HHPN and MCN) and chromatographic methods (reversed-phase and ion-pair) for the speciation of selenium in nutritional supplements, using H_2/He as a reaction/collision gas, has been reported by Marchante-Gayon et al. [64]. While the HHPN in combination with either chromatography offered the best relative detection limits (35–90 pg/ml), the lowest absolute detection limit (500 femtogram range) was obtained with MCN coupled to reversed-phase chromatography. Selenium species were hot-water-extracted from commercial nutritional supplements, and several were identified through their retention times. The fraction of organic and inorganic selenium varies dramatically with supplement type and brand.

The determination of V and Cr in serum and urine are reported by Nixon et al. [153,154]. The samples were diluted 1:10 and analyzed directly by aspiration/nebulization. Ammonia reaction gas provided effective suppression of the ClO^+ and ArC^+ interferences, yielding detection limits in the serum and urine in the range of 12 ng/l (V) and 55–80 ng/l (Cr). These detection limits are substantially better than those obtained using GFAAS, and equivalence for determination of these elements in real patient samples by the two methods is shown. Similarly, determination of Se in serum and urine using methane as reaction gas is capable of detection limits on the order of 50 ng/l in the undiluted sample [155]. The determination of Fe and Cu in liver tissue, with detection limits of 20 and 2 ng/g (in the tissue) respectively, is shown by Nixon et al. [156], using ammonia to suppress the ArO^+, $ArOH^+$ and $ArNa^+$ interferences.

The degree of phosphorylation of isolated or chromatographically separated proteins is an important diagnostic in proteomics. The usual

analytical method involves radioisotope labeling with ^{32}P [157]. Wind et al. [158] have shown the power of using ICP-MS for the determination of natural ^{31}P. Both a quadrupole ICP-MS with a hexapole collision/reaction cell, operated with H_2/He, and a high mass resolution instrument were used to resolve the $^{15}N^{16}O^+$ and $^{14}N^{16}O^1H^+$ interferences. The collision cell approach required the concomitant use of desolvation, which appeared to result in some suppression of the signals, and it was concluded that the high resolution approach is preferred. In a very recent report [159], they note that the concomitant measurement of S^+ (with high mass resolution) allows effective determination of the degree of phosphorylation through the ratio of P^+/S^+ for homologous proteins that contain cysteine or methionine. Bandura et al. [160] show that P^+ and S^+ may be efficiently oxidized using O_2 as a reaction gas, allowing determination of these elements at less-interfered masses. The BECs under optimum conditions in DIW are 0.5 and 5 ppb, respectively, and detection limits of 0.1 and 0.2 ppb are reported. The BECs of the oxide ions do not appear to be affected by a sample matrix containing 5% acetonitrile, 5% formic acid and 1 mM ammonium bicarbonate, whereas one would expect these to impact at the atomic ion masses. The method was shown to correctly yield the number of P-atoms and the P/S ratio for α-casein, and the residual phosphate of dephosphorylated α-casein was determined.

10. Summary

The r.f.-driven reaction/collision cell in combination with a quadrupole mass filter has become an essential tool in many analytical laboratories. It provides an effective means for the chemical resolution of plasma-based isobaric interferences as well as complementary benefits such as improved sensitivity (through collisional focusing), improved mass resolution and abundance sensitivity (through collisional energy damping) and improved precision (through temporal homogenization of high frequency signal fluctuations derived from the plasma source).

Collisional fragmentation is a relatively ineffective process for the ICP-MS application. Ion–molecule chemistry, used either to remove an isobaric interference or to shift the analyte to a less-interfered mass, can be exceptionally efficient. Our preference for chemical reaction derives from the specificity of thermal ion–molecule reactions, the large rate constants resulting from the ion–dipole interaction, and the general lack of activation energy barriers that allow prediction of the relevant chemistry from thermochemical information. An extensive database of thermal ion–molecule reaction rate constants facilitates method development. In order to best take advantage of these characteristics, the reaction cell should be operated under near-thermal conditions. Accordingly, we distinguish collision cells from reaction cells on the basis of the thermal characteristics of the ions extracted from the cell.

The r.f.-driven reaction cell necessarily operates under conditions that deviate from strictly thermal. The relatively large axial energy of the ions at the entrance, required in order to accelerate ions into the cell that is commonly operated above the ambient pressure, is initially converted into radial excitation. After a number of collisions, the radial and axial energies relax together, with a residual degree of radial excitation derived from the secular and applied drive frequencies. This r.f. contribution to the collision energy is a function of the operating conditions including the amplitudes of the r.f. and DC voltages applied between pole pairs, the drive frequency and the number of collisions per r.f. cycle. The rate of thermalization of the ions is a function of the operating conditions and the ratio of the ion and neutral masses. The energy and spatial focusing that derives from these collisional processes results in improved transmission of ions through an on-axis exit aperture (collisional focusing) and an improvement in the resolution of the downstream mass filter.

Efficient primary ion–molecule chemistry that distinguishes analyte ions from plasma-based interference ions is accompanied by efficient secondary reactions that create new isobaric interferences within the cell. Either of two methods is commonly used to suppress the appearance of these secondary interference ions: post-cell kinetic energy discrimination and in-cell bandpassing. The former may be applied when the cell conditions are such as to

retain a fraction of the initial kinetic energy of the ions introduced into the cell; that is, under non-thermal conditions. When the number of collisions suffered by the ions is sufficiently small to allow distinction of the energies of the primary ions from those of the secondary ions produced within the cell, kinetic energy discrimination does provide high efficiency of suppression of the secondary ions. The efficiency of post-cell kinetic energy discrimination is antagonistic to efficiency of the primary reaction chemistry: the former is favored under conditions of few collisions and the latter is favored under conditions of many collisions. Operation of the cell with a bandpass that excludes at least one of the precursor ions of the secondary chemistry suppresses the formation of the secondary interference ions and allows operation of the cell under many-collision conditions that optimize the efficiency of the primary chemistry.

Under multiple collision conditions, the purity of the reaction gas is very important: relatively small traces of impurities can have a disproportionate effect on the overall chemistry if their reaction rate constants with the ions are large. Therefore, when high efficiency of the primary chemistry is required, it is necessary to use the highest purity gases available and to minimize incursion of other gases (plasma gas, ambient vacuum chamber gas) into the cell.

While originally thought to be of most value for the determination of interfered elements in high purity materials, especially those used in the semiconductor industry, the cell has found wide acceptance in other areas already adapted to the ICP-MS method. Many commercial and industrial laboratories have already adopted the method for quality assurance of reagents and products, and for direct determinations in complex samples such as seawater, urine and serum. New opportunities also arise, for instance in geochronology where the ion–molecule chemistry can be used for in situ isobar resolution and the temporal homogenization characteristics of the cell provide isotope ratio precision limited by counting statistics. It is to be anticipated that new applications will continue to develop and these will yet further broaden the scope of the ICP-MS method. It is also obvious that an outstanding opportunity for fundamental research is facilitated.

Acknowledgments

The authors appreciate the stimulating discussions and observations of John Olesik (Ohio State University), Sam Houk (Iowa State University), Bodo Hattendorf (ETH, Zurich) and other practitioners that have inspired us to this work. The patience and encouragement of the editor, Ralph Sturgeon, is much appreciated. We thank Drs Ken Neubauer and Ruth Wolf (Perkin Elmer, Connecticut) for their thorough review of the manuscript.

References

[1] H.I. Schiff, D.K. Bohme, An ion–molecule scheme for the synthesis of hydrocarbon-chain and organonitrogen molecules in dense interstellar clouds, Astrophysical J. 232 (1979) 740–746.

[2] D. Smith, The ion chemistry of interstellar clouds, Chem. Rev. 92 (1992) 1473–1485.

[3] S.G. Lias, P. Ausloos, Ion–Molecule Reactions: Their Role in Radiation Chemistry, American Chemical Society, Washington, 1975.

[4] G. Gioumousis, D.P. Stevenson, Reactions of gaseous molecule ions with gaseous molecules V. theory, J. Chem. Phys. 29 (1958) 294–299.

[5] R.A. Barker, D.P. Ridge, Ion–polar neutral momentum transfer collision frequencies: a theoretical approach, J. Chem. Phys. 64 (1976) 4411–4416.

[6] L. Bass, T. Su, W.J. Chesnavich, M.T. Bowers, Ion–polar molecule collisions. A modification of the average dipole orientation theory: the cos model, Chem. Phys. Lett. 34 (1975) 119–122.

[7] T. Su, W.J. Chesnavich, Parameterization of the ion–polar molecule collision rate constant by trajectory calculations, J. Chem. Phys. 76 (1982) 5183–5185.

[8] T. Su, E.C.F. Su, M.T. Bowers, Ion–polar molecule collisions. Conservation of angular momentum in the average dipole orientation theory. The AADO theory, J. Chem. Phys. 69 (1978) 2243–2250.

[9] S.G. Lias, J.E. Bartmess, J.F. Liebman, J.L. Holmes, R.D. Levin, W.G. Mallard, Gas-phase ion and neutral thermochemistry, J. Phys. Chem. Ref. Data 17 1 (Suppl. 1) (1988) 1–861, Available from http://webbook.nist.gov/chemistry/.

[10] V.G. Anicich, A survey of bimolecular ion–molecule reactions for use in modeling the chemistry of planetary atmospheres, cometary comae and interstellar clouds, Astrophysical J. Suppl. Series 84 (1993) 215, Available from http://astrochem.jpl.nasa.gov/asch/.

[11] D.K. Bohme, Experimental studies of positive ion chemistry with flow-tube mass spectrometry: birth, evolution, and achievements in the 20th century, Int. J. Mass Spectrom. 200 (2000) 97–136.

[12] D. Gerlich, Inhomogeneous RF fields: a versatile tool for the study of processes with slow ions, in: C.-Y. Ng, M. Baer (Eds.), State-Selected and State-to-State Ion–Molecule Reaction Dynamics Part l. Experiment, Adv. Chem. Physics Series, vol. LXXXII, Wiley, 1992, pp. 1–176.

[13] K.M. Ervin, P.B. Armentrout, Translational energy dependence of $Ar^+ + XY \rightarrow ArX^+ + Y$ ($XY = H_2$, D_2, HD) from thermal to 30 eV cm, J. Chem. Phys. 83 (1985) 166–189.

[14] P.B. Armentrout, Kinetic energy dependence of ion–molecule reactions: guided ion beams and threshold measurement, Int. J. Mass Spectrom. 200 (2000) 219–241.

[15] R.A. Yost, C.G. Enke, Selected ion fragmentation with a tandem quadrupole mass spectrometer, J. Amer. Chem. Soc. 100 (1978) 2274–2275.

[16] R.A. Yost, C.G. Enke, Triple quadrupole mass spectrometry for direct mixture analysis and structure elucidation, Anal. Chem. 51 (1979) 1251A–1264A.

[17] R.A. Yost, C.G. Enke, D.C. McGilvery, D. Smith, J.D. Morrison, High efficiency collision-induced dissociation in an rf-only quadrupole, Int. J. Mass Spectrom. Ion Phys. 30 (1979) 127–136.

[18] P.H. Dawson, J.B. French, J.A. Buckley, D.J. Douglas, D. Simmons, The use of triple quadrupoles for sequential mass spectrometry: 1 the instrument parameters, Org. Mass Spectrom. 17 (1982) 205–211.

[19] P.H. Dawson, J.B. French, J.A. Buckley, D.J. Douglas, D. Simmons, The use of triple quadrupoles for sequential mass spectrometry: 2 a detailed case study, Org. Mass Spectrom. (1982) 212–217.

[20] D.J. Douglas, Some current perspectives on ICP-MS, Can. J. Spectroscopy 34 (1989) 38–49.

[21] J.T. Rowan, R.S. Houk, Attenuation of polyatomic ion interferences in inductively coupled plasma mass spectrometry by gas-phase collisions, Appl. Spectroscopy 43 (1989) 976–980.

[22] C.J. Barinaga, D.W. Koppenaal, Ion-trap mass spectrometry with an inductively coupled plasma source, Rapid Commun. Mass Spectrom. 8 (1994) 71–76.

[23] D.W. Koppenaal, C.J. Barinaga, M.R. Smith, Performance of an inductively coupled plasma source ion trap mass spectrometer, J. Anal. At. Spectrom. 9 (1994) 1053–1058.

[24] G.C. Eiden, C.J. Barinaga, D.W. Koppenaal, Selective removal of plasma matrix ions in plasma source mass spectrometry, J. Anal. At. Spectrom. 11 (1996) 317–322.

[25] G.C. Eiden, C.J. Barinaga, D.W. Koppenaal, Beneficial ion/molecule reactions in elemental mass spectrometry, Rapid Commun. Mass Spectrom. 11 (1997) 37–42.

[26] G.C. Eiden, C.J. Barinaga, D.W. Koppenaal, Analytical performance of the plasma source RF quadrupole ion trap in elemental and isotopic MS, J. Anal. At. Spectrom. 14 (1999) 1129–1132.

[27] P. Turner, T. Merren, J. Speakman, C. Haines, Interface studies in the ICP-mass spectrometer, in: G. Holland, S.D. Tanner (Eds.), Plasma Source Mass Spectrometry: Developments and Applications, The Royal Society of Chemistry, Cambridge, 1997, pp. 28–34.

[28] V.I. Baranov, S.D. Tanner, A dynamic reaction cell for inductively coupled plasma mass spectrometry (ICP-DRC-MS). I. The RF-field energy contribution in thermodynamics of ion–molecule reactions, J. Anal. At. Spectrom. 14 (1999) 1133–1142.

[29] S.D. Tanner, V.I. Baranov, A dynamic reaction cell for inductively coupled plasma mass spectrometry (ICP-DRC-MS). II. Reduction of interferences produced within the cell, J. Am. Soc. Mass Spectrom. 10 (1999) 1083–1094.

[30] S.D. Tanner, V.I. Baranov, U. Vollkopf, A dynamic reaction cell for inductively coupled plasma mass spectrometry (ICP-DRC-MS). III. Analytical performance, J. Anal. At. Spectrom. 15 (2000) 1261–1269.

[31] P.H. Dawson, Quadrupole Mass Spectrometry and Its Applications, American Institute of Physics, Woodbury, New York, 1995.

[32] J.E.P. Syka, Characteristics of multipole collision cells, presented at the 36th ASMS Conference on Mass Spectrometry and Allied Topics, San Francisco, 1988, Book of abstracts, 1328–1329.

[33] I. Szabo, New ion-optical devices utilizing oscillatory electric fields. I. Principle of operation and analytical theory of multipole devices with two-dimensional electric fields, Int. J. Mass Spectrom. Ion Processes 73 (1986) 197–235.

[34] C. Hagg, I. Szabo, New ion-optical devices utilizing oscillatory electric fields. II. Stability of motion in a two-dimensional hexapole field, Int. J. Mass Spectrom. Ion Processes 73 (1986) 237–275.

[35] C. Hagg, I. Szabo, New ion-optical devices utilizing oscillatory electric fields. IV. Computer simulations of transport of an ion beam through an ideal quadrupole, hexapole, and octapole operating in the rf-only mode, Int. J. Mass Spectrom. Ion Processes 73 (1986) 295–312.

[36] C. Hagg, I. Szabo, New ion-optical devices utilizing oscillatory electric fields. III. Stability of ion motion in a two-dimentional octapole field, Int. J. Mass Spectrom. Ion Processes 73 (1986) 277–294.

[37] R.E. March, J.F.J. Todd, Practical Aspects of Ion Trap Mass Spectrometry, 1. Fundamentals of Ion Trap Mass Spectrometry; 2. Ion Trap Instrumentation; 3. Chemical, Environmental and Biomedical Applications, CRC Series, Modern Mass Spectrometry, Boca Raton, FL, 1995.

[38] J.D. Morrison, K.A. Stanney, J. Tedder, The design and development of a quinquequadrupole mass spectrometer,

presented at the 34th Annual Conference on Mass Spectrometry and Allied Topics, Ohio, 1986, Book of abstracts, 222–223.

[39] C. Beaugrand, G. Devant, S.N. Nermag, C. Rolando, D. Jaouen, A multiquad triple analyzer MS/MS/MS, presented at the 34th Annual Conference on Mass Spectrometry and Allied Topics, Cincinnati, 1986, Book of abstracts, 220–221.

[40] B.A. Collings, J.M. Campbell, D. Mao, D.J. Douglas, A combined linear ion trap time-of-flight system with improved performance and MS^n capabilities, Rapid Commun. Mass Spectrom. 15 (2001) 1777–1795.

[41] C.G. Enke, R.A. Yost, J.D. Morrison, Tandem quadrupole mass spectrometer for selected ion fragmentation studies and low energy collision induced dissociator therefore, US patent 4,234,791 (1980).

[42] M. Morris, P. Thibault, R.K. Boyd, Low-energy ion/molecule products from collisions with ammonia, Rapid Commun. Mass Spectrom. 7 (1993) 1136–1140.

[43] J.T. Watson, C. Jaouen, H. Mestdagh, C. Rolando, A technique for mass selective ion rejection in a quadrupole reaction chamber, Int. J. Mass Spectrom. Ion Processes 93 (1989) 225–235.

[44] T. Sakuma, N. Gurprasad, S.D. Tanner, A. Ngo, W.R. Davidson, H.A. McLeod, B.P.-Y. Lau, J.J. Ryan, The application of rapid gas chromatography–tandem mass spectrometry in the analysis of complex samples for chlorinated dioxins and furans, in: L.H. Keith, C. Rappe, G. Choudhary (Eds.), Chlorinated Dioxins and Dibenzofurans in the Total Environment II, Butterworth Publishers, Boston, 1985, pp. 139–152.

[45] I.I. Stewart, Electrospray mass spectrometry: a tool for elemental speciation, Spectrochim. Acta Part B 54 (1999) 1649–1695.

[46] M.S. Lee, E.H. Kerns, LC/MS applications in drug development, Mass Spectrom. Rev. 18 (1999) 187–279.

[47] R. Aebersold, D.R. Goodlett, Mass spectrometry in proteomics, Chem. Rev. 101 (2001) 269–295.

[48] J. Godovac-Zimmerman, L.R. Brown, Perspectives for mass spectrometry and functional proteomics, Mass Spectrom. Rev. 20 (2001) 1–57.

[49] K.L. Busch, G.L. Glish, S.A. McLuckey, Mass Spectrometry/Mass Spectrometry: Techniques and Applications of Tandem Mass Spectrometry, VCH, New York, 1988.

[50] D.J. Douglas, J.B. French, Collisional focusing effects in radio frequency quadrupoles, J. Am. Soc. Mass Spectrom. 3 (1992) 398–408.

[51] D.J. Douglas, Applications of collision dynamics in quadrupole mass spectrometry, J. Am. Soc. Mass Spectrom. 9 (1998) 101–113.

[52] A.N. Krutchinsky, I.V. Chernushevich, V.L. Spicer, W. Ens, K.G. Standing, Collisionally damping interface for an electrospray time-of-flight mass spectrometer, J. Am. Soc. Mass Spectrom. 9 (1998) 569–579.

[53] B.A. Thomson, D.J. Douglas, J.J. Corr, J.W. Hager, C.L. Jolliffe, Improved collisionally activated dissociation efficiency and mass resolution on a triple quadrupole mass spectrometer system, Anal. Chem. 67 (1995) 1696–1704.

[54] M. Nicholls, Z. Palacz, P. Turner, High precision isotope ratio measurement by multicollector ICP-MS, presented at Winter Conference on Plasma Spectrochemistry, Scottsdale, Arizona, 1998, Book of abstracts, 413.

[55] M. Splendore, F.A. Londry, R.E. March, R.J.D. Morrision, P. Perrier, J. Andre, A simulation study of ion kinetic energies during resonant excitation in a stretched ion trap, Int. J. Mass Spectrom. Ion Processes 156 (1996) 11–29.

[56] R.E. March, R.J. Hughes, Quadrupole Storage Mass Spectrometry, Wiley, New York, 1989.

[57] D. Duckworth, D.E. Goering, G.V. Van Berkel, S.A. McLuckey, Gas-phase metal ion chemistry investigations using quadrupole ion traps: Unimolecular dissociation, ion/molecule and ion/ion reactions, presented at Federation of Analytical Chemistry and Spectroscopy Societies (FACSS), 1999, Book of abstracts, paper number 57.

[58] S.A. McLuckey, G.L. Glish, D.C. Duckworth, R.K. Marcus, Radio-frequency glow discharge ion trap mass spectrometry, Anal. Chem. 64 (1992) 1606–1609.

[59] N. Furuta, A. Takeda, J. Zheng, Evaluation of inductively coupled plasma–ion trap mass spectrometry, in: G. Holland, S.D. Tanner (Eds.), Plasma Source Mass Spectrometry: The New Millennium, The Royal Society of Chemistry, Cambridge, 2001, pp. 90–96.

[60] A. Dodonov, V. Kozlovski, A. Loboda, V. Raznikov, I. Soulimenkov, A. Tolmachev, A. Kraft, H. Wollnik, A new technique for decomposition of selected ions in molecule ion reactor coupled with ortho-time-of-flight mass spectrometry, Rapid Commun. Mass Spectrom. 11 (1997) 1649–1656.

[61] E.R. Denoyer, S.D. Tanner, U. Vollkopf, A new dynamic reaction cell for reducing ICP-MS interferences using chemical resolution, Spectroscopy 14 (1999) 43–54.

[62] I. Feldmann, N. Jakubowski, D. Steuwer, Application of a hexapole collision and reaction cell in ICP-MS part I: instrumental aspects and operational optimization, Fresenius' J. Anal. Chem. 365 (1999) 415–421.

[63] I. Feldmann, N. Jakubowski, C. Thomas, D. Steuwer, Application of a hexapole collision and reaction cell in ICP-MS part II: analytical figures of merit and first applications, Fresenius' J. Anal. Chem. 365 (1999) 422–428.

[64] J.M. Marchante-Gayon, C. Thomas, I. Feldmann, N. Jakubowski, Comparison of different nebulisers and chromatographic techniques for the speciation of selenium in nutritional commercial supplements by hexapole collision and reaction cell ICP-MS, J. Anal. At. Spectrom. 15 (2000) 1093–1102.

[65] D.R. Bandura, V.I. Baranov, S.D. Tanner, Reaction chemistry and collisional processes in multipole devices for resolving isobaric interferences in ICP-MS, Fresenius' J. Anal. Chem. 370 (2001) 454–470.

[66] N.G. Adams, D. Smith, The selected ion flow tube (SIFT); a technique for studying ion-neutral reactions, Int. J. Mass Spectrom. Ion Phys. 21 (1976) 349–359.
[67] P.R.D. Mason, K. Kaspers, M.J. vanBergen, Determination of sulfur isotope ratios and concentrations in water samples using ICP-MS incorporating hexapole ion optics, J. Anal. At. Spectrom. 14 (1999) 1067–1074.
[68] H. Niu, R.S. Houk, Fundamental aspects of ion extraction in inductively coupled plasma mass spectrometry, Spectrochim. Acta Part B 51 (1996) 779–815.
[69] R.S. Houk, N. Praphairaksit, Dissociation of polyatomic ions in the inductively coupled plasma, Spectrochim. Acta Part B 56 (2001) 1069–1096.
[70] V.V. Lavrov, D.K. Bohme, Personal communication, 2000.
[71] M.V. Sussman, Elementary General Thermodynamics, Addison-Wesley Publishing, Toronto, Canada, 1972.
[72] P. Kebarle, Gas phase ion thermochemistry based on ion-equilibria: from the ionosphere to the reactive centers of enzymes, Int. J. Mass Spectrom. 200 (2000) 313–330.
[73] J.L. Beauchamp, M.C. Caserio, T.B. McMahon, Ion–molecule reactions of *tert*-butyl alcohol by ion cyclotron resonance spectroscopy, J. Amer. Chem. Soc. 96 (1974) 6243–6251.
[74] F.C. Fehsenfeld, A.L. Schmeltekopf, P.D. Goldan, H.I. Schiff, E.E. Ferguson, Thermal energy ion-neutral reaction rates. 1. Some reactions of helium ions, J. Chem. Phys. 44 (1966) 4078–4094.
[75] G.K. Koyanagi, V.V. Lavrov, V. Baranov, D. Bandura, S.D. Tanner, J.W. McLaren, D.K. Bohme, A novel ICP/SIFT mass spectrometer for the study of reactions of atomic and atomic oxide ions, Int. J. Mass Spectrom. 194 (2000) L1–L5.
[76] G.K. Koyanagi, V.I. Baranov, S.D. Tanner, D.K. Bohme, An inductively coupled plasma/selected-ion flow tube mass spectrometric study of the chemical resolution of isobaric interferences, J. Anal. At. Spectrom. 15 (2000) 1207–1210.
[77] G.K. Koyanagi, D.K. Bohme, Oxidation reactions of lanthanide cations with N_2O and O_2: periodicities in reactivity, J. Phys. Chem. 105 (2001) 8964–8968.
[78] C. Rue, P.B. Armentrout, I. Kretzschmar, D. Schroder, H. Schwarz, Guided ion beam studies of the reactions of Fe^+ and Co^+ with CS_2 and COS, J. Phys. Chem. A 105 (2001) 8456–8464.
[79] B. Hattendorf, D. Günther, Characteristics and capabilities of an ICP-MS with a dynamic reaction cell for dry aerosols and laser ablation, J. Anal. At. Spectrom. 15 (2000) 1125–1131.
[80] D.R. Bandura, S.D. Tanner, V.I. Baranov, G.K. Koyanagi, V.V. Lavrov, D.K. Bohme, Ion–molecule chemistry solutions to the ICP-MS analytical challenge, in: G. Holland, S.D. Tanner (Eds.), Plasma Source Mass Spectrometry: The New Millennium, The Royal Society of Chemistry, Cambridge, 2001, pp. 130–147.
[81] J.R. Gibson, S. Taylor, Numerical investigation of the effect of electrode size on the behaviour of quadrupole mass filters, Rapid Commun. Mass Spectrom. 15 (2001) 1960–1964.
[82] W. Paul, H.P. Reinhard, U. von Zahn, Das elektrische massenfilter als massenspektrometer und isotopentrenner, Z. Physik. 152 (1958) 143–182.
[83] I.E. Dayton, F.C. Shoemaker, R.F. Mozley, The measurement of two-dimensional fields. Part II. Study of a quadrupole magnet, Rev. Sci. Instru. 25 (1954) 485–489.
[84] D.J. Douglas, N.V. Konenkov, Influence of the sixth and tenth spatial harmonics on the peak shape of quadrupole mass filter with round rods', Rapid Commun. Mass Spectrom. 16 (2002) 1425–1431.
[85] D.R. Denison, Operating parameters of a quadrupole in a grounded cylindrical housing, J. Vac. Sci. Technol. 8 (1971) 266–269.
[86] V.V.K.R. Rao, A. Bhutani, Electric hexapoles and octapoles with optimized circular section rods, Int. J. Mass Spectrom. 202 (2000) 31–36.
[87] W.M. Brubaker, Comparison of quadrupole mass spectrometers with round and hyperbolic rods, J. Vac. Sci. Technol. 4 (1967) 326, abstract only.
[88] W.M. Brubaker, W.S. Chamberlin, Theoretical and experimental comparison of quadrupole mass analyzers with round and hyperbolic field-forming surfaces, presented at Recent Developments in Mass Spectrometry, Proceedings International Conference Mass Spectroscopy, University Park Press, Baltimore, MD, 1970, pp. 98–103.
[89] W.M. Brubaker, An improved quadrupole mass analyzer, Adv. Mass Spectrom. 4 (1968) 293–299.
[90] J.E. Fulford, D.J. Douglas, Ion kinetic energies in inductively coupled plasma/mass spectrometry (ICP-MS), Appl. Spectroscopy 40 (1986) 971–974.
[91] S.D. Tanner, Experimental studies of ion kinetic energies in ICP-MS, in: G. Holland, A.N. Eaton (Eds.), Application of Plasma Source Mass Spectrometry II, The Royal Society of Chemistry, Cambridge, 1993, pp. 222–234.
[92] D.J. Douglas, S.D. Tanner, Fundamental considerations in ICP-MS, in: A. Montaser (Ed.), Inductively Coupled Plasma Mass Spectrometry, VCH, 1998, pp. 615–679.
[93] F. Muntean, Transmission study for rf-only quadrupoles by computer simulation, Int. J. Mass Spectrom. Ion Processes 151 (1995) 197–206.
[94] K. Blaum, Ch. Geppert, P. Muller, K. Nortershauser, K. Wendt, B.A. Bushaw, Peak shape for a quadrupole mass spectrometer: comparison of computer simulation and experiment, Int. J. Mass Spectrom. 202 (2000) 81–89.
[95] M. Morris, P. Thibault, R.K. Boyd, Characterization of a high-pressure quadrupole collision cell for low-energy collision-induced dissociation, J. Am. Soc. Mass Spectrom. 5 (1994) 1042–1063.
[96] C.M. Lock, E. Dyer, Characterisation of high pressure quadrupole collision cells possessing direct current axial

fields, Rapid Commun. Mass Spectrom. 13 (1999) 432–448.

[97] G. Javahery, B. Thomson, A segmented radiofrequency—only quadrupole collision cell for measurements of ion collision cross section on a triple quadrupole mass spectrometer, J. Am. Soc. Mass Spectrom. 8 (1997) 697–702.

[98] B.A. Thomson, C.L. Jolliffe, Spectrometer with axial field, US patent 5,847,386 (1998).

[99] A. Loboda, A. Krutchnisky, J. McNabb, V. Spicer, W. Ens, K. Standing, Novel LINAC II electrode geometry to create an axial field in a multipole ioon guide, presented at the 48th Am. Soc. Mass Spectrom. Meeting, Long Beach, California, 2000, Book of abstracts, poster number WPA016.

[100] A. Loboda, A. Krutchnisky, O. Loboda, J. McNabb, V. Spicer, W. Ens, K. Standing, Novel Linac II electrode geometry for creating an axial field in a multipole ion guide, Eur. J. Mass Spectrom. 6 (2000) 531–536.

[101] D.R. Bandura, V.I. Baranov, S.D. Tanner, Inductively coupled plasma mass spectrometer with an axial field in a quadrupole reaction cell, J. Am. Soc. Mass Spectrom. (2002), in press.

[102] D.R. Bandura, V. Baranov, S.D. Tanner, Dynamic reaction cell with axial field, presented at the 47th International Conference on Analytical Sciences and Spectroscopy, Toronto, 2001.

[103] D.J. Douglas, J.B. French, Gas dynamics of the inductively coupled plasma mass spectrometry interface, J. Anal. At. Spectrom. 3 (1988) 743–747.

[104] S.D. Tanner, L.M. Cousins, D.J. Douglas, Reduction of space charge effects using a three-aperture gas dynamic vacuum interface for inductively coupled plasma-mass spectrometry, Appl. Spectroscopy 48 (1994) 1367–1372.

[105] S.D. Tanner, D.J. Douglas, J.B. French, Gas and ion dynamics of a three-aperture vacuum interface for inductively coupled plasma-mass spectrometry, Appl. Spectroscopy 48 (1994) 1373–1378.

[106] T.N. Olney, W. Chen, D.J. Douglas, Gas dynamics of the ICP-MS interface: impact pressure probe measurements of gas flow profiles, J. Anal. At. Spectrom. 14 (1999) 9–17.

[107] V.I. Baranov, S.D. Tanner, Multi-thermal plasma distributions from ion kinetic energy measurements, presented at the 24th Federation of Analytical Chemistry and Spectroscopy Societies, Providence, Rhode Island, 1997, Book of abstracts, 133.

[108] A.N. Krutchinsky, A.V. Loboda, V.L. Spicer, R. Dworschak, W. Ens, K.G. Standing, Orthogonal injection of matrix-assisted laser desorption/ionization ions into a time-of-flight spectrometer through a collisional damping interface, Rapid Commun. Mass Spectrom. 12 (1998) 508–518.

[109] D.R. Bandura, V.I. Baranov, S.D. Tanner, Effect of collisional damping and reactions in a dynamic reaction cell on the precision of isotope ratio measurements, J. Anal. At. Spectrom. 15 (2000) 921–928.

[110] D.R. Bandura, S.D. Tanner, Effect of collisional damping in the dynamic reaction cell on the precision of isotope ratio measurements, At. Spectroscopy 20 (1999) 69–72.

[111] S.F. Boulyga, J.S. Becker, ICP-MS with hexapole collision cell for isotope ratio measurements of Ca, Fe and Se, Fresenius' J. Anal. Chem. 370 (2001) 618–623.

[112] S.F. Boulyga, J.S. Becker, Inductively coupled plasma mass spectrometry with hexapole collision cell: figures of merit and applications, Entwicklung und Adwendung massenspektrometrischer Methoden zur Spuren-, Ultraspuren,-Isotopen- und Oberflachenanalytik fur Forchungsaufgaben des Forschungszentrums Julich, Tei 12 (2000) 13–44.

[113] V. Baranov, G. Javahery, A.C. Hopkinson, D.K. Bohme, Intrinsic coordination properties of iron in FeO^+: kinetics at 294 ± 3 K for gas-phase reactions of the ground states of Fe^+ and FeO^+ with inorganic ligands containing hydrogen, nitrogen, and oxygen, J. Am. Chem. Soc. 117 (1995) 12801–12809.

[114] R.K. Milburn, V.I. Baranov, A.C. Hopkinson, D.K. Bohme, Sequential ligation of Mg^+, Fe^+, $(c\text{-}C_5H_5)Mg^+$, and $(c\text{-}C_5H_5)Fe^+$ with ammonia in the gas phase: transition from coordination to solvation in the sequential ligation of Mg^+, J. Phys. Chem. A 102 (1998) 9803–9810.

[115] G.K. Koyanagi, D.K. Bohme, Personal communication, 2001.

[116] J.W. Olesik, Personal communication, 2001.

[117] K. Neubauer, Personal communication, 2001.

[118] L.J. Moens, F.F. Vanhaecke, D.R. Bandura, V.I. Baranov, S.D. Tanner, Elimination of isobaric interferences in ICP-MS, using ion–molecule reaction chemistry: Rb/Sr age determination of magmatic rocks, a case study, J. Anal. At. Spectrom. 16 (2001) 991–994.

[119] U. Vollkopf, V.I. Baranov, S.D. Tanner, ICP-MS multielement analysis at sub-ppt levels applying new instrumental design concepts, in: G. Holland, S.D. Tanner (Eds.), Plasma Source Mass Spectrometry: New Developments and Applications, The Royal Society of Chemistry, Cambridge, 1999, pp. 63–79.

[120] F. Abou-Shakra, The determination of arsenic in seawater by platform ICP-HEX-MS, in: G. Holland, S.D. Tanner (Eds.), Plasma Source Mass Spectrometry: New Developments and Applications, The Royal Society of Chemistry, Cambridge, 1999, pp. 120–131.

[121] P. Leonhard, R. Pepelnik, A. Prange, N. Yamada, T. Yamada, Analysis of diluted seawater at the ng l^{-1} level using an ICP-MS with an octapole reaction cell, J. Anal. At. Spectrom. 17 (2002) 189–196.

[122] J.J. Sloth, E.H. Larsen, The application of inductively coupled plasma dynamic reaction cell mass spectrometry for measurement of selenium isotopes, isotope ratios and chromatographic detection of selenoamino acids, J. Anal. At. Spectrom. 15 (2000) 669–672.

[123] J.R. deLaeter, Mass spectrometry and geochronology, Mass Spectrom. Rev. 17 (1998) 97–125.
[124] F. Vanhaecke, G. De Wannemacker, L. Moens, J. Hertogen, The determination of strontium isotope ratios by means of quadrupole-based ICP mass spectrometry: a geochronological case study, J. Anal. At. Spectrom. 14 (1999) 1691–1696.
[125] P.J. Turner, T.O. Merren, J. Speakman, R.C. Haines, Z. Palacz, Ion optics of multi-collector ICP-MS systems for precise and accurate isotope ratio measurement, presented at Winter Conference on Plasma Spectrochemistry, Ft. Lauderdale, 2000, Book of abstracts, 330–331.
[126] J.P. Guzowski, G.M. Hieftje, Characteristics of a hexapole ion-guide interface for plasma-source time-of-flight mass spectrometry, J. Anal. At. Spectrom. 16 (2001) 781–792.
[127] A.M. Leach, G.M. Hieftje, Use of an ion guide collision cell to improve the analytical performance of an inductively coupled plasma time-of-flight mass spectrometer', Int. J. Mass Spectrom. 212 (2001) 49–63.
[128] S.F. Boulyga, J.S. Becker, J.L. Matusevitch, H.-J. Dietze, Isotope ratio measurements of spent reactor uranium in environmental samples by using inductively coupled plasma mass spectrometry, Int. J. Mass Spectrom. 203 (2000) 143–154.
[129] J.S. Becker, H.-J. Dietze, Precise and accurate isotope ratio measurements by ICP-MS, Fresenius' J. Anal. Chem. 368 (2000) 23–30.
[130] K. Sakata, K. Kawabata, Reduction of fundamental polyatomic ions in inductively coupled plasma mass spectrometry, Spectrochim. Acta Part B 49 (1994) 1027–1038.
[131] S.D. Tanner, Characterization of ionization and matrix suppression in inductively coupled 'cold' plasma mass spectrometry, J. Anal. At. Spectrom. 10 (1995) 905–921.
[132] S.D. Tanner, V.I. Baranov, Fundamental processes impacting performance of an ICP-MS dynamic reaction cell, in: G. Holland, S.D. Tanner (Eds.), Plasma Source Mass Spectrometry: New Development and Applications, The Royal Society of Chemistry, Cambridge, 1999, pp. 46–62.
[133] D.S. Bollinger, A.J. Schleisman, Analysis of high purity acids using a dynamic reaction cell ICP-MS, At. Spectroscopy 20 (1999) 60–63.
[134] D.S. Bollinger, A.J. Schleisman, Initial experiences with the dynamic reaction cell ICP-MS, in: G. Holland, S.D. Tanner (Eds.), Plasma Source Mass Spectrometry: New Developments and Applications, The Royal Society of Chemistry, Cambridge, 1999, pp. 80–92.
[135] J.W. Olesik, C. Hensman, S. Rabb, D. Rago, Sample introduction, plasma-sample interactions, ion transport and ion–molecule reactions: fundamental understanding and practical improvements in ICP-MS, in: G. Holland, S.D. Tanner (Eds.), Plasma Source Mass Spectrometry: The New Millennium, The Royal Society of Chemistry, Cambridge, 2001, pp. 3–16.
[136] U. Vollkopf, K. Klemm, M. Pfluger, The analysis of high purity hydrogen peroxide by dynamic reaction cell ICP-MS, At. Spectroscopy 20 (1999) 53–59.
[137] Y. Kishi, K. Kawabata, Effect of Plasma Parameters on the Analysis of Semiconductor Process Chemicals by ICP-MS, D-6482, Perkin Elmer Instruments, Shelton, CT, 2001.
[138] A.F. Porche, Y. Kishi, R.E. Wolf, Analysis of Silicon Wafers Using the ELAN DRC ICP-MS, Application Note D-6444, Perkin Elmer Instruments, Shelton, CT, 2001.
[139] J. Godfrey, J. Cantle, P. Sigsworth, Multi-element analysis of potable water using the VG PQ ExCell ICP-MS incorporating Collision Cell Technology (CCT), presented at ninth ISMAS-WS, 2000, 114–123.
[140] Available from http://www.chem.yorku.ca/profs/bohme/research/research.html (last accessed June 4, 2002).
[141] Z. Du, R.S. Houk, Attenuation of metal oxide ions in inductively coupled plasma mass spectrometry with hydrogen in a hexapole collision cell, J. Anal. At. Spectrom. 15 (2000) 383–388.
[142] L.A. Simpson, M. Thomsen, B.J. Alloway, A reaction mechanism for solving the oxide problem in ICP-MS analysis of the noble metals, in: G. Holland, S.D. Tanner (Eds.), Plasma Source Mass Spectrometry: The New Millennium, The Royal Society of Chemistry, Cambridge, 2001, pp. 148–161.
[143] M.L. Huertas, J. Fontan, Evolution times of tropospheric positive ions, Atmos. Environ. 9 (1975) 1018–1026.
[144] V.I. Baranov, D.R. Bandura, S.D. Tanner, Reaction cell approach to the oxide problem, presented at Winter Conference on Plasma Spectrochemistry, Ft. Lauderdale, Florida, 2000, Book of abstracts, 375.
[145] B. Hattendorf, D. Günther, Experimental evidence for the formation of doubly charged oxide and hydroxide ions in inductively coupled plasma mass spectrometry, Fresenius' J. Anal. Chem. 370 (2001) 483–487.
[146] W. Lindinger, Reactions of doubly charged ions at near thermal energies, Physica Scripta T3 (1983) 115–119.
[147] Z. Herman, Dynamics of charge transfer and chemical reactions of doubly-charged ions at low collision energies, Int. Rev. Phys. Chem. 15 (1996) 299–324.
[148] W. Lindinger, A. Hansel, Z. Herman, Ion–molecule reactions, Adv. Atomic Mol. Optical Phys. 43 (2000) 243–294.
[149] P.R.D. Mason, Expanding the capabilities of laser ablation ICP-MS with collision and reaction cells, in: P. Sylvester (Ed.), Laser-Ablation-ICPMS in the Earth Sciences—Principles and Applications, The Mineralogical Association of Canada, Ottawa, Canada, 2001, pp. 63–81.
[150] B. Hattendorf, D. Gunter, M. Schonbachler, A. Halliday, Simultaneous ultra trace determination of Zr and Nb in chromium matrices with ICP Dynamic Reaction Cell MS, Anal. Chem. 73 (2001) 5494–5498.

[151] D. Günther, B. Hattendorf, A. Audetat, Multi-element analysis of melt and fluid inclusions with improved detection capabilities for Ca and Fe using laser ablation with a dynamic reaction cell ICP-MS, J. Anal. At. Spectrom. 16 (2001) 1085–1090.

[152] N. Jakubowski, Instrumental concepts in ICP-MS to cope with spectral interferences, presented at International Congress of Pacific Basic Societies, 2000, paper number ANAL 0384.

[153] D.E. Nixon, J. Butz, S. Eckdahl, M.F. Burritt, K.R. Neubauer, Determination of Vanadium in Serum and Urine Using the ELAN DRC ICP-MS, Application Note D-6456, Perkin Elmer Instruments, Shelton, CT, 2001.

[154] D.E. Nixon, J. Butz, S.J. Eckdahl, M.F. Burritt, K.R. Neubauer, Determination of Chromium in Serum and Urine, Application Note D6356, Perkin Elmer Instruments, Shelton, CT, 2000.

[155] D.E. Nixon, J. Butz, S.J. Eckdahl, M.F. Burritt, K.R. Neubauer, R.E. Wolf, Determination of Selenium in Serum and Urine Using the ELAND DRC ICP-MS, Application Note D-6420, Perkin Elmer Instruments, Shelton, CT, 2000.

[156] D.E. Nixon, J. Butz, S.J. Eckdahl, M.F. Burritt, K.R. Neubauer, R.E. Wolf, Determination of Copper and Iron in Liver Tissue Using the ELAN DRC ICP-MS, Application Note D6419, Perkin Elmer Instruments, Shelton, CT, 2000.

[157] K. Wilson, J. Walker, Principals and Techniques of Practical Biochemistry, Cambridge University Press, 2000, pp. 319–322.

[158] M. Wind, M. Edler, N. Jakubowski, M. Linsheid, H. Wesch, W.D. Lehmann, Analysis of protein phosphorylation by capillary liquid chromatography coupled to element mass spectrometry with ^{31}P detection and to electrospray mass spectrometry, Anal. Chem. 73 (2001) 29–35.

[159] M. Wind, H. Wesch, W.D. Lehmann, Protein phosphorylation degree: determination by capillary liquid chromatography and inductively coupled plasma mass spectrometry, Anal. Chem. 73 (2001) 3006–3010.

[160] D.R. Bandura, V.I. Baranov, S.D. Tanner, Detection of ultra-trace phosphorous and sulfur by quadrupole ICP-MS with Dynamic Reaction Cell', Anal. Chem. 74 (2002) 1497–1502.

[161] K.R. Ludwig, Using Isoplot/Ex (version 1.00): A Geochronological Toolkit for Microsoft Excel, Berkeley Geochronology Center, Berkeley, CA, 1998, Special Publication No. 1.